US Army Corps of Engineers®

Acoustic Doppler Current Profiler Study of Water and Sediment Movement through a Deep Scour Hole in the Lower Mississippi River

MRG&P Report No. 45 • August 2023

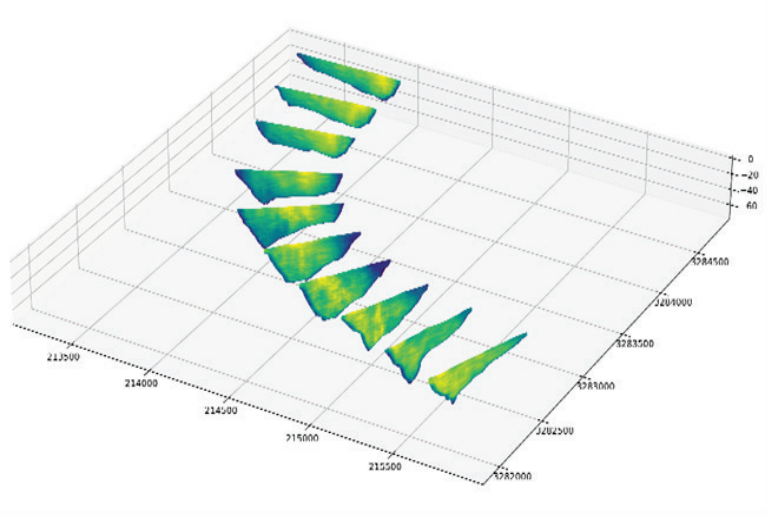

MRG&P
Mississippi River Geomorphology & Potamology Program

This page intentionally left blank.

Mississippi River Geomorphology and Potamology Program

MRG&P Report No. 45
August 2023

Acoustic Doppler Current Profiler Study of Water and Sediment Movement through a Deep Scour Hole in the Lower Mississippi River

Michael T. Ramirez, Travis A. Dahl, and Gary L. Brown

US Army Engineer Research and Development Center
Coastal and Hydraulics Laboratory
3909 Halls Ferry Road
Vicksburg, MS 39180-6199

Final report

Prepared for Mississippi River Geomorphology and Potamology Program
US Army Corps of Engineers, Mississippi Valley Division
Vicksburg, MS 39180-0080

Under Funding provided by the Mississippi Valley Division through the Mississippi River Geomorphology and Potamology Program

Abstract

A series of acoustic Doppler current profiler (ADCP) transects were collected through a deep scour hole at the bend near River Mile 60 on the Lower Mississippi River. The measurements were collected during both a low and a high flow. The ADCP results show a 3D flow field through the deep bend. The backscatter intensity of the ADCP measurements indicates the majority of the sediment remains close to the inside of the bend and high in the water column, with minimal concentrations at the bottom of the bend. These findings have implications for numerical sediment transport models, which tend to deposit material at the bottom of deep scour holes like the one in this study.

Contents

Figures and Tables iv

Preface v

1 Introduction 1

1.1 Background 1
1.2 Objective 2
1.3 Approach 2

2 Methods 3

2.1 Study Area 3
2.2 Study Period 4
2.3 Data Collection 7
2.4 Data Processing 7

3 Results 8

3.1 Hydrodynamics 8
3.1.1 September 2020 8
3.1.2 March 2021 12
3.2 Sediment Transport 17

4 Discussion 20

4.1 Hydrodynamics 20
4.2 Acoustic Backscatter and Sediment Transport 21
4.3 Numerical Modeling Implications 23

5 Conclusions and Recommendations 25

5.1 Conclusions 25
5.2 Recommendations 25

Appendix A: ADCP Plots from 17 September 2020 27

Appendix B: ADCP Plots from 19 March 2021 58

Report Documentation Page (SF 298) 89

Figures and Tables

Figures

1. Map showing river channel bathymetry and locations of the 30 cross-sectional and 3 longitudinal survey lines. 4
2. Streamwise water velocity measured in September 2020. Locations for the eight sequential survey lines are shown in *red* overlaid on the channel bathymetry. Cross sections are displayed from right descending bank (0.0 m distance) to left (approximately 700 m distance)..... 9
3. Cross-stream water velocity measured in September 2020. Locations for the eight sequential survey lines are shown in *red* overlaid on the channel bathymetry. The cross sections are shown from upstream at the top to downstream at the bottom. For the cross-stream component, positive values reflect flow directed towards the outside of the bend, and negative values reflect flow directed towards the inside of the bend. 10
4. Vertical component water velocity measured in September 2020. Locations for the eight sequential survey lines are shown in *red* overlaid on the channel bathymetry. Positive values reflect flow directed upwards, and negative values reflect flow directed downwards. 11
5. Depth-averaged flow vectors from September 2020. The reference vector in the northeast quadrant represents 1 m/s flow. The colors represent bathymetry, with *red*s and *yellow*s in shallow areas and *blue* to *magenta* colors in the deepest areas..... 12
6. Streamwise water velocity measured in March 2021. Locations for the eight sequential survey lines are shown in *red* overlaid on the channel bathymetry..... 14
7. Cross-stream water velocity measured in March 2021. Locations for the eight sequential survey lines are shown in *red* overlaid on the channel bathymetry. For the cross-stream component, positive values reflect flow directed towards the outside of the bend, and negative values reflect flow directed towards the inside of the bend. 15
8. Vertical water velocity measured in March 2021. Locations for the eight sequential survey lines are shown in *red* overlaid on the channel bathymetry. Positive values reflect flow directed upwards, and negative values reflect flow directed downwards. 16
9. Depth-averaged flow vectors from March 2021. The reference vector in the northeast quadrant represents 1 m/s flow. 17
10. Cross sections of acoustic backscatter observed in September 2020. 18
11. Cross sections of acoustic backscatter observed in March 2021. 19

Tables

1. Dates, times, and measured discharge for each survey transect. Longitudinal survey lines do not result in a measured discharge and were excluded from this table..... 5

Preface

The investigation documented in this report was conducted for the US Army Corps of Engineers, Mississippi Valley Division (MVD), as part of the Mississippi River and Tributaries Project, funding provided by the Mississippi Valley Division through Mississippi River Geomorphology and Potamology (MRG&P) program and published through the MRG&P program. At the time of publication of this report, the MRG&P program director was Mr. Jonathan Andrew (Andy) Ashley. The MVD commander was MG Kimberly A. Peeples, and Mr. James A. Bodron was the MVD director of programs.

The work was performed by the Field Data Collection and Analysis Branch of the Navigation Division and the River and Estuarine Engineering Branch of the Flood and Storm Protection Division, US Army Engineer Research and Development Center (ERDC), Coastal and Hydraulics Laboratory (CHL).

At the time of publication of this report, Mr. William C. Butler was chief of the Field Data Collection and Analysis Branch; Ms. Ashley E. Frey was chief of the Navigation Division; Mr. David P. May was chief of the River and Estuarine Engineering Branch; and Ms. Lauren M. Dunkin was acting chief of the Flood and Storm Protection Division. The deputy director of CHL was Mr. Keith W. Flowers, and Dr. Ty V. Wamsley was the director.

The commander of ERDC was COL Christian Patterson, and the director was Dr. David W. Pittman.

This page intentionally left blank.

1 Introduction

1.1 Background

The US Army Corps of Engineers and other agencies use sediment transport models of the Mississippi River to inform management decisions, especially regarding proposed sediment diversions and long-term dredging needs. All current sediment transport models of the Mississippi River (e.g., Copeland and Lombard 2020; Brown et al. 2019; Dahl et al. 2018) tend to predict deposition in very deep scour holes that actually persist in the river, often in meander bends. The anomalous deposition occurs in 1D, 2D, and 3D models. Repeated bathymetric survey data of these scour holes indicate that they are over 50 m* deep (approximately twice the depth of the adjacent river thalweg) and are not filling over time. This phenomenon also occurs in other rivers (Gibson et al. 2019). It is important to understand why the numerical models fail to match the observed conditions at these points to increase model fidelity and better support management decisions.

Previous work in smaller rivers identified potential sediment transport patterns through meander bends. The US Geological Survey analyzed acoustic Doppler current profiler (ADCP) data from a meander bend on the Sacramento River in California to identify indicators of secondary flow (Dinehart and Burau 2005). In data collected at flows ranging from 679 to 1,580 m^3/s, they detected areas of high backscatter intensity (strong acoustic returns) over the point bar. These areas coincided with outward cross-stream flow and low backscatter intensity in the outside of the meander bend where inward cross-stream flows moved through the deeper pool.

Czuba et al. (2011) used a series of ADCP cross sections to look at flows in a bend at the upstream end of the St. Clair River, between Port Huron, Michigan, and Sarnia, Ontario. The data, collected at a flow rate of 5,200 m^3/s, indicated that higher sediment concentrations were found

* For a full list of the spelled-out forms of the units of measure and unit conversions used in this document, please refer to *US Government Publishing Office Style Manual*, 31st ed. (Washington, DC: US Government Publishing Office 2016), 248–52 and 345–347, respectively. https://www.govinfo.gov/content/pkg/GPO-STYLEMANUAL-2016/pdf/GPO-STYLEMANUAL-2016.pdf.

along the banks, particularly the inside bank, going into the bend. As the river widened in the bend, backscatter intensities declined but were still lowest in the middle of the channel.

1.2 Objective

The goal of this effort was to collect velocity and acoustic backscatter data to better understand the hydraulic and sediment dynamics of deep scour holes in the Lower Mississippi River. The hypothesis for the study was that the 3D flow field in the deep scour holes allows sand particles to either stay in suspension or to preferentially move along shorter flow paths than simulated by current numerical models. These data and subsequent analysis from this study will lead to improved numerical models that support sediment and dredging management decisions.

1.3 Approach

This study consisted of a high-resolution data collection effort focused on a single, deep scour hole in the Lower Mississippi River. A US Army Engineer Research and Development field crew collected a grid of ADCP transects with sufficient detail to allow interpretation of the 3D flow field through the scour hole during two different flow regimes. The strength of backscatter returns along each transect was utilized as a surrogate for the relative amount of sediment in the water. These measurements were analyzed to draw conclusions about the flow of sediment through the deep scour hole.

2 Methods

2.1 Study Area

The study site is located at approximately N 29.65°, W 89.95°, 96 km upstream of the Mississippi River mouth at Head of Passes (River Mile 60), in a tight leftward (i.e., towards the left descending bank) bend. The survey area encompassed a 4 km reach of the river extending above and below the apex of the bend. A total of 33 survey lines were planned: 30 cross sections and 3 longitudinal sections (Figure 1). The cross sections were spaced 100 m apart in the tightest section of the bend, where flow conditions were expected to be the most dynamic, and 300 m spacing was used away from the apex of the bend. The three longitudinal sections were spaced at approximately 25%, 50%, and 75% along the width of the channel, parallel to the river course.

Morphologically, the river in this reach consists of two distinct geometries: bar-and-thalweg and channel-crossing. The bar-and-thalweg morphology is characterized by an asymmetric cross section, with a relatively shallow, dune-mantled sand bar alongside a channel thalweg generally devoid of sand cover (as evidenced by a lack of bedforms). The channel-crossing morphology is more symmetrical in cross section, a U-shaped profile with sand cover across the width of the channel. These two morphologies are characteristic of the meandering lower Mississippi River, with channel-crossing morphologies situated between alternate bar-and-thalweg sections, which generally correlate with the curvature of the river's meanders.

Note that the backwater control associated with the proximity of the Gulf of Mexico mitigates stage variation in this reach. Hence, the bars are never emergent and are generally referred to as submerged lateral bars.

Figure 1. Map showing river channel bathymetry and locations of the 30 cross-sectional and 3 longitudinal survey lines.

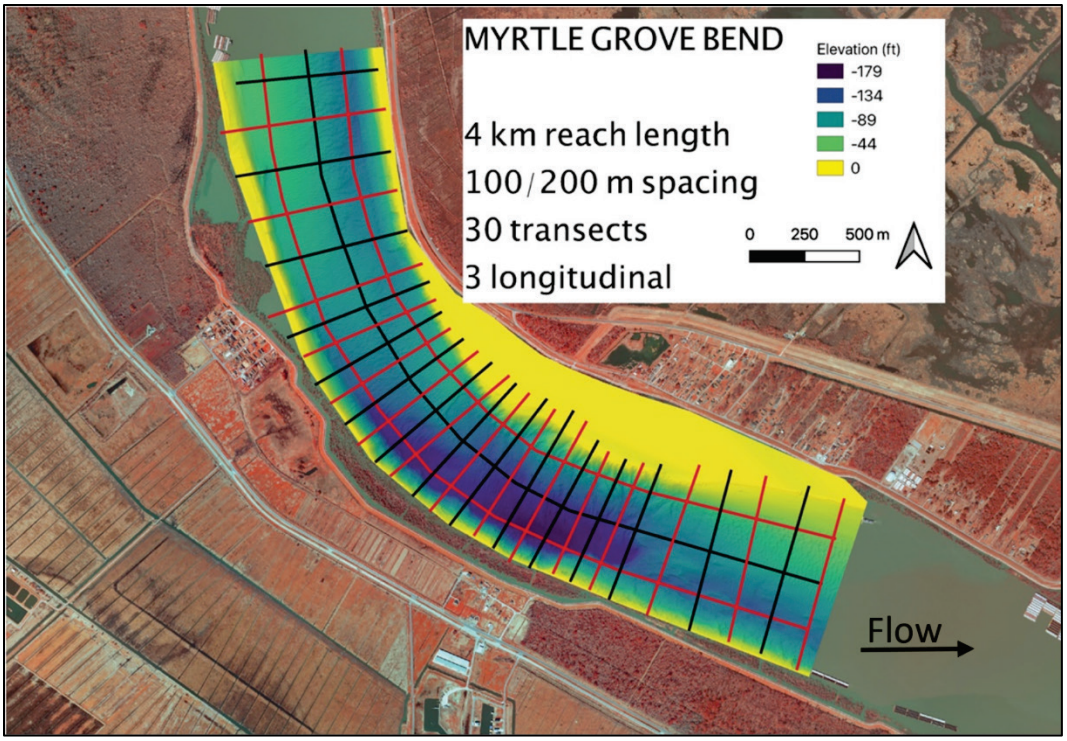

2.2 Study Period

The surveys were performed 17 September 2020 (average river discharge 9,745 m^3/s) and 19 March 2021 (average river discharge 24,651 m^3/s) to capture the hydrodynamic conditions at two distinct river stages representing low flow in the fall and high flow in the spring. The September survey coincided with spring tide (new moon) conditions and low flow, so this sampling event can be expected to show the maximum possible influence of tidal modulation on river conditions. The March survey had nearly the exact opposite: neap tide (3 days prior to first quarter moon) and high flow conditions, so tidal modulation was expected to be minimal. Nevertheless, each survey was performed by surveying even-numbered lines (*black lines* in Figure 1) in the morning and odd-numbered lines (*red lines* in Figure 1) in the afternoon to ensure that half of the data represents ebb tidal conditions and the other half represents flood tidal conditions. The exact times and measured discharge for each ADCP transect are shown in Table 1.

Table 1. Dates, times, and measured discharge for each survey transect. Longitudinal survey lines do not result in a measured discharge and were excluded from this table.

ADCP Line Number	Date	Time (UTC)	Discharge (m^3/s)	Tidal Phase
1	9/17/2020	13:18	9,789	Flood
2	9/17/2020	18:31	9,494	Ebb
3	9/17/2020	13:29	9,805	Flood
4	9/17/2020	18:44	9,683	Ebb
5	9/17/2020	13:42	9,911	Flood
6	9/17/2020	18:59	9,631	Ebb
7	9/17/2020	13:53	9,901	Flood
8	9/17/2020	19:14	9,755	Ebb
9	9/17/2020	14:08	9,905	Flood
10	9/17/2020	19:29	9,685	Ebb
11	9/17/2020	14:24	9,880	Flood
12	9/17/2020	19:47	9,653	Ebb
13	9/17/2020	14:37	9,595	Flood
14	9/17/2020	20:00	9,782	Ebb
15	9/17/2020	14:59	9,710	Flood
16	9/17/2020	20:18	9,833	Ebb
17	9/17/2020	15:17	9,657	Flood
18	9/17/2020	20:30	9,857	Ebb
19	9/17/2020	15:30	9,333	Flood
20	9/17/2020	20:46	9,909	Ebb
21	9/17/2020	15:44	9,892	Flood
22	9/17/2020	21:00	9,698	Ebb
23	9/17/2020	15:59	9,708	Ebb*
24	9/17/2020	21:15	9,717	Ebb
25	9/17/2020	16:14	9,503	Ebb*
26	9/17/2020	21:30	9,971	Ebb
27	9/17/2020	16:30	9,486	Ebb*
28	9/17/2020	21:45	9,930	Ebb
29	9/17/2020	16:45	9,501	Ebb*
30	9/17/2020	21:59	10,179	Ebb

*Collected after the high tide at 15:47 UTC as part of the flood tide measurements.

Table 1 (cont.). Dates, times, and measured discharge for each survey transect. Longitudinal survey lines do not result in a measured discharge and were excluded from this table.

ADCP Line Number	Date	Time (UTC)	Discharge (m^3/s)	Tidal Phase
1	3/19/2021	14:16	25,131	Flood
2	3/19/2021	18:31	24,518	Ebb
3	3/19/2021	14:29	24,597	Flood
4	3/19/2021	18:44	24,136	Ebb
5	3/19/2021	14:44	24,881	Flood
6	3/19/2021	18:57	24,951	Ebb
7	3/19/2021	14:59	24,631	Flood
8	3/19/2021	19:13	24,416	Ebb
9	3/19/2021	15:16	25,240	Flood
10	3/19/2021	19:32	24,793	Ebb
11	3/19/2021	15:30	24,801	Flood
12	3/19/2021	19:46	25,308	Ebb
13	3/19/2021	15:51	25,882	Flood
14	3/19/2021	19:59	24,316	Ebb
15	3/19/2021	16:04	25,612	Flood
16	3/19/2021	20:13	23,783	Ebb
17	3/19/2021	16:18	25,270	Flood
18	3/19/2021	20:26	25,238	Ebb
19	3/19/2021	16:32	24,749	Flood
20	3/19/2021	20:38	24,479	Ebb
21	3/19/2021	16:44	25,084	Flood
22	3/19/2021	20:57	23,233	Ebb
23	3/19/2021	16:54	25,077	Flood
24	3/19/2021	21:15	24,147	Ebb
25	3/19/2021	17:04	23,609	Flood
26	3/19/2021	21:29	24,567	Ebb
27	3/19/2021	17:14	24,471	Flood
28	3/19/2021	21:42	23,782	Ebb
29	3/19/2021	17:28	24,149	Flood
30	3/19/2021	21:58	24,684	Ebb

The September survey began at 12:34 UTC and concluded at 22:38 UTC. Personnel performing this survey were Mr. Charles Ellis and Mr. Michael Ramirez utilizing the Research Vessel (R/V) *Clara Jean*.

The March survey began at 13:35 UTC and concluded at 22:12 UTC. Personnel were Mr. Mike Kirklin and Mr. Tommy Kirklin aboard the R/V *Landing Craft*.

2.3 Data Collection

ADCP data were collected with a 600 kHz RD Instruments Workhorse Rio Grande mounted on a custom adjustable instrument arm deployed off the side of the survey vessels (Teledyne RD Instruments, Inc.; Poway, California 92064, https://www.teledynemarine.com/brands/rdi/). GPS data were collected using a Trimble differential system with dual antennas for accurate heading information (Trimble; Westminster, Colorado, https://www.trimble.com/en). Both data streams were incorporated using Teledyne RD Instruments, Inc., WinRiver II software. Instrument mounting angular offsets were calculated by surveying a straight line in both the upstream and downstream directions and subtracting the mean flow vectors from each other. Instrument mounting depth was measured directly at survey speed and used as input to the software.

2.4 Data Processing

ADCP data were post processed using RD Instruments WinRiver II software and Python scripts. WinRiver was used to confirm data quality and to output the data in ASCII format. The ASCII outputs were processed with python scripts to separate the data into header data and collected data in appropriate python data structures. The header data contained information such as instrument frequency and settings, and the ensemble data contained ping-by-ping information such as individual bin depths, overall river depth, calculated water velocity, and backscatter intensity.

The first step in data processing was to remove invalid data. Bins beyond the depth of the river and pings with missing returns show an overflow value of −32768 in the ASCII outputs and are easily filtered out. Then, ping-by-ping, bin-by-bin velocities were calculated as magnitude, direction, north component, east component, and vertical components. The north and east components were also rotated into river-oriented space to calculate streamwise and cross-stream components. Each of these variables were tied to individual *XYZ* points in space and UTC timestamps. Additionally, data were depth averaged by ensemble so that they could be displayed in 2D plan views.

3 Results

The full study results for the September and March surveys are reported in Appendix A and Appendix B, respectively. What is shown in this chapter is a selection of the survey results that best highlight the observed river characteristics.

3.1 Hydrodynamics

3.1.1 September 2020

Cross sections of streamwise velocity through the study area in September 2020 (Figure 2) show a classic river-bend flow pattern. At the upstream end of the study area, which exhibits the bar-and-thalweg morphology, water velocity increases with distance from the riverbed and therefore is greatest (exceeding 1 m/s) in surface waters over the thalweg along the left descending bank, where distance from the bed is greatest. Other, shallower parts of the river exhibit lower velocities, several tens of cubic meters per second. Moving through the study area into the bend section, the core of high velocity shifts towards the right descending bank, slightly lagging the bathymetry due to inertia of the downstream flow. Some very low (<10 cm/s) upstream-directed flow is observed near the inside bank in the tightest part of the bend (*dark blue-magenta* colors of cross sections *E* and *F* in Figure 3). This is a recirculation eddy caused by flow separation. Near the downstream end of the study area, the high-velocity core has fully shifted from the left side of the channel to the right side of the channel when looking downstream.

The vertical velocity components measured in September 2020 (Figure 4) were the smallest of the three components (less than a few cubic meters per second). The vertical velocity components exhibit slight deviations as the flow dips downward into the deep scour hole (*blue* colors in Figure 4) and rises coming out of the hole (*yellow* colors in Figure 4).

The characteristics seen in the individual velocity components can be observed in a plan view showing depth-averaged velocity vectors (Figure 5). The highest velocity flows largely follow the thalweg bathymetry, slightly lagging the bathymetry where the channel first begins to bend. The lowest velocities are observed along channel margins and in the flow-separation zone near the inside of the bend.

Figure 2. Streamwise water velocity measured in September 2020. Locations for the eight sequential survey lines are shown in *red* overlaid on the channel bathymetry. Cross sections are displayed from right descending bank (0.0 m distance) to left (approximately 700 m distance).

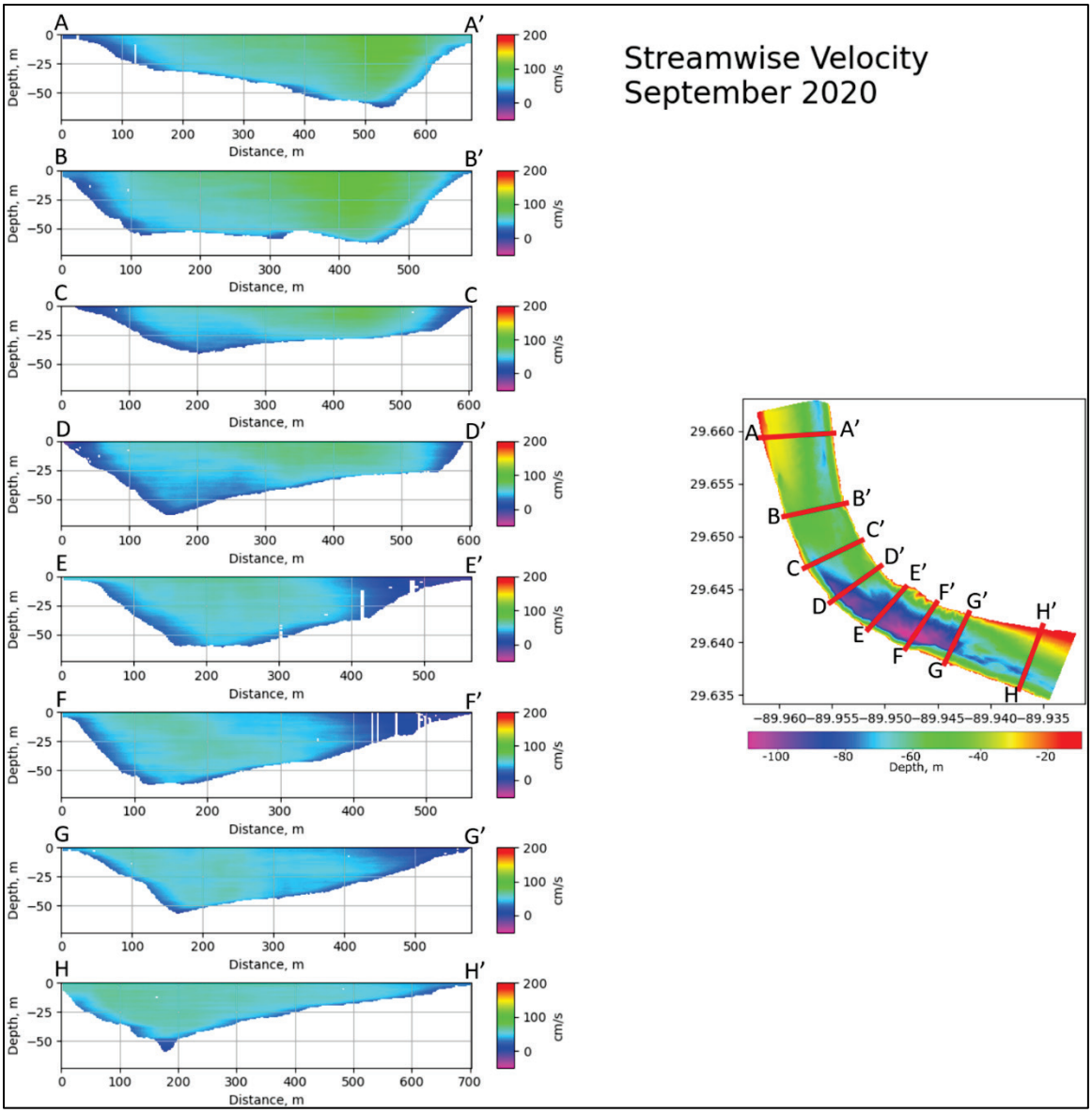

Figure 3. Cross-stream water velocity measured in September 2020. Locations for the eight sequential survey lines are shown in *red* overlaid on the channel bathymetry. The cross sections are shown from upstream at the top to downstream at the bottom. For the cross-stream component, positive values reflect flow directed towards the outside of the bend, and negative values reflect flow directed towards the inside of the bend.

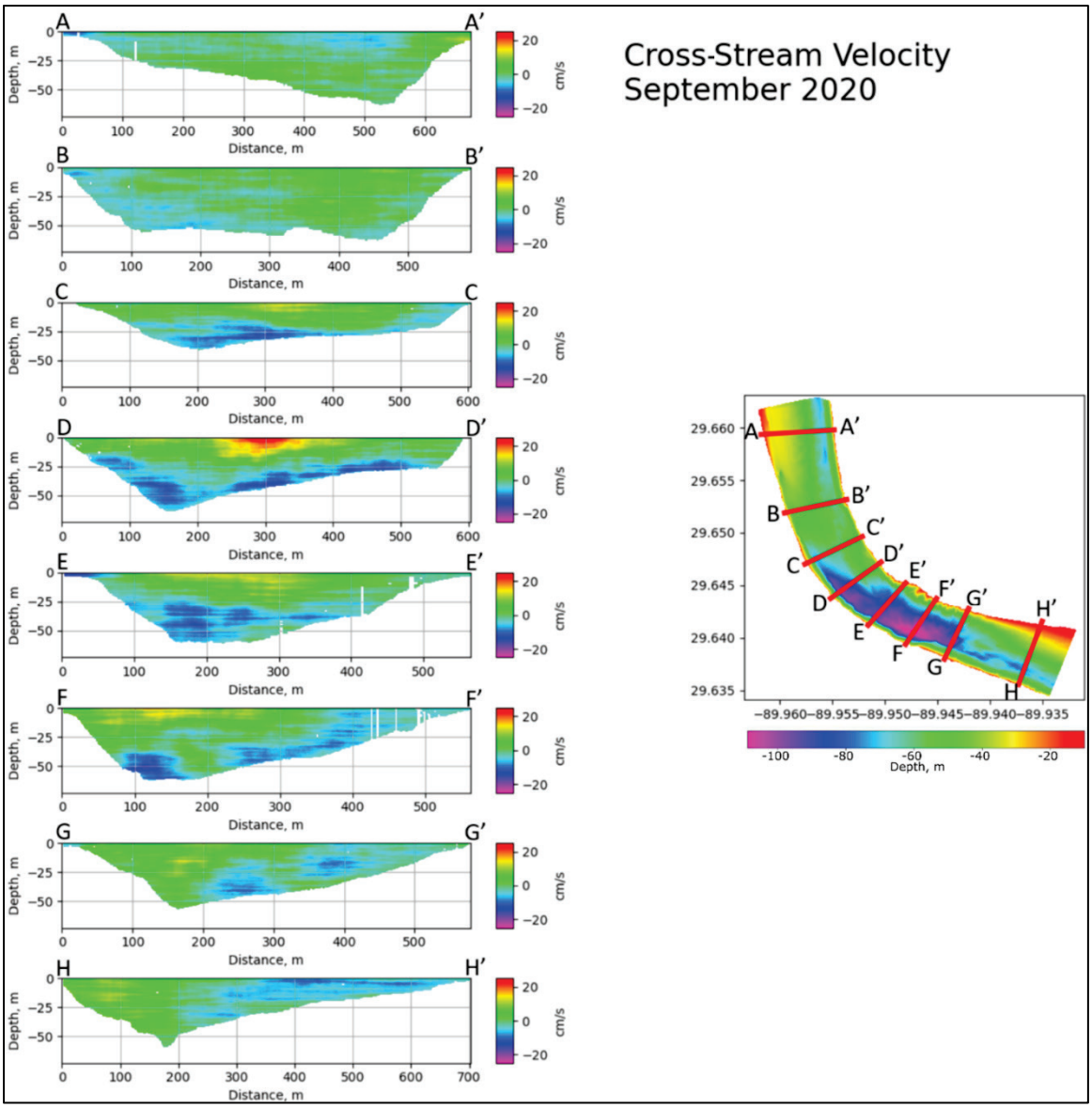

Figure 4. Vertical component water velocity measured in September 2020. Locations for the eight sequential survey lines are shown in *red* overlaid on the channel bathymetry. Positive values reflect flow directed upwards, and negative values reflect flow directed downwards.

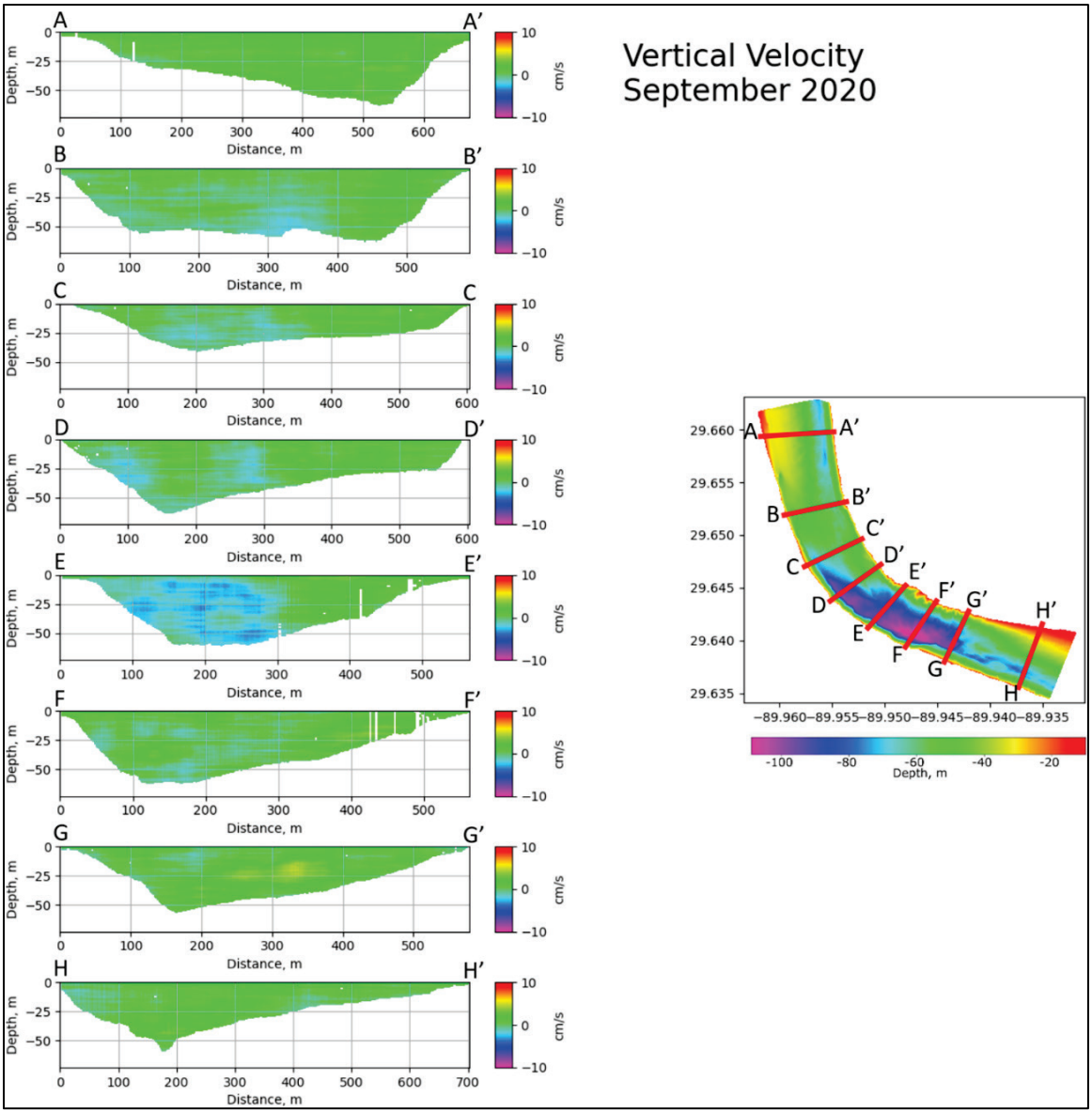

Figure 5. Depth-averaged flow vectors from September 2020. The reference vector in the northeast quadrant represents 1 m/s flow. The colors represent bathymetry, with *reds* and *yellows* in shallow areas and *blue* to *magenta* colors in the deepest areas.

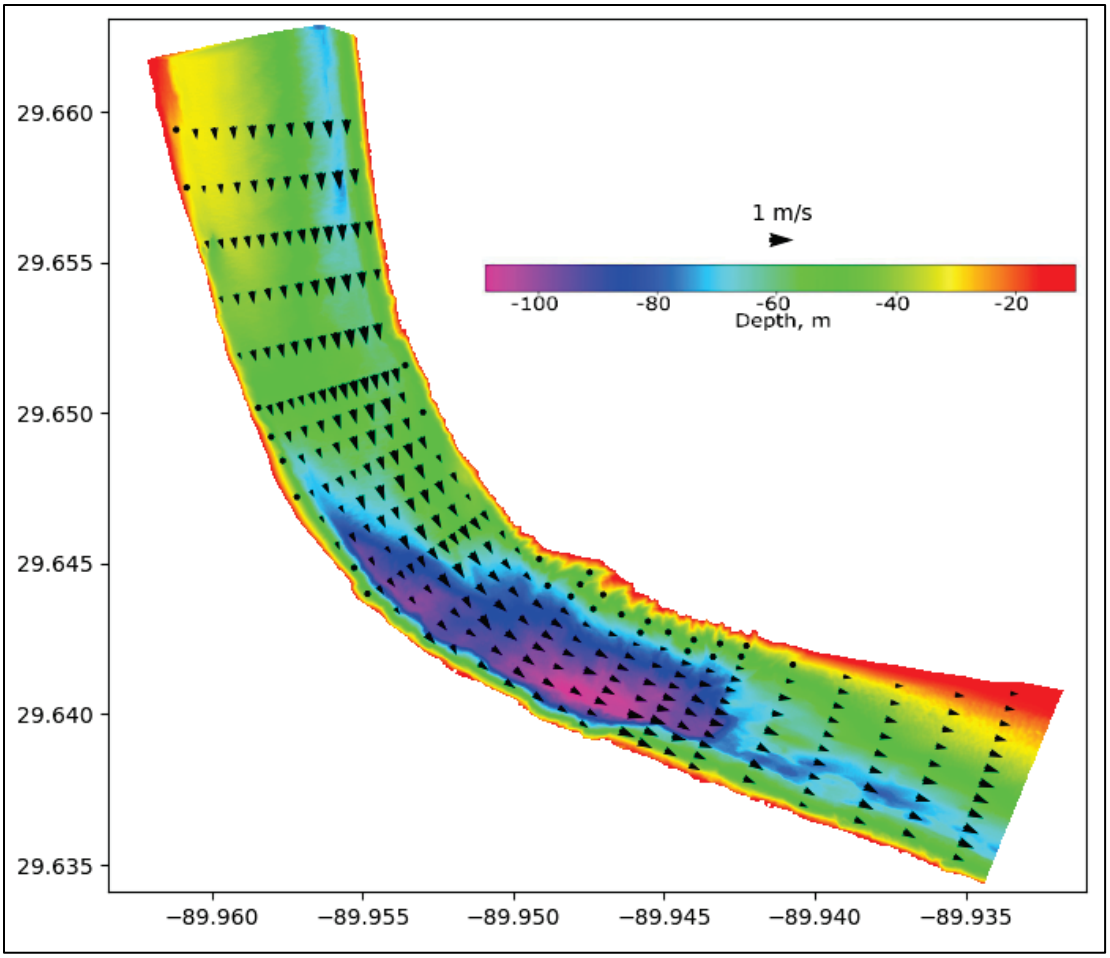

3.1.2 March 2021

The patterns of flow observed during the March 2021 study mimic those observed in September 2020, but they are amplified greatly in magnitude due to the much higher water discharge in March 2021 (Figure 6). The high-velocity flow over the thalweg exceeds 2 m/s and extends over a greater width of the channel (including the western half of the sand bar). Entering the bend, this high-velocity zone shifted towards the right descending bank until the thalweg is reestablished in the next straight bar-and-thalweg section of the river. Negative streamwise velocities (i.e., flow moving upstream) were observed in the innermost bend segment along the left descending bank.

Patterns of cross-stream velocity were also greatly amplified in the March 2021 study (Figure 7). Here the helical flow pattern was much more

coherent, with cross-stream component velocities exceeding 25 cm/s. These can be observed most clearly in the tightest bend segment where surface waters were moving towards the right descending bank and deeper waters were moving in toward the left descending bank as a result of the pressure differential (cross sections *E* and *F* in Figure 7). At the downstream end of the study area, the vertical stratification gave way to a lateral stratification with water in the thalweg moving towards the right descending bank and water over the sand bar moving towards the left descending bank. At the upper end of the study area, this pattern is reversed, likely due to lingering effects of the previous bend segment.

Patterns of vertical velocity in the March 2021 study period were much less coherent than observed in the low flow measurement, possibly a reflection of the greater turbulence at this higher water discharge (Figure 8). There is generally negative velocity (downward) entering the deep bend segment and positive velocity (upward) moving out of the deep scour hole, however the overall pattern is much more chaotic than the low flow measurement.

In a depth-averaged plan view (Figure 9), the difference between water velocity from September to March is very dramatic. The high-velocity zone (>2 m/s) can be seen shifting from the left descending bank to the right descending bank. Flow separates along the tightest bend segment, and upstream recirculating eddies are seen in the wake zone.

Figure 6. Streamwise water velocity measured in March 2021. Locations for the eight sequential survey lines are shown in *red* overlaid on the channel bathymetry.

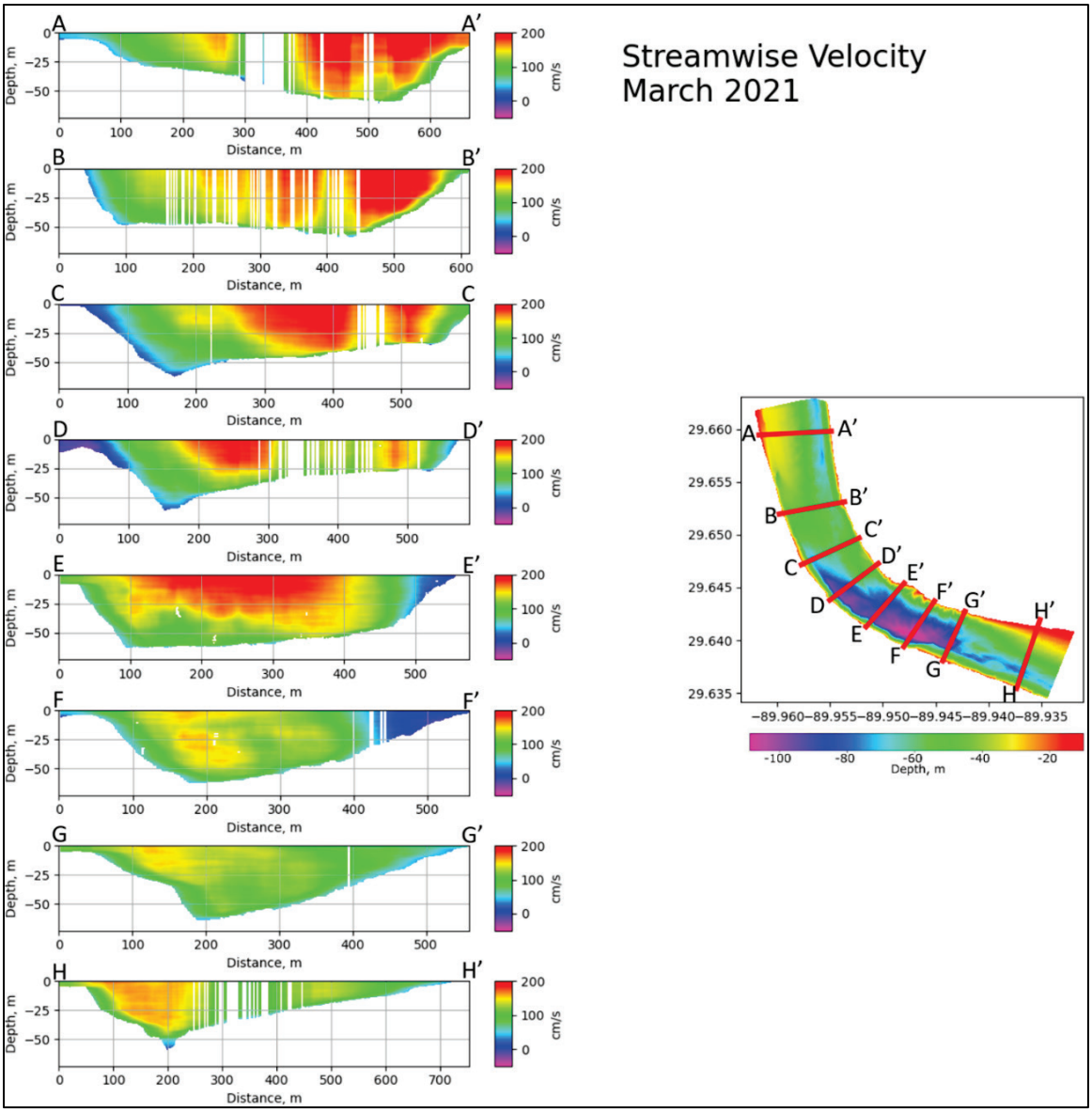

Figure 7. Cross-stream water velocity measured in March 2021. Locations for the eight sequential survey lines are shown in *red* overlaid on the channel bathymetry. For the cross-stream component, positive values reflect flow directed towards the outside of the bend, and negative values reflect flow directed towards the inside of the bend.

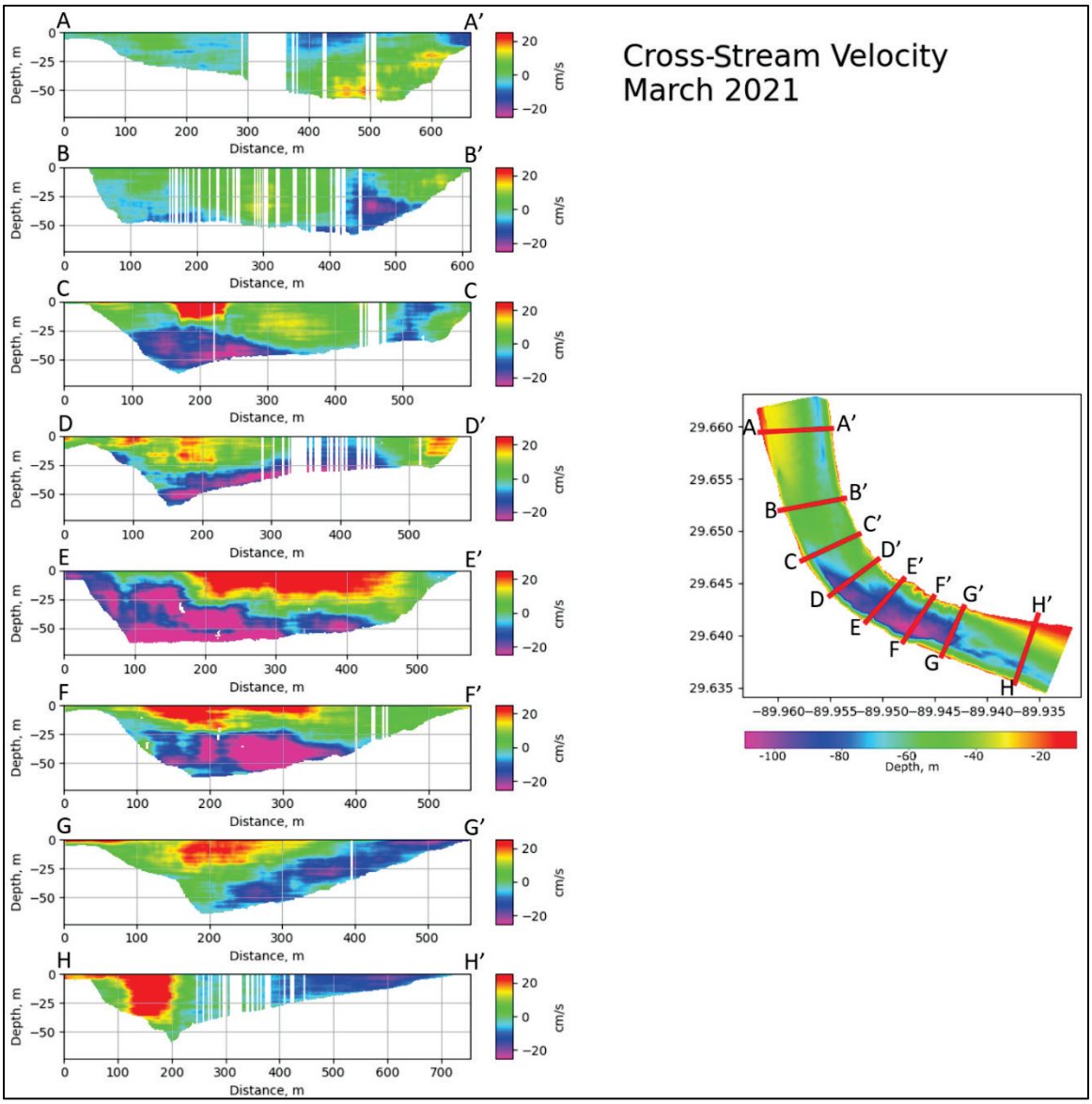

Figure 8. Vertical water velocity measured in March 2021. Locations for the eight sequential survey lines are shown in *red* overlaid on the channel bathymetry. Positive values reflect flow directed upwards, and negative values reflect flow directed downwards.

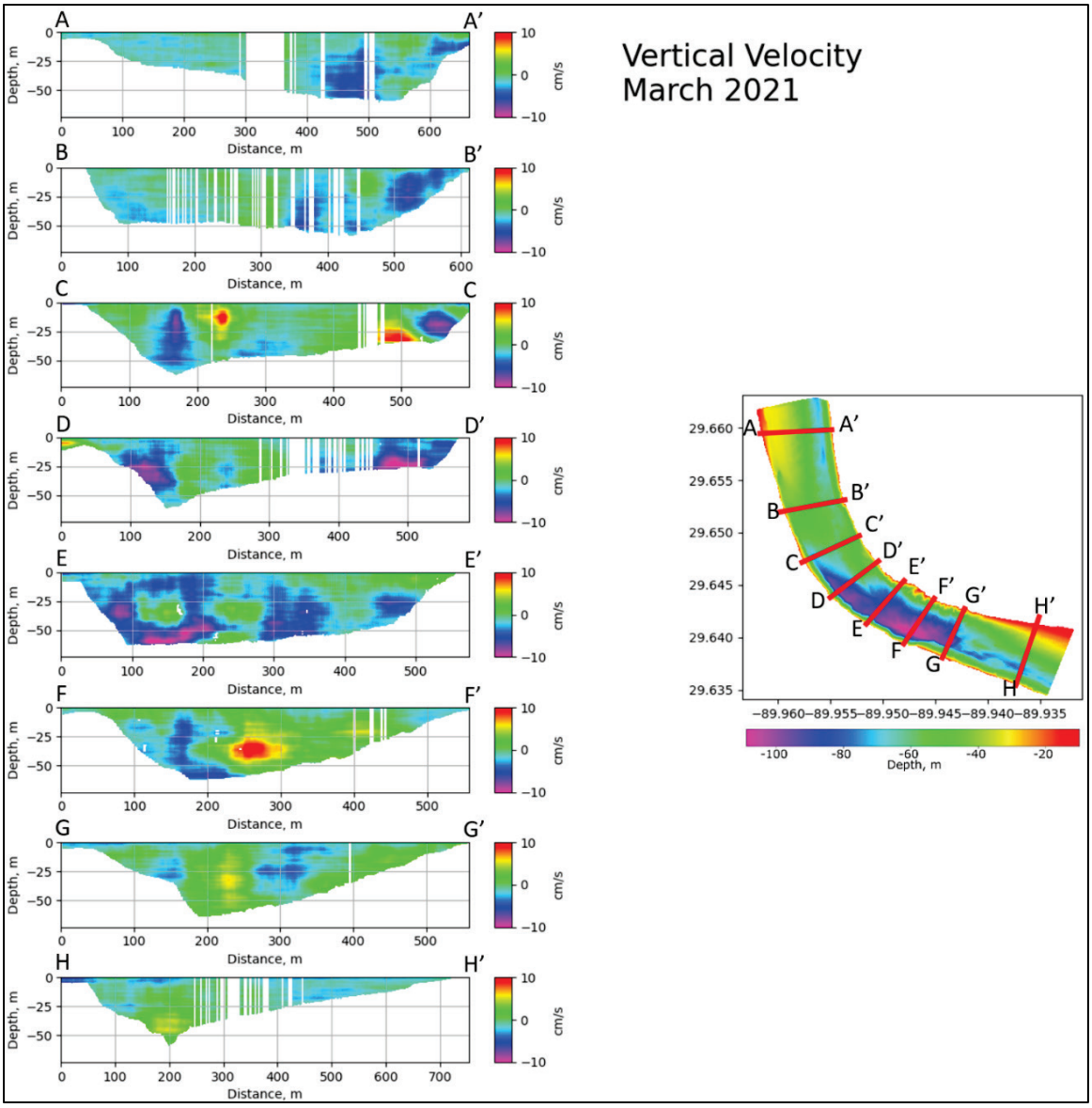

Figure 9. Depth-averaged flow vectors from March 2021. The reference vector in the northeast quadrant represents 1 m/s flow.

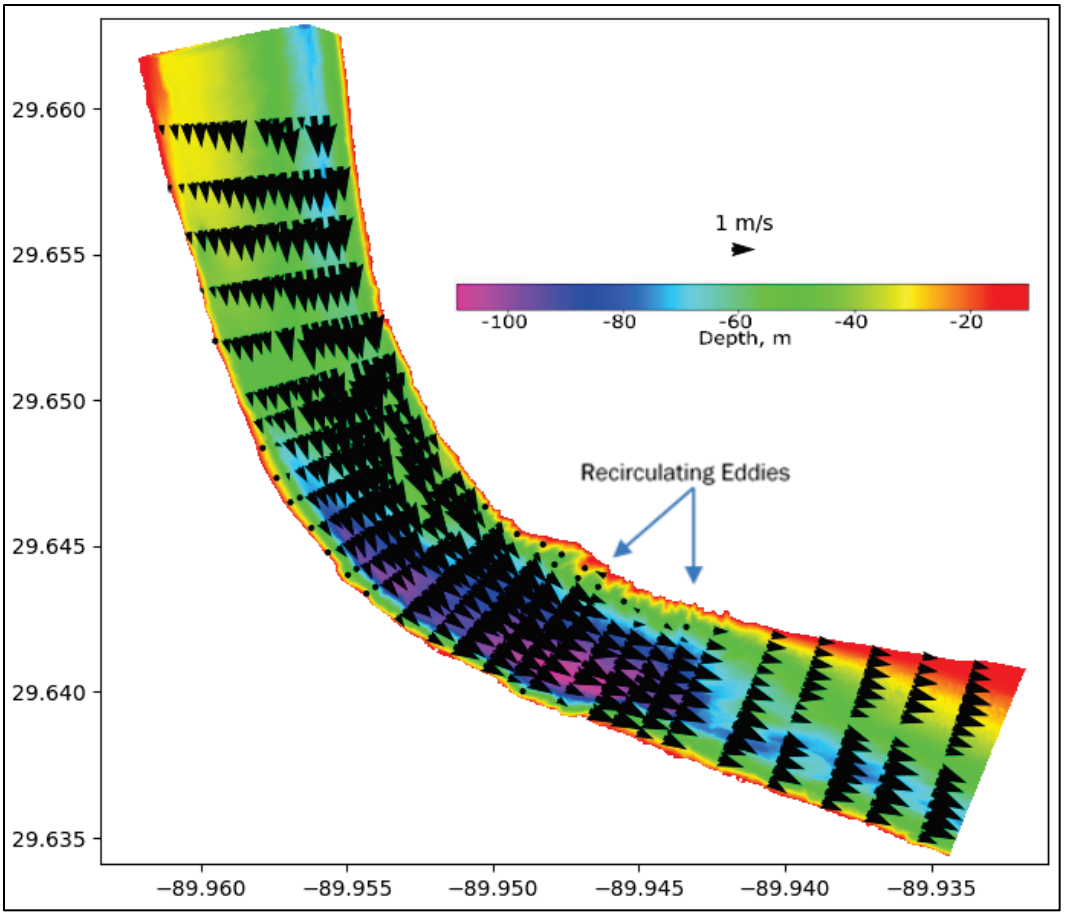

3.2 Sediment Transport

Suspended sediment transport in this reach of the river is a function of (1) the presence of wash load (i.e., sediment small enough that it has no significant contact with bed), (2) the presence of supercritical shear stress capable of resuspending bed sediment, and (3) the presence of sediment on the bed able to be resuspended. By examining the intensity of backscatter returns, it is possible to visualize relative differences in suspended sediment concentrations. At the low flow of September 2020, the critical shear stress appears to be exceeded only in deeper parts of the river while bed sediment is available only on the sand bar, resulting in the backscatter intensity patterns in Figure 10. Therefore, the zone of greatest suspended sediment concentration in the bend occurs at the interface between the thalweg and the bar (cross sections *E* through *H* in Figure 10, approximately 300–600 m from the right descending bank). In the tight

bend segment, this sediment is pushed towards the left descending bank due to the inward cross-stream vectors of the deeper water there.

Figure 10. Cross sections of acoustic backscatter observed in September 2020.

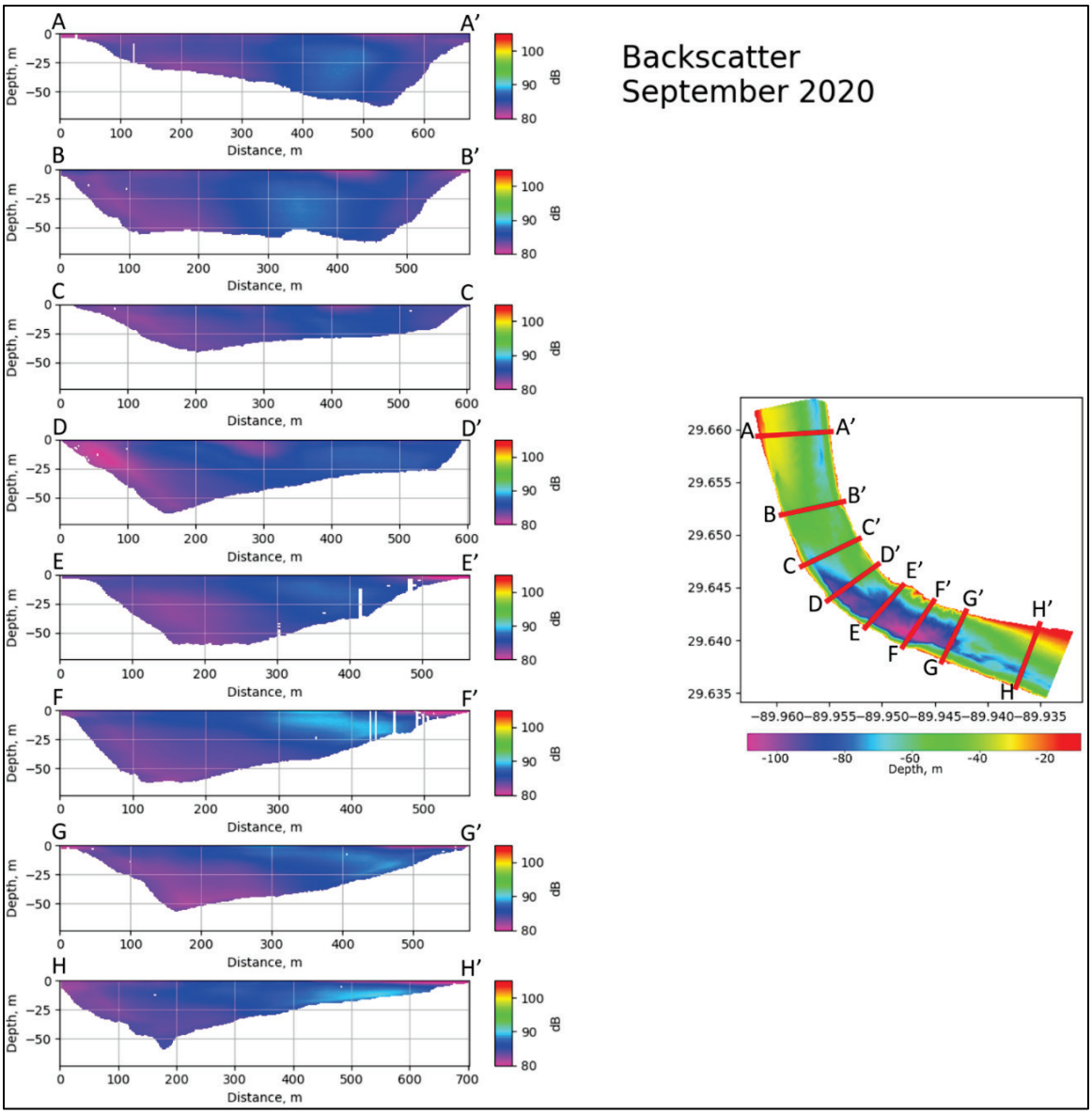

In March 2021, all of the backscatter intensities were higher, indicating greater sediment concentrations (Figure 11). The zone of critical shear stress appears to cover a wider area, as the high-velocity water is spread over more of the channel. These greater shears stresses are able to resuspend sand in shallower areas of the sand bar. Entering the segment with the deep bend, this suspended sediment is again pushed towards the left descending bank due to the higher magnitude of deep-water circulation in that direction.

It appears the helical recirculation is drawing sediment-lean surface water toward the bed as the surface water dives toward the bed along the right descending bankline (*left side* of the plots). This sediment-lean water then flows across the bottom of the river channel toward the left descending bankline as the downstream flow passes through the bend.

Figure 11. Cross sections of acoustic backscatter observed in March 2021.

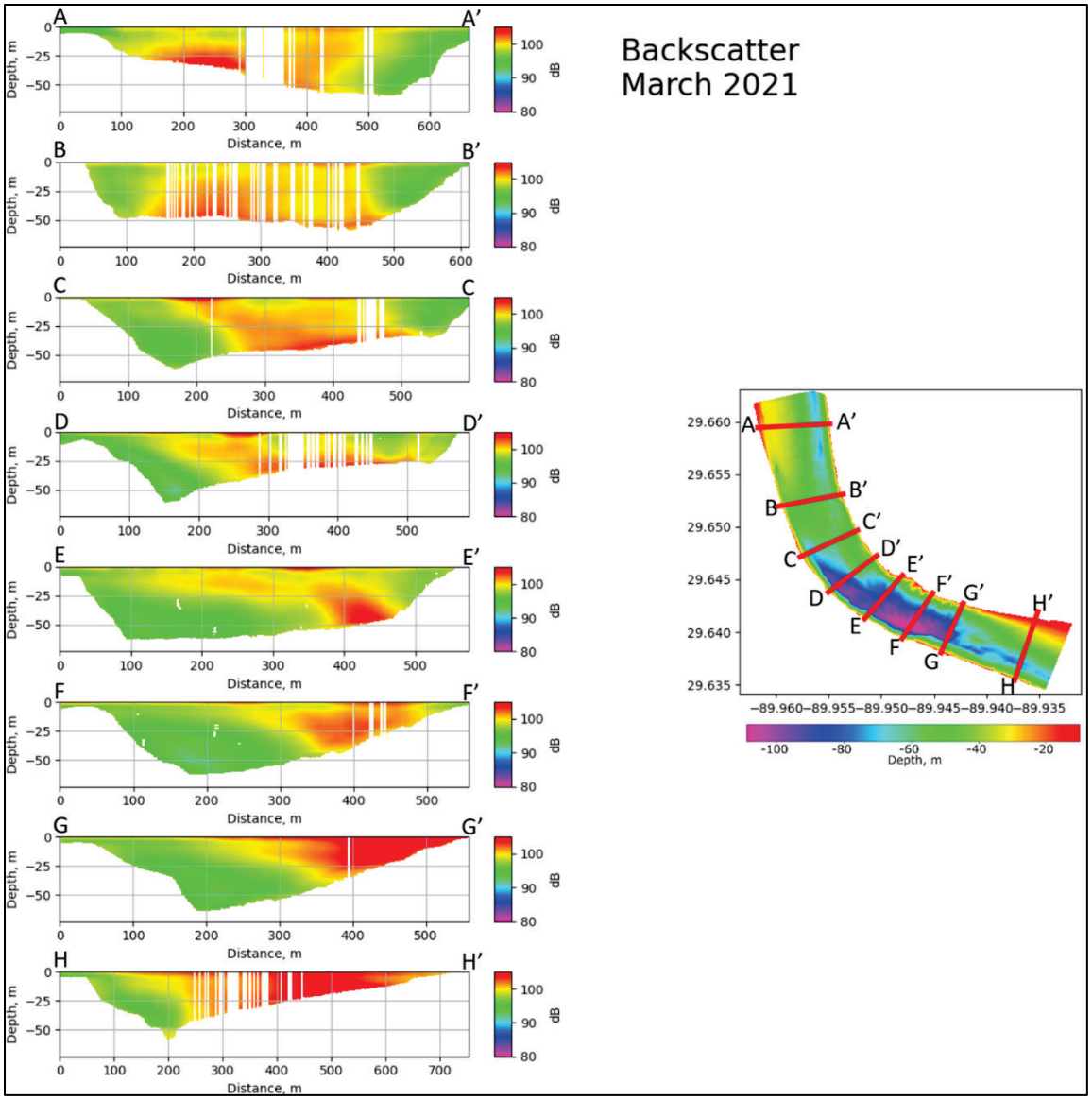

4 Discussion

4.1 Hydrodynamics

The hydrodynamics observed during this study were consistent with the study hypothesis (i.e., a 3D flow field is present in the deep scour hole that impacts sediment transport). The river bend (as a divergence in both planform and bathymetric morphology) induces a perturbation to the flow field in the surrounding river reach. The core of the downstream flow enters this reach following the thalweg along the left descending bank. As the flow proceeds through the bend, the angular momentum of the flow around the bend is balanced by a transverse water surface slope, resulting in a superelevation of the water surface on the outside of the bend. Since the surface water entering the bend flows faster than the near-bed water, it has more downstream momentum than the near-bed water. Hence, the surface flow overshoots the bend until it begins to interact with the right descending bank. Here, the flow decelerates, and the momentum of the surface water combines with the transverse pressure gradient to direct flow vectors downward. The water at the bottom of the channel flows inward due to conservation of mass. This stream-transverse pattern of outward surface flow and inward bottom flow (in this case, clockwise downstream), superimposed on the overall downstream flow field, leads to the classic helical hydrodynamics of the river bend.

The vortices set up by this perturbation persist downstream until they are dissipated as turbulent kinetic energy. The boundaries of this study did not extend far enough downstream to observe the full dissipation of these eddies, but the observation of counterclockwise circulation at the upstream end of the study area (likely leftover from the previous bend upstream) suggests they can persist for several river miles following a perturbation.

These patterns were observed during both the low-flow September 2020 study period and the high-flow March 2021 study period but were greatly amplified by the higher velocities observed at flood stage. Downstream, cross-stream, and vertical velocities during the low-flow study were on the order of 100 cm/s, 10 cm/s, and 2 cm/s, respectively. While all velocities were greater during the high-flow study, the ratio of downstream velocity (approximately 200 cm/s) to cross-stream velocity (approximately 20 cm/s) was similar to that of the low-flow study while the vertical component of the high-flow study (exceeding 10 cm/s in many places)

made up a far greater proportion of the overall flow. This suggests vertical turbulent eddies are a more important characteristic of the flow field at high discharge. These high-magnitude inward- and upward-directed flow vectors along the sand-covered point bar have important implications for sediment transport.

4.2 Acoustic Backscatter and Sediment Transport

Sediment transport through the study reach, as indicated by the backscatter intensity, is concentrated along the inside of the bend. Backscatter intensities at both high and low flows are greater over the point bar. It is not clear from this study whether this is an effect of, caused by, or a complex response of the sediment availability on the outside of the bend. Note that nearly all of the banks along the Lower Mississippi River, including the study area, have large amounts of revetment present. The revetment prevents the natural outward and downstream migration of meander bends, eliminating the outside banks as a sediment source and potentially increasing vertical velocities in the bend.

Dinehart and Burau (2005) found a similar concentration of backscatter intensity over the point bar in the much smaller Sacramento River (maximum depth approximately 15 m). Their results differed, however, by showing a narrow layer of high backscatter intensity adjacent to the bed across the entire channel width. This layer may have been caused by saltating particles or other bed material load. No equivalent layer of near-bed backscatter returns was observed at the much deeper (approximately 60 m deep) Mississippi River study site.

Based on the ADCP data, the pool at River Mile 60 on the Mississippi River is not filling in because the highest concentrations of transported material do not go through the bottom of the pool. There is also no evidence of material eroding based on the ADCP data. This may be due to the composition of the material at the bottom of the scour hole. Zumberge et al. (2022) found that there is a Pleistocene-Holocene boundary at 38 m deep near the River Mile 60 site. Stanley et al. (1996), summarizing existing boring data, found that the base of the Holocene deltaic sequence in this area is 31 m to 38 m deep. Nittrouer et al. (2011) found that the deep scour holes in the lowermost Mississippi River, including the one at River Mile 60, protrude into Pleistocene material as far downstream as 35 km above Head of Passes, but the crossings are typically well above this

horizon. Based on the age and depth of this Pleistocene material, it is reasonable to assume it is very resistant to erosion and is effectively arresting or slowing the rate of incision in the scour holes.

Based on these observations, a plausible hypothesis for the tendency for these scour holes to be deeper than those resulting from model simulations may be associated with the observed tendency for sediment-lean surface water to be entrained into the near-bed return currents flowing over the bed across the deep scour hole. The hypothesized mechanism for how this could result in scour holes deeper than those predicted by models is as follows:

- The sediment-lean surface water is drawn toward the bed when the surface water interacts with the right descending bankline.
- Sediment is then eroded from the scour hole in greater quantities that it would be under more typical conditions because the water is sediment lean and can therefore carry more sediment than would typically be entrained by the sediment-rich water.
- This process deepens the scour hole more than it would deepen under more typical circumstances (i.e., if the sediment profile in the flow were more typical, with the highest concentrations near the bed).

In this bend, the extent of the deepening is apparently controlled by the presence of relict material that is nonerodible. Hence, for these observations, no evidence is observed of re-entrainment of sediment into the sediment-lean water because the supply is limited by the nonerodible condition. That is, the scour hole is already established, so the erosion process is not seen in the observations.

Depth-averaged numerical models cannot simulate this exchange of sediment-lean surface water with the bed because they usually assume a sediment profile that is either uniform or a more typical, Rouse-type profile (i.e., sediment concentrations are greatest near the bed). One might assume that 3D models should be able to resolve this observed behavior, but most of the 3D models that are used in sediment transport modeling employ a hydrostatic assumption whereby the vertical velocity is assumed to have no acceleration component. The strong downward vertical velocities near the right descending bankline violates this assumption (i.e., the acceleration components are significant). Therefore, the vertical velocities that draw the surface water rapidly toward the bed may be

poorly represented in 3D hydrostatic models. Also, any excess numerical or applied diffusion in the models may mix the sediment-lean water with more sediment-rich water in the layers above the bed, limiting the tendency for the concentrations to be low near the bed.

4.3 Numerical Modeling Implications

Current sediment transport models tend to deposit more sediment in deep scour holes like the one in this study than observed in the field. That is, the scour-holes form in the models, but they are not as deep as the ones observed. Since the ADCP observations show 2D and 3D flows and suspended sediment distribution patterns, it is not surprising that 1D models (e.g., Hydrologic Engineering Center–River Analysis System [HEC-RAS]) do not fully capture these sediment dynamics. It is curious, however, that the multidimensional models also struggle with fully capturing the sediment dynamics.

As stated in the previous section, one possible source of this discrepancy is the inability of the models to properly resolve the entrainment of sediment-lean surface water into the near-bed region flowing across the scour hole. It is hypothesized this entrainment of sediment-lean water to the near bed increases the capacity for erosion of the bed sediment, thereby deepening the scour hole.

Depth-averaged models cannot resolve this phenomenon. They typically impose either a uniform sediment profile or a Rouse-type sediment profile (i.e., the highest concentrations are assumed to be near the bed) on the model solution. This contradicts the observed reduction in concentration, apparently associated with the entrained sediment-lean surface water.

Many of the 3D models typically used for sediment transport calculations invoke the hydrostatic assumption (i.e., vertical accelerations are assumed to be negligible). This includes both temporal and convective accelerations (i.e., change in direction). The large changes in vertical velocities associated with flow interacting with the bankline, like those shown in Figure 8, likely violate this assumption. Hence, 3D hydrostatic models may resolve these near-bank vertical velocities poorly.

Another potential source of error in the 3D models may be excessive vertical diffusion of the sediment. This would tend to reduce the difference

in concentration between the surface and bed for the regions where the sediment-lean surface water has moved into the near-bed region. This, in turn, would reduce the ability to erode sediment into this water.

Recent versions of HEC-RAS include the capability to designate individual, 1D cross sections as pass-through nodes, with no deposition (Gibson and Sánchez 2020). HEC-RAS has two types of pass-through nodes: a classic pass through where all sediment is moved through to the downstream cross section and a pool pass through. The pool pass-through method sets the transport capacity through the pool either to the next upstream cross section or the average of the upstream cross section from the current time-step and the downstream cross section in the previous step. These methods have not yet been extensively tested in models of the Lower Mississippi River.

Multidimensional models should more accurately simulate the movement of the water through the scour hole and, therefore, the sediment. Some models, such as Adaptive Hydraulics (AdH) (Coastal and Hydraulics Laboratory 2021), do have the ability to designate specific regions as scour-only regions (i.e., they do not allow deposition). However, this is not a physics-based solution to the problem; it merely imposes conditions specified by the user. The lessons learned from this study can be used to develop improved methods that rely on either process-based or physics-based solutions.

5 Conclusions and Recommendations

5.1 Conclusions

The ADCP results show there is a 3D flow field through the deep bend at River Mile 60 (Figure 2–Figure 4; Figure 6–Figure 8). The backscatter intensity shows the majority of the sediment remains close to the inside of the bend and high in the water column, with minimal concentrations at the bottom of the bend (Figure 10 and Figure 11). These findings have implications for numerical sediment transport models, which tend to deposit material at the bottom of deep scour holes like the one in this study.

5.2 Recommendations

Additional data collection efforts can improve the understanding of the complex hydraulic and sediment transport dynamics through deep scour holes and meander bends on large rivers. Future data collection efforts should couple ADCP measurements with suspended sediment sampling to verify the acoustic backscatter findings. Bathymetry data should be reviewed to determine whether there are bedforms present that could be transporting bed material.

Numerical models like HEC-RAS and AdH have functionality to allow users to specify areas to be nonerodible, but these features depend on the user's knowledge of the system and may not be appropriate for predicting the effects of system modifications. Existing hydraulic models should be modified, where practical, to incorporate this improved understanding of sediment transport in reaches with deep scour holes. This will require both conceptual and code development.

References

Brown, G. L., J. N. McAlpin, K. C. Pevey, P. V. Luong, C. R. Price, and B. A. Kleiss. 2019. *Mississippi River Hydrodynamic and Delta Management Study: Delta Management Modeling; AdH/SEDLIB Multi-Dimensional Model Validation and Scenario Analysis Report*. ERDC/CHL TR-19-2. Vicksburg, MS: US Army Engineer Research and Development Center, Coastal and Hydraulics Laboratory.

Coastal and Hydraulics Laboratory. 2021. *Adaptive Hydraulics Version 4.7 Sediment Transport User's Manual*. Vicksburg, MS: US Army Engineer Research and Development Center, Coastal and Hydraulics Laboratory.

Copeland, R. R., and L. Lombard. 2020. *Numerical Sedimentation Investigation, Mississippi River, Cairo to Pilots Station*. MRG&P Report No. 30. Vicksburg, MS: US Army Engineer Research and Development Center.

Czuba, Jonathan A., James L. Best, Kevin A. Oberg, Daniel R. Parsons, P. Ryan Jackson, Marcelo H. Garcia, and Peter Ashmore. 2011. "Bed Morphology, Flow Structure, and Sediment Transport at the Outlet of Lake Huron and in the Upper St. Clair River." *Journal of Great Lakes Research* 37 (3) :480–493. https://doi.org/10.1016/j.jglr.2011.05.011.

Dahl, T. A., S. A. Gibson, C. J. Nygaard, and R. E. Heath. 2018. *HEC-RAS Unsteady Flow and Sediment Model of the Mississippi River: Tarbert Landing to the Gulf*. MRG&P Report No. 25. Vicksburg, MS: US Army Engineer Research and Development Center.

Dinehart, R. L., and J. R. Burau. 2005. "Averaged Indicators of Secondary Flow in Repeated Acoustic Doppler Current Profiler Crossings of Bends." *Water Resources Research* 41(9). https://doi.org/10.1029/2005WR004050.

Gibson, S., A. Osorio, C. Creech, R. Amorim, M. Dircksen, T. Dahl, and M. Koohafkan. 2019. "Two Pool-to-Pool Spacing Periods on Large Sand-Bed Rivers: Mega-Pools on the Madeira and Mississippi." *Geomorphology* 328: 196–210.

Gibson, S., and A. Sánchez. 2020. *HEC-RAS Sediment Transport User's Manual Version 6.0*. Davis, CA: US Army Corps of Engineers Institute for Water Resources, Hydrologic Engineering Center.

Nittrouer, Jeffrey A., David Mohrig, Mead A. Allison, and Aymeric-Pierre B. Peyret. 2011. "The Lowermost Mississippi River: A Mixed Bedrock-Alluvial Channel." *Sedimentology* 58 (7): 1914–1934. https://doi.org/10.1111/j.1365-3091.2011.01245.x.

Stanley, Daniel Jean, Andrew G. Warne, and Joseph B. Dunbar. 1996. "Eastern Mississippi Delta: Late Wisconsin Unconformity, Overlying Transgressive Facies, Sea Level and Subsidence." *Engineering Geology* 45 (1): 359–381.

Zumberge, Mark A., Surui Xie, Frank K. Wyatt, Michael S. Steckler, Guandong Li, William Hatfield, Donald Elliott, Timothy H. Dixon, Jonathan G. Bridgeman, Elizabeth L. Chamberlain, Mead Allison, and Torbjörn E. Törnqvist. 2022. "Novel Integration of Geodetic and Geologic Methods for High-Resolution Monitoring of Subsidence in the Mississippi Delta." *Journal of Geophysical Research: Earth Surface* 127 (9): e2022JF006718. https://doi.org/10.1029/2022JF006718.

Appendix A: ADCP Plots from 17 September 2020

The following 30 figures display the ADCP data collected on 17 September 2020. Each transect has its own figure. The *right side* of the figure indicates the location of the transect and bathymetric data for the reach. The panels on the *left side* show, from top to bottom, streamwise velocity, cross-stream velocity, and acoustic backscatter intensity.

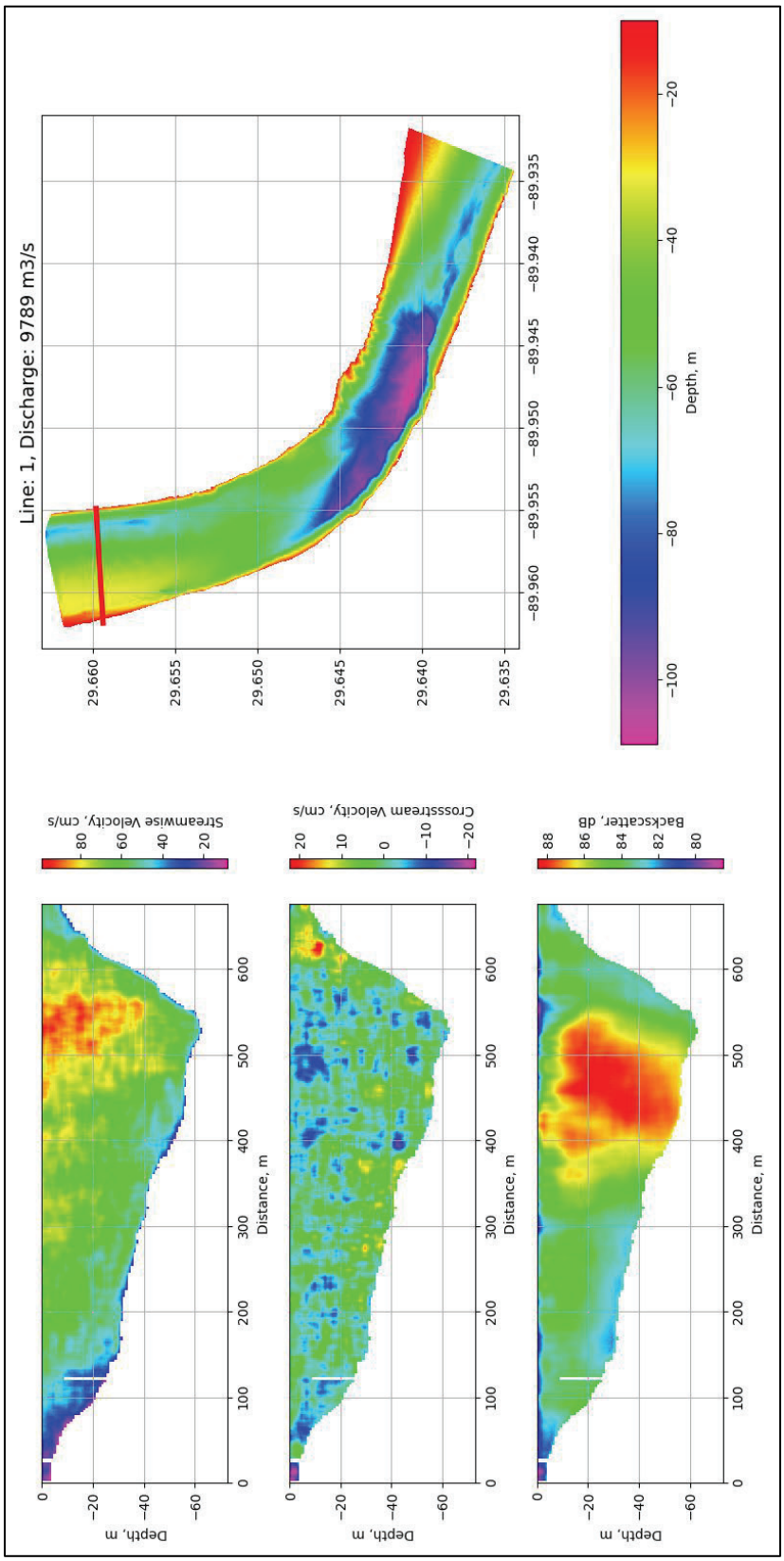
Line: 1, Discharge: 9789 m3/s
29.660
29.655
29.650
29.645
29.640
29.635
−89.960
−89.955
−89.950
−89.945
−89.940
−89.935
Depth, m
−20
−40
−60
−80
−100
Backscatter, dB
88
86
84
82
80
Crossstream Velocity, cm/s
20
10
0
−10
−20
Streamwise Velocity, cm/s
80
60
40
20
Depth, m
0
−20
−40
−60
Distance, m
0
100
200
300
400
500
600

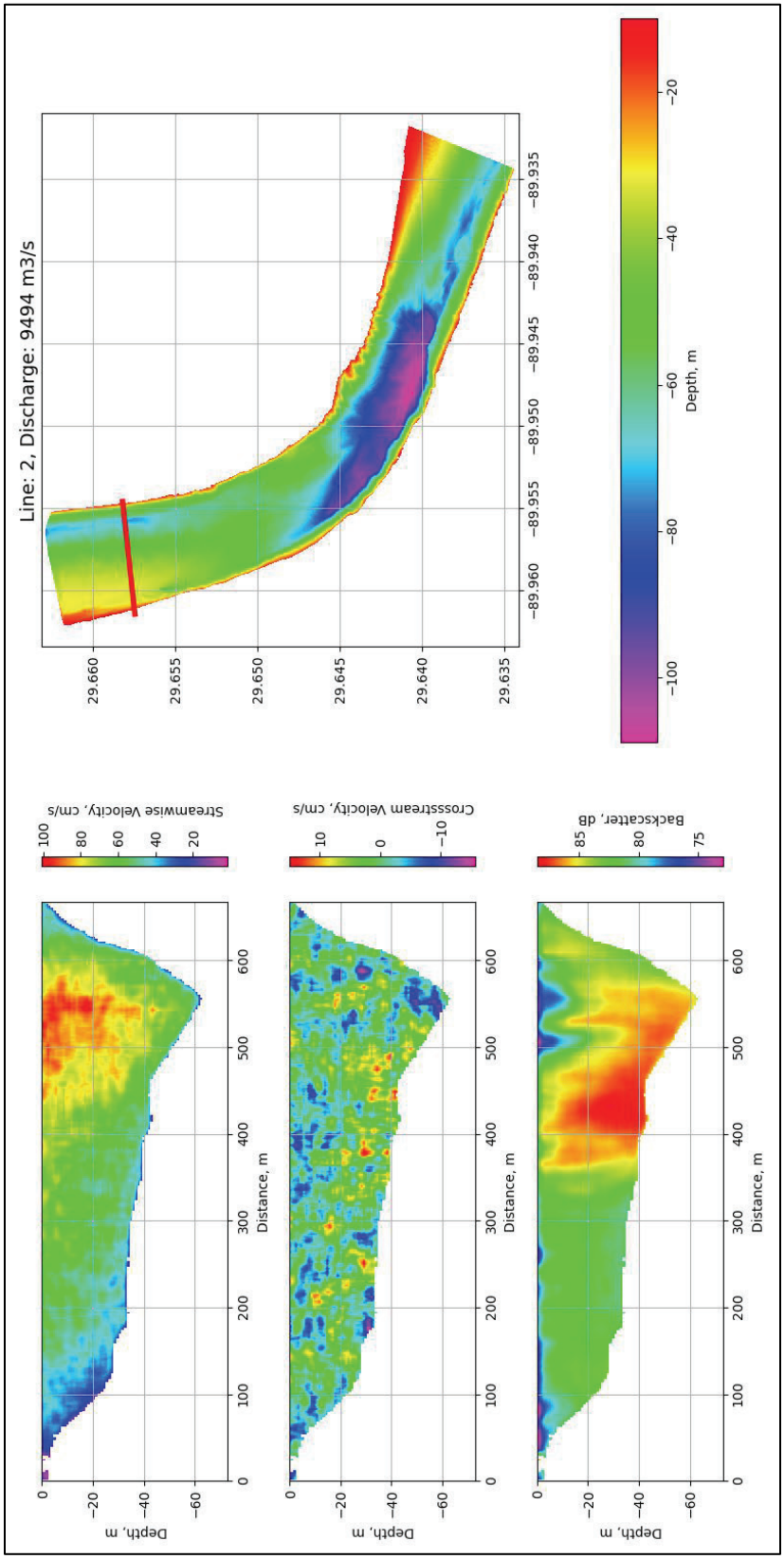
Line: 2, Discharge: 9494 m3/s
29.660
29.655
29.650
29.645
29.640
29.635
−89.960
−89.955
−89.950
−89.945
−89.940
−89.935
Depth, m
−20
−40
−60
−80
−100
Backscatter, dB
85
80
75
Crossstream Velocity, cm/s
10
0
−10
Streamwise Velocity, cm/s
100
80
60
40
20
Depth, m
Distance, m
0
100
200
300
400
500
600
−20
−40
−60

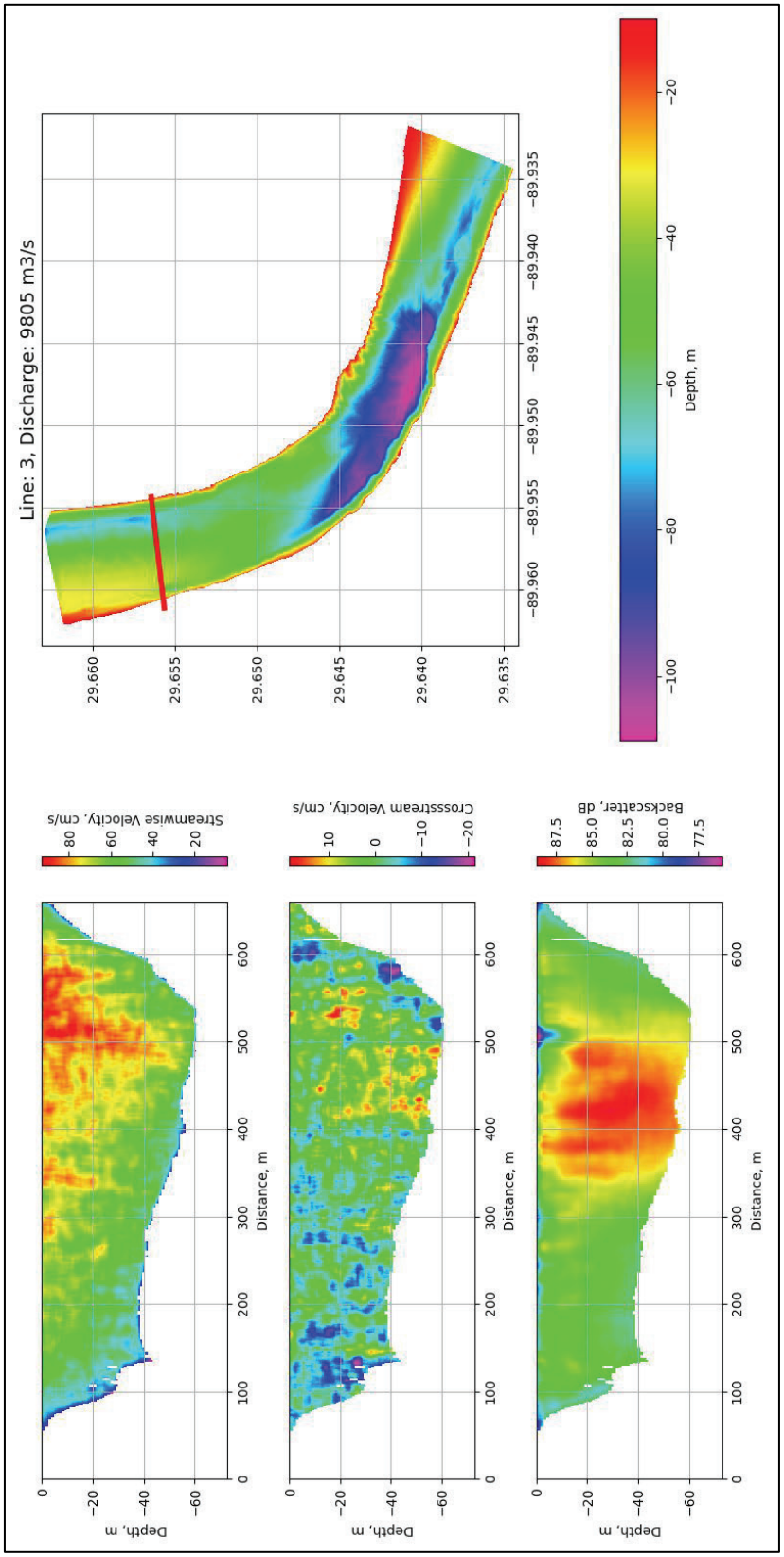
Line: 3, Discharge: 9805 m3/s
29.660
29.655
29.650
29.645
29.640
29.635
−89.960
−89.955
−89.950
−89.945
−89.940
−89.935
Depth, m
−20
−40
−60
−80
−100
Backscatter, dB
87.5
85.0
82.5
80.0
77.5
Crossstream Velocity, cm/s
10
0
−10
−20
Streamwise Velocity, cm/s
80
60
40
20
Depth, m
Distance, m
0
100
200
300
400
500
600
−20
−40
−60

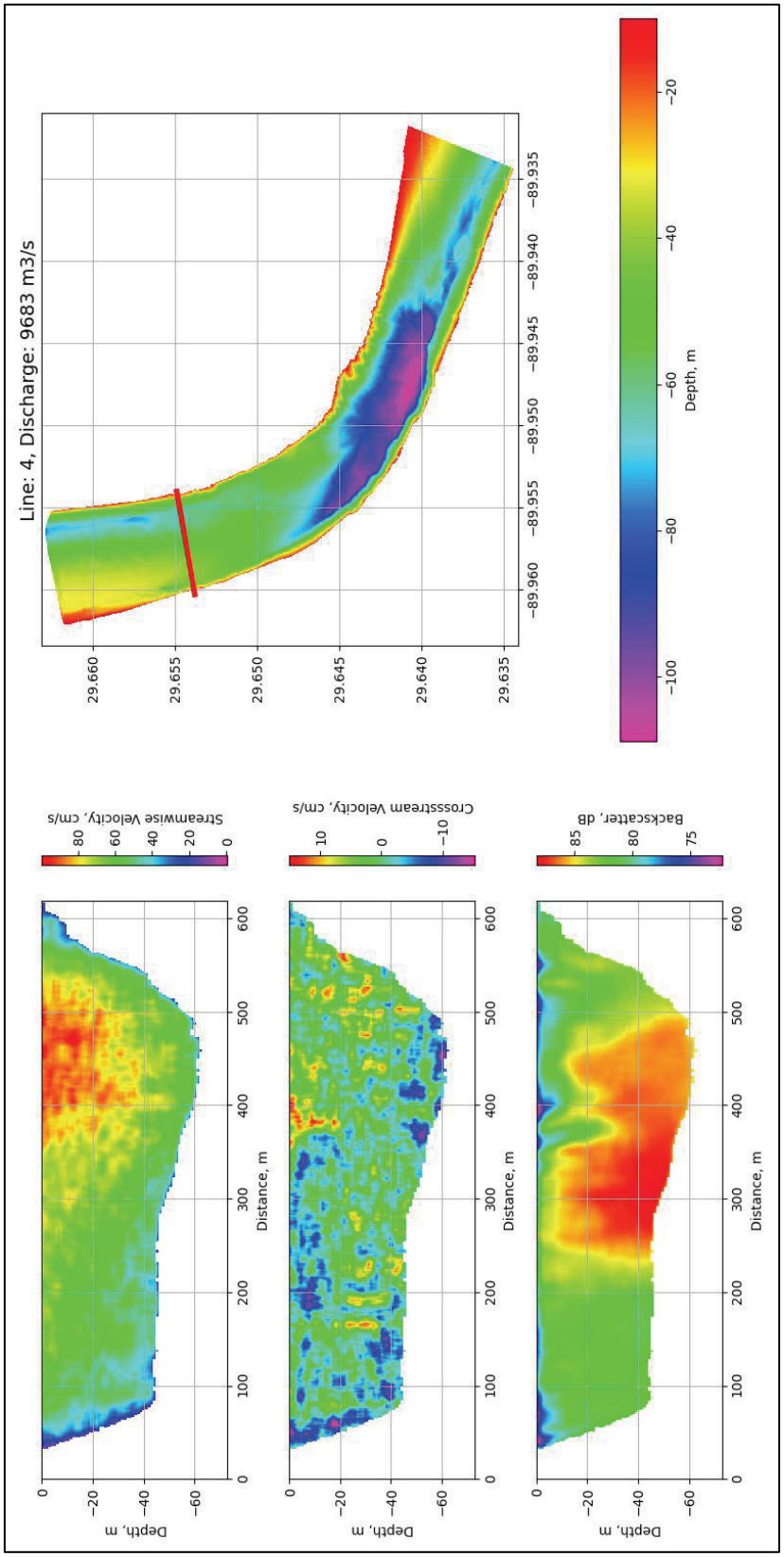
Line: 4, Discharge: 9683 m3/s
29.660
29.655
29.650
29.645
29.640
29.635
−89.960
−89.955
−89.950
−89.945
−89.940
−89.935
Depth, m
−20
−40
−60
−80
−100
Backscatter, dB
85
80
75
Crossstream Velocity, cm/s
10
0
−10
Streamwise Velocity, cm/s
80
60
40
20
0
Depth, m
Distance, m
0
100
200
300
400
500
600
−20
−40
−60

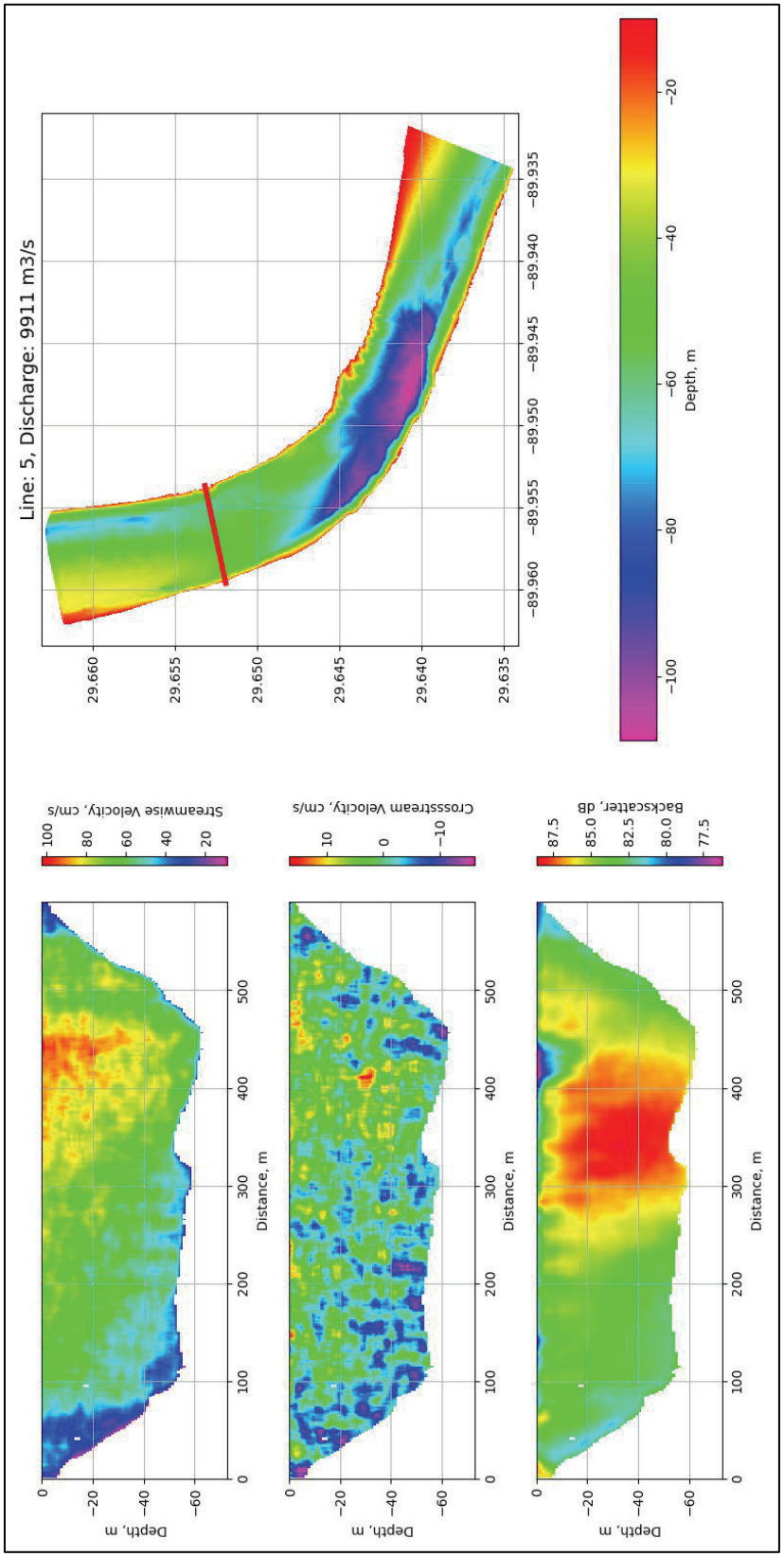
Line: 5, Discharge: 9911 m3/s
Depth, m
Distance, m
Streamwise Velocity, cm/s
Crossstream Velocity, cm/s
Backscatter, dB

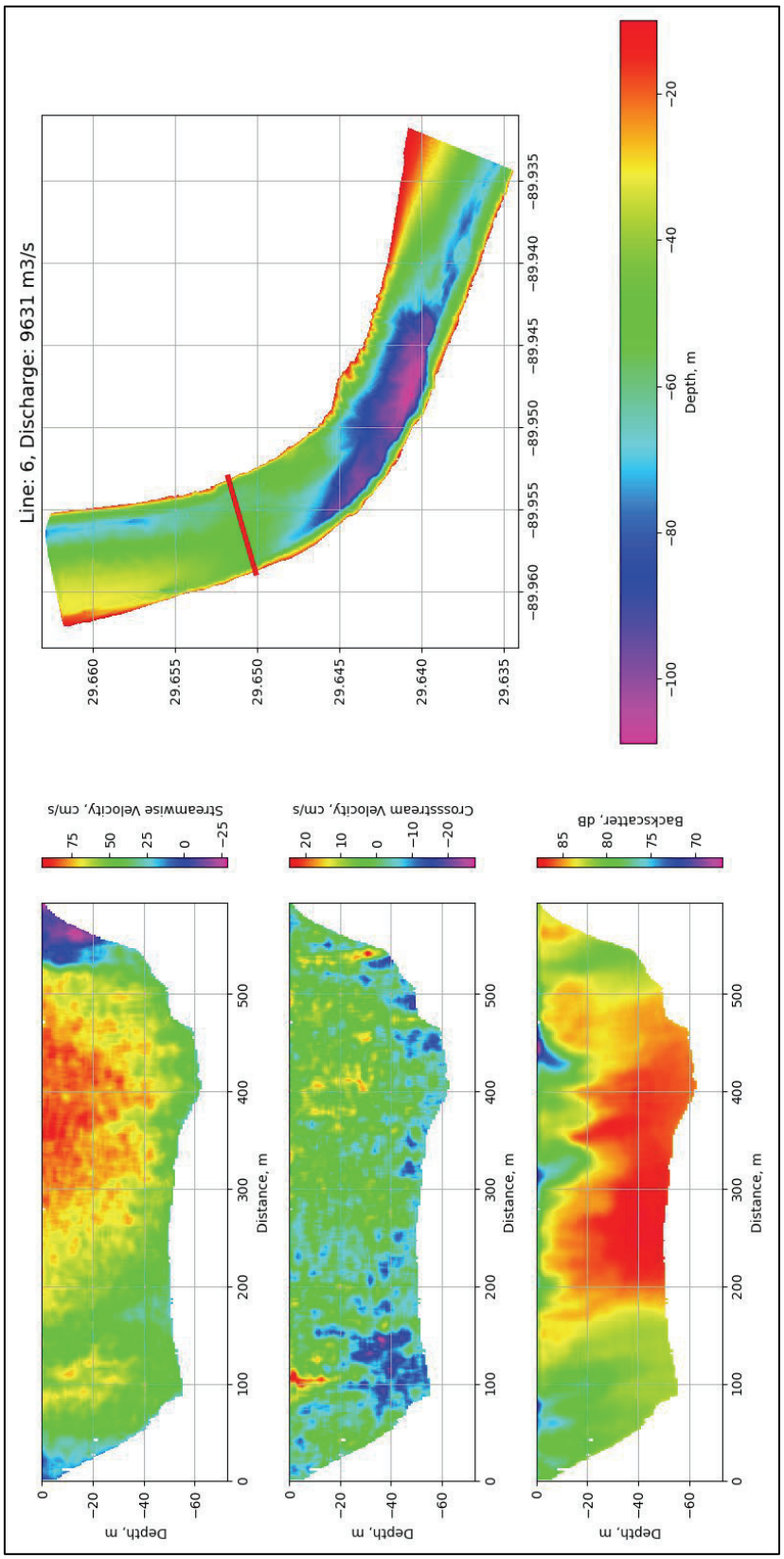
Line: 6, Discharge: 9631 m3/s
29.660
29.655
29.650
29.645
29.640
29.635
−89.960
−89.955
−89.950
−89.945
−89.940
−89.935
Depth, m
−20
−40
−60
−80
−100
Backscatter, dB
85
80
75
70
Crossstream Velocity, cm/s
20
10
0
−10
−20
Streamwise Velocity, cm/s
75
50
25
0
−25
Depth, m
Distance, m
0
100
200
300
400
500
−20
−40
−60

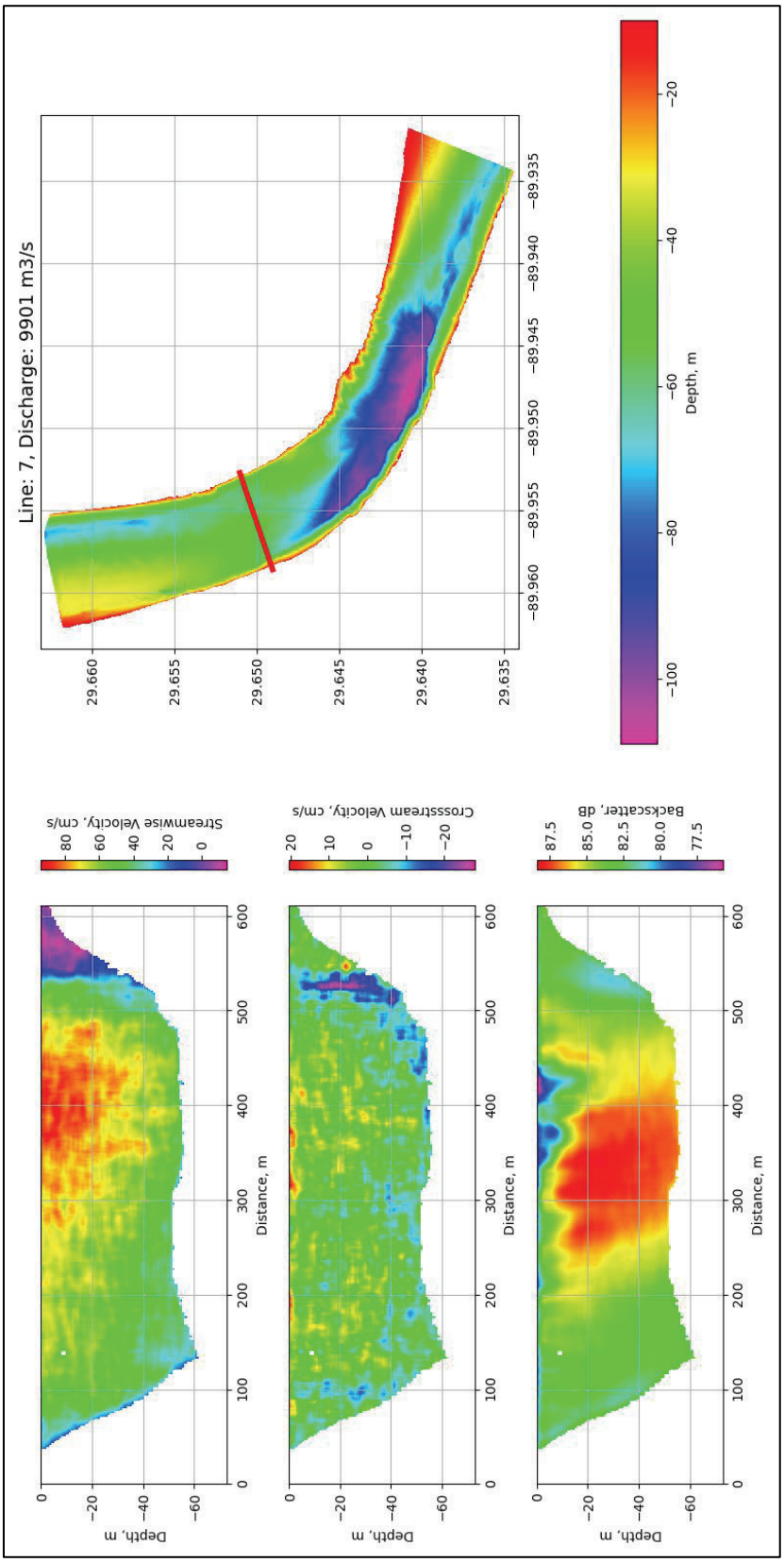
Line: 7, Discharge: 9901 m3/s
29.660
29.655
29.650
29.645
29.640
29.635
−89.960
−89.955
−89.950
−89.945
−89.940
−89.935
Depth, m
−100
−80
−60
−40
−20
Backscatter, dB
87.5
85.0
82.5
80.0
77.5
Crossstream Velocity, cm/s
20
10
0
−10
−20
Streamwise Velocity, cm/s
80
60
40
20
0
Depth, m
0
−20
−40
−60
Distance, m
0
100
200
300
400
500
600

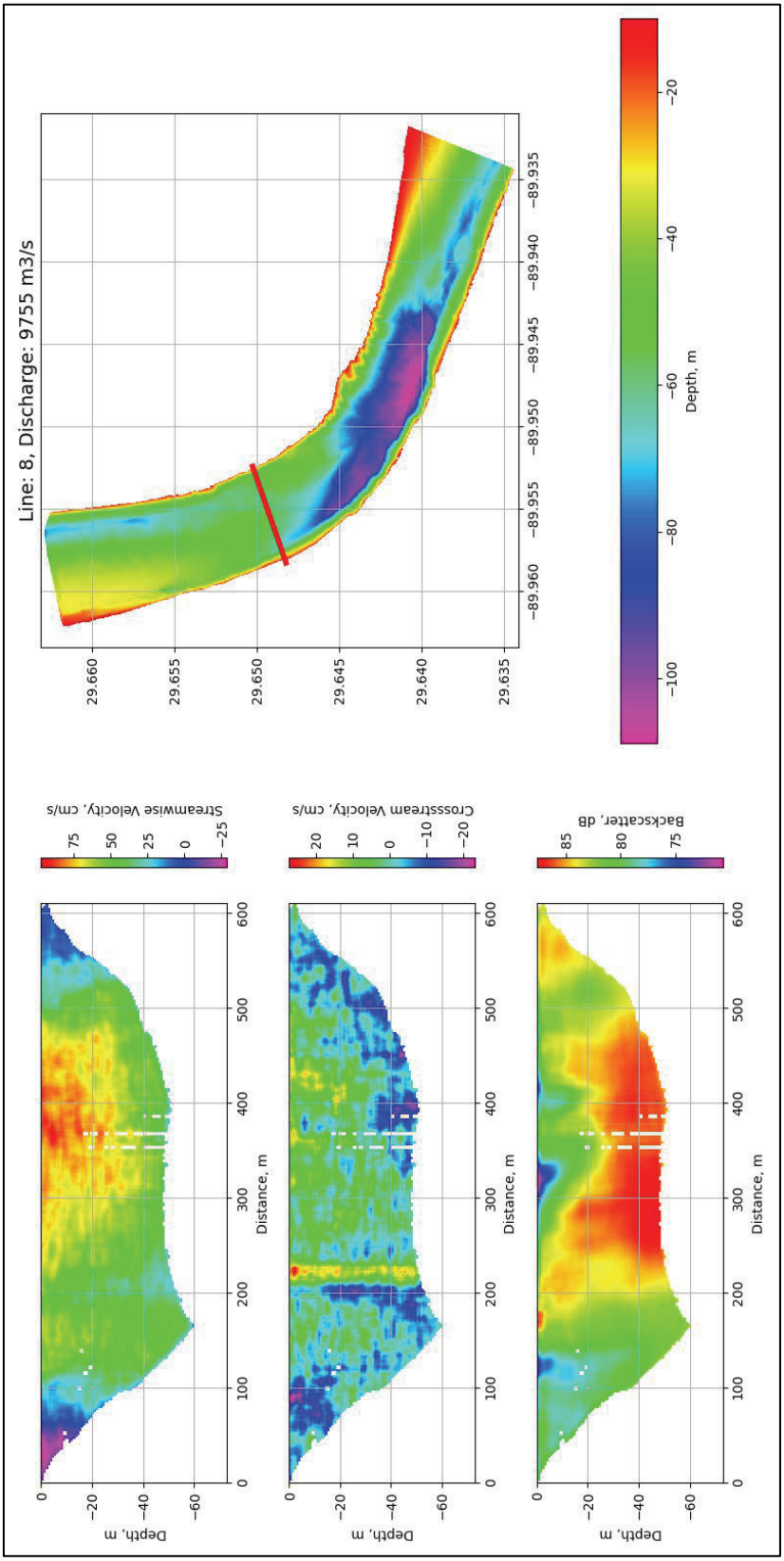
Line: 8, Discharge: 9755 m3/s
29.660
29.655
29.650
29.645
29.640
29.635
−89.960
−89.955
−89.950
−89.945
−89.940
−89.935
Depth, m
−20
−40
−60
−80
−100
Backscatter, dB
85
80
75
Crossstream Velocity, cm/s
20
10
0
−10
−20
Streamwise Velocity, cm/s
75
50
25
0
−25
Depth, m
Distance, m
0
100
200
300
400
500
600
−20
−40
−60

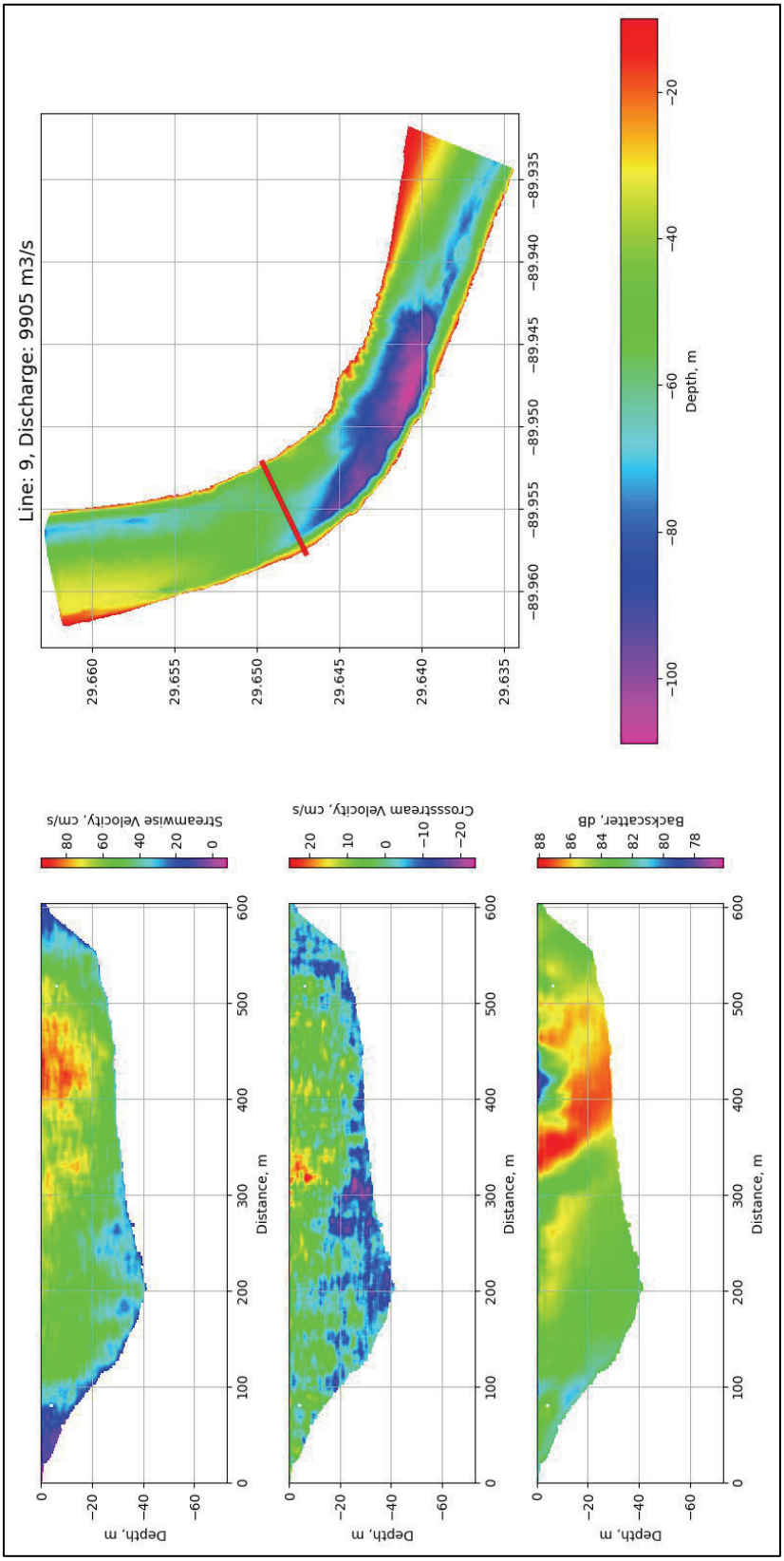
Line: 9, Discharge: 9905 m3/s
Depth, m
Distance, m
Backscatter, dB
Crossstream Velocity, cm/s
Streamwise Velocity, cm/s

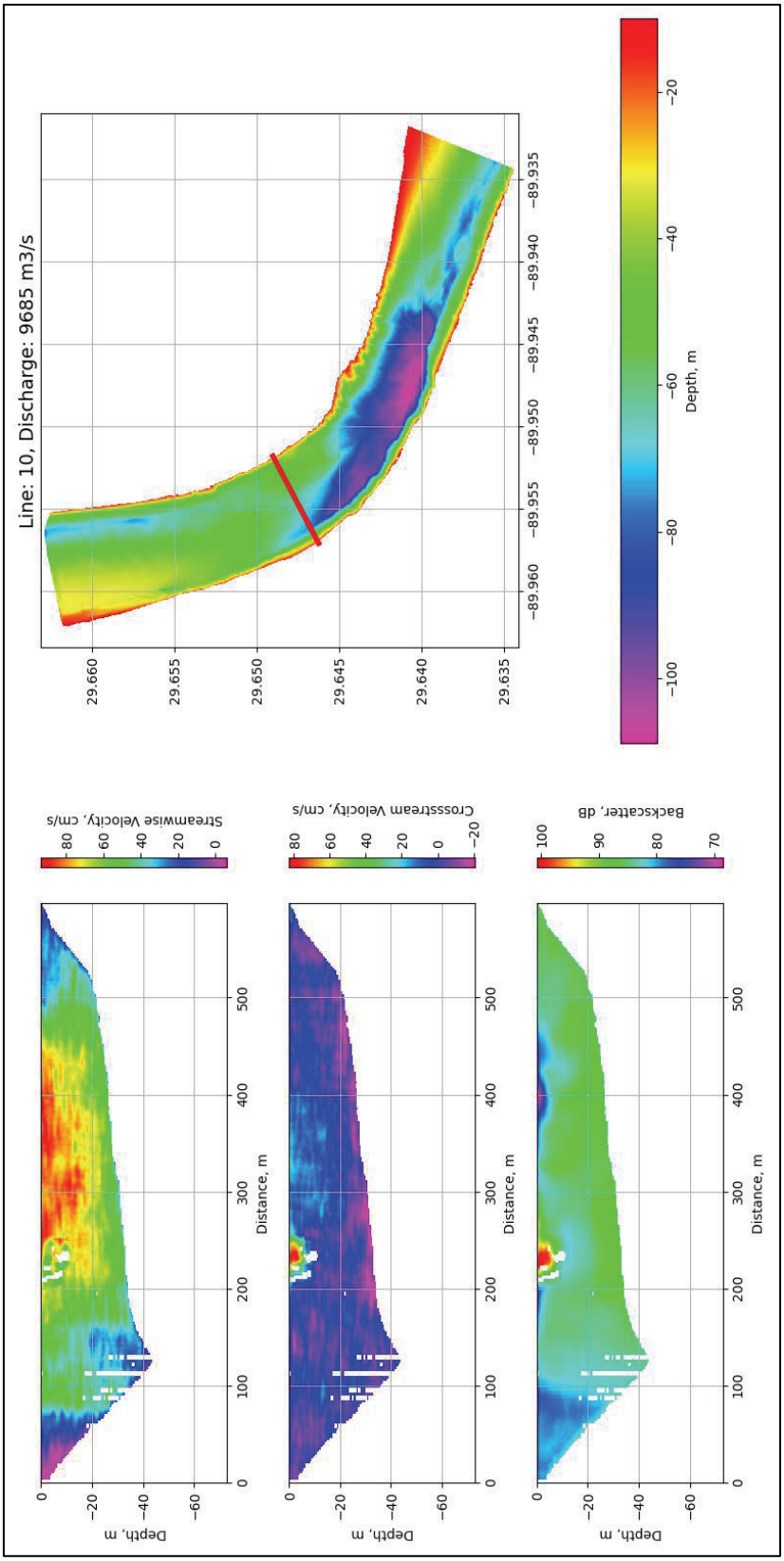
Line: 10, Discharge: 9685 m3/s
Depth, m
Backscatter, dB
Crossstream Velocity, cm/s
Streamwise Velocity, cm/s
Distance, m

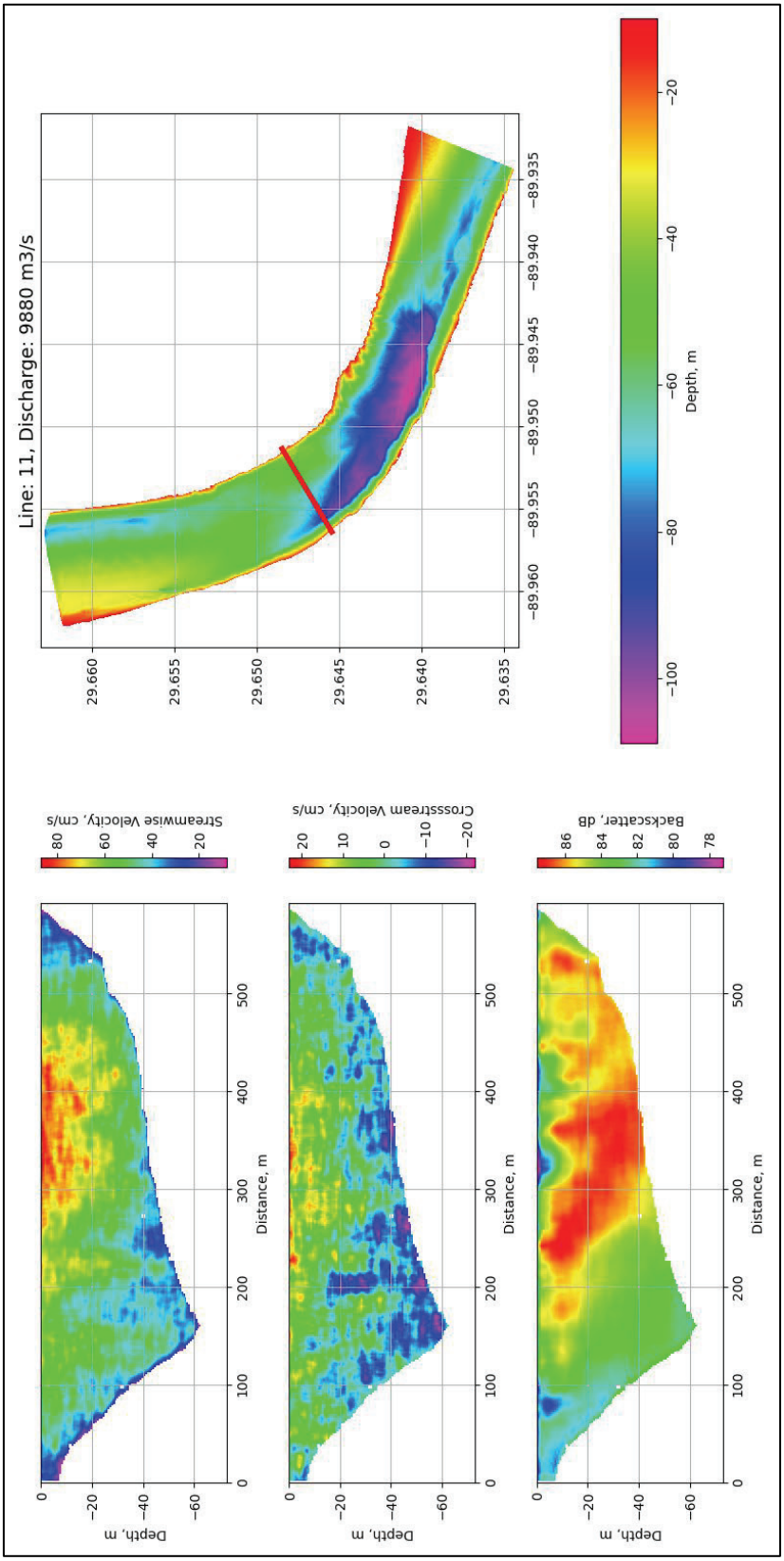
Line: 11, Discharge: 9880 m3/s
29.660
29.655
29.650
29.645
29.640
29.635
−89.960
−89.955
−89.950
−89.945
−89.940
−89.935
Depth, m
−20
−40
−60
−80
−100
Backscatter, dB
86
84
82
80
78
Crossstream Velocity, cm/s
20
10
0
−10
−20
Streamwise Velocity, cm/s
80
60
40
20
Depth, m
0
−20
−40
−60
Distance, m
0
100
200
300
400
500

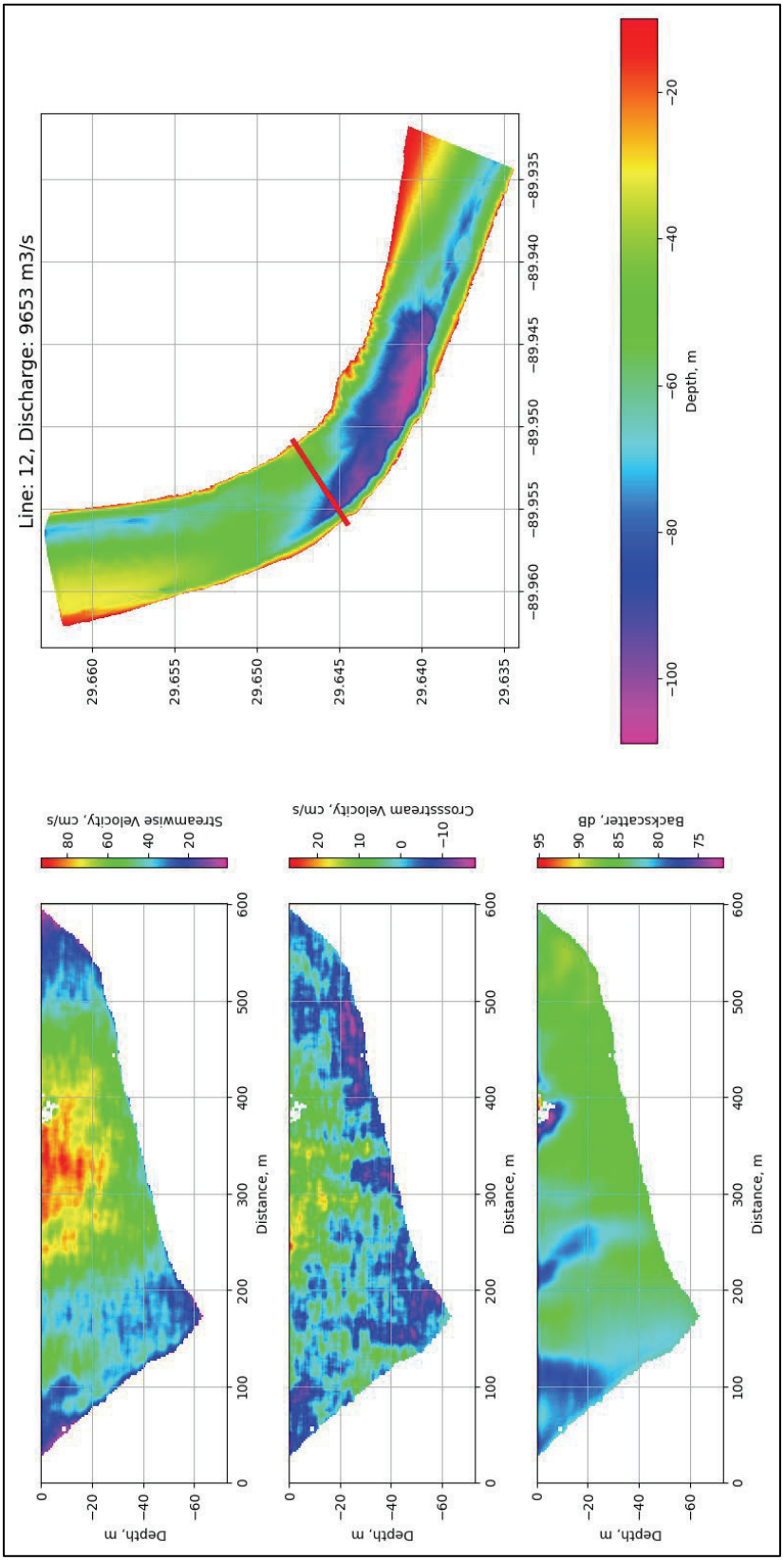
Line: 12, Discharge: 9653 m3/s
Depth, m
Distance, m
Backscatter, dB
Crossstream Velocity, cm/s
Streamwise Velocity, cm/s

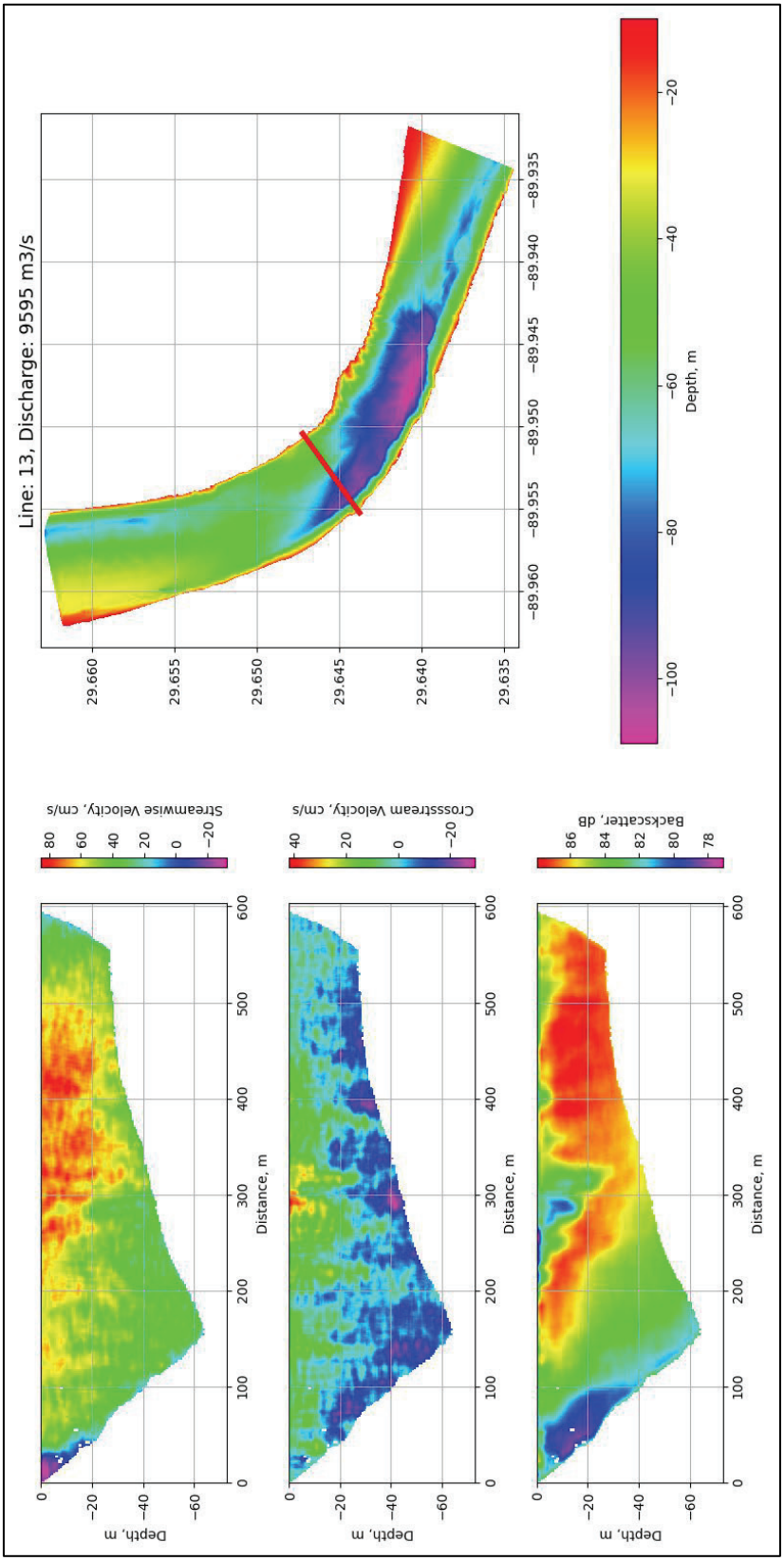
Line: 13, Discharge: 9595 m3/s
29.660
29.655
29.650
29.645
29.640
29.635
−89.960
−89.955
−89.950
−89.945
−89.940
−89.935
Depth, m
−20
−40
−60
−80
−100
Backscatter, dB
86
84
82
80
78
Crossstream Velocity, cm/s
40
20
0
−20
Streamwise Velocity, cm/s
80
60
40
20
0
−20
Depth, m
Distance, m
0
100
200
300
400
500
600
−20
−40
−60

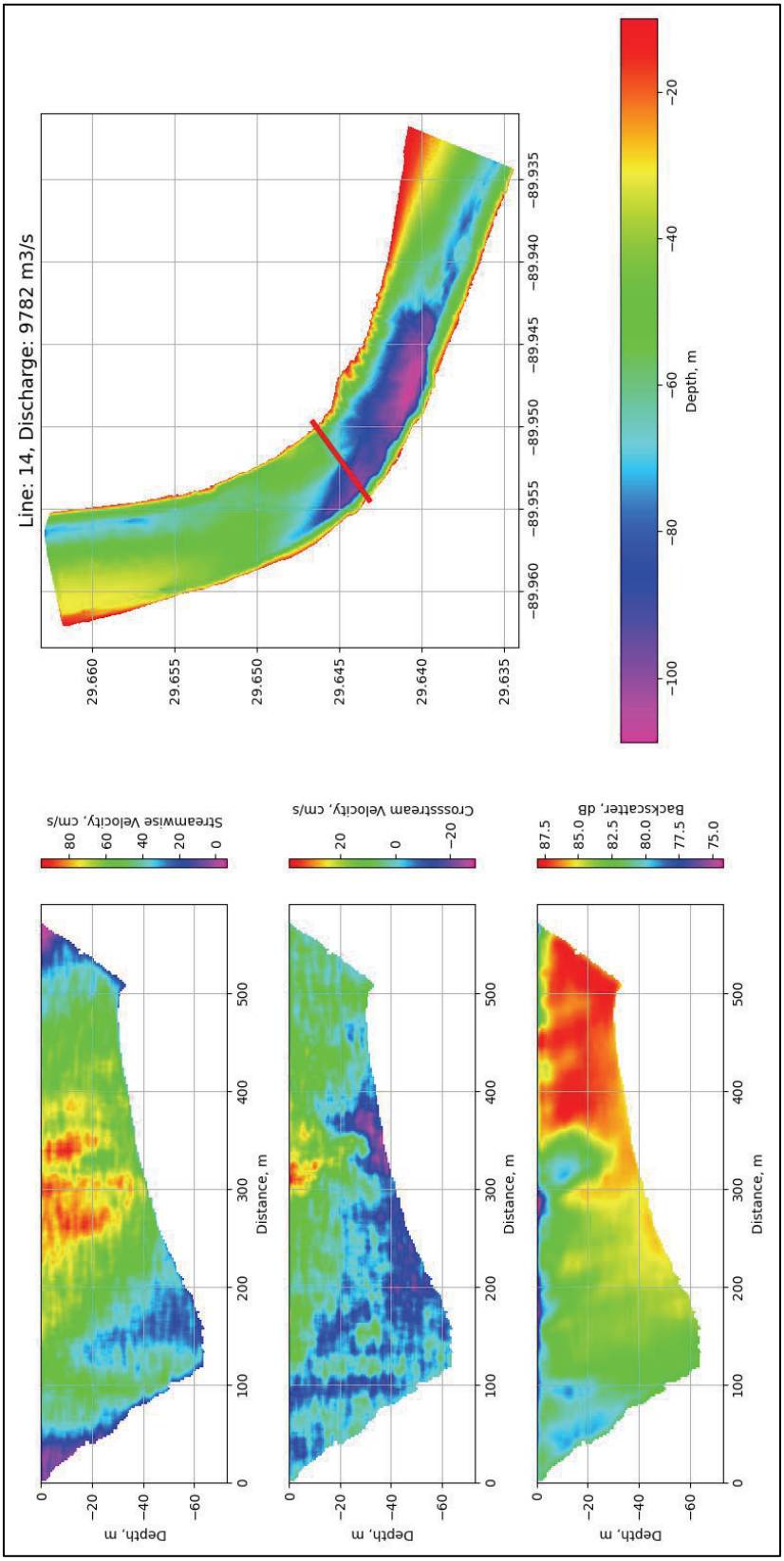
Line: 14, Discharge: 9782 m3/s
29.660
29.655
29.650
29.645
29.640
29.635
−89.960
−89.955
−89.950
−89.945
−89.940
−89.935
Depth, m
−20
−40
−60
−80
−100
Backscatter, dB
87.5
85.0
82.5
80.0
77.5
75.0
Crossstream Velocity, cm/s
20
0
−20
Streamwise Velocity, cm/s
80
60
40
20
0
Depth, m
Distance, m
0
100
200
300
400
500
−20
−40
−60

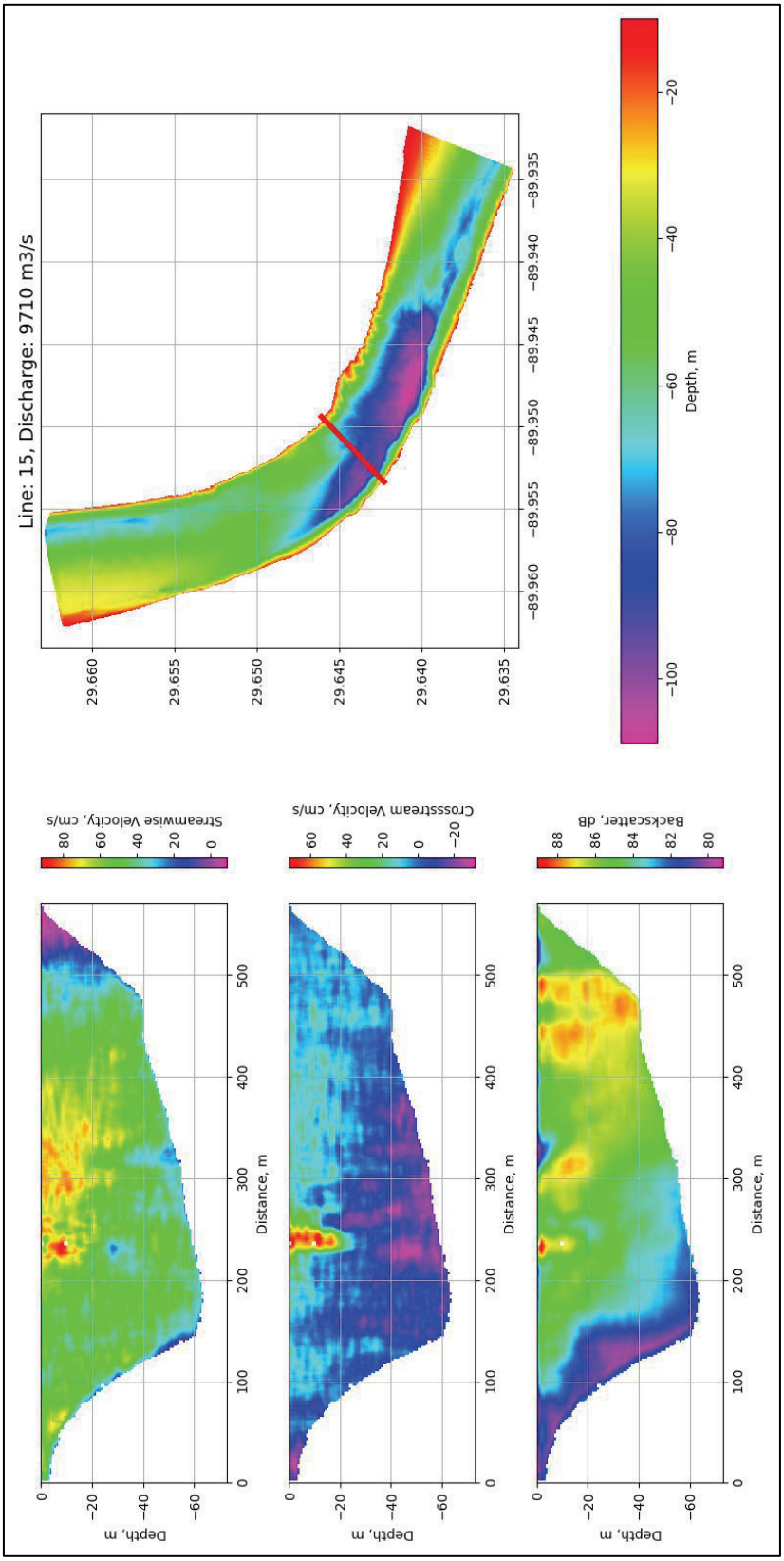
Line: 15, Discharge: 9710 m3/s
29.660
29.655
29.650
29.645
29.640
29.635
−89.960
−89.955
−89.950
−89.945
−89.940
−89.935
Depth, m
−20
−40
−60
−80
−100
Backscatter, dB
Crossstream Velocity, cm/s
Streamwise Velocity, cm/s
Depth, m
Distance, m
0
100
200
300
400
500
−20
−40
−60

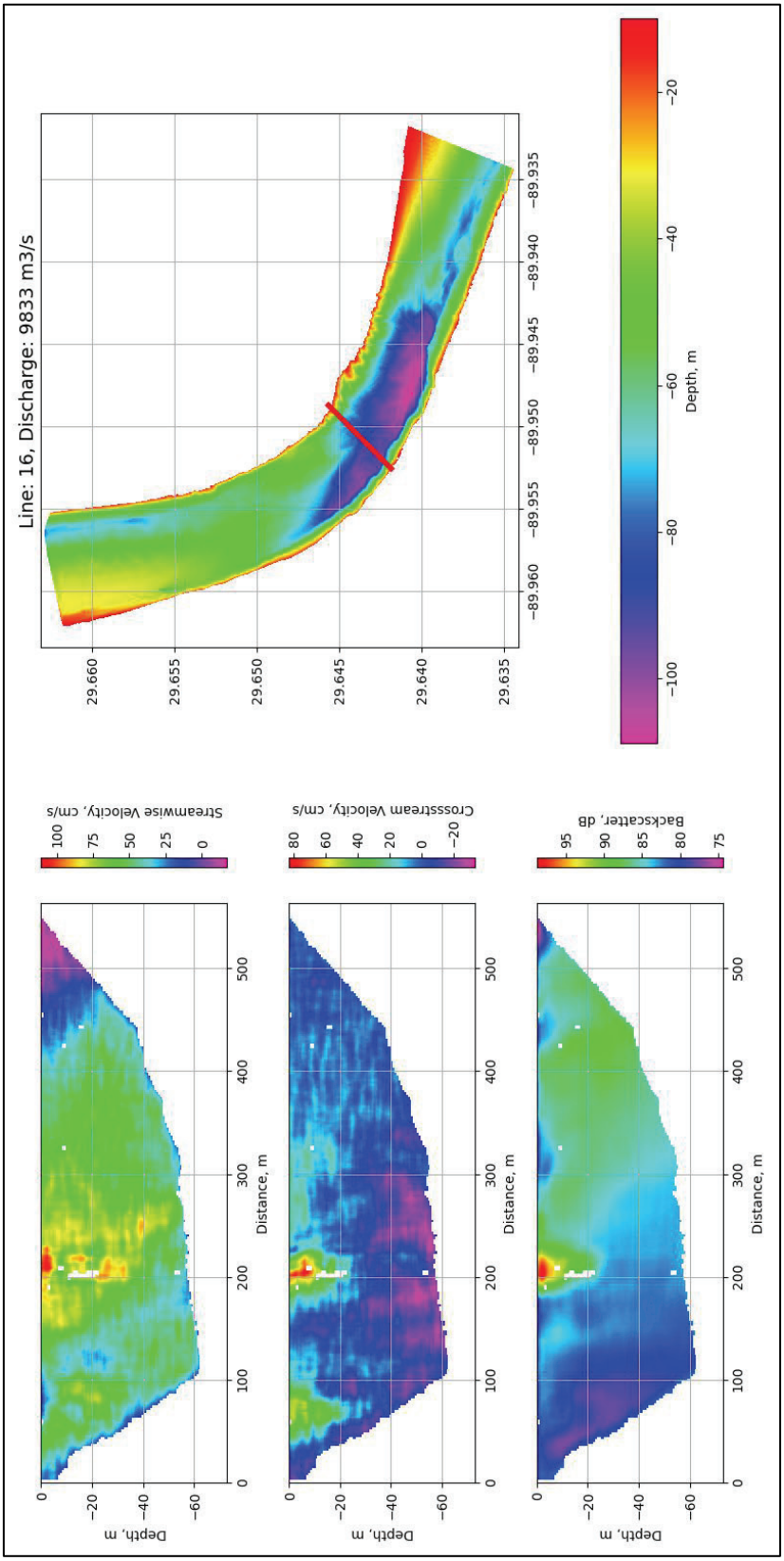
Line: 16, Discharge: 9833 m3/s
29.660
29.655
29.650
29.645
29.640
29.635
−89.960
−89.955
−89.950
−89.945
−89.940
−89.935
Depth, m
−20
−40
−60
−80
−100
Backscatter, dB
95
90
85
80
75
Crossstream Velocity, cm/s
80
60
40
20
0
−20
Streamwise Velocity, cm/s
100
75
50
25
0
Depth, m
0
−20
−40
−60
Distance, m
0
100
200
300
400
500

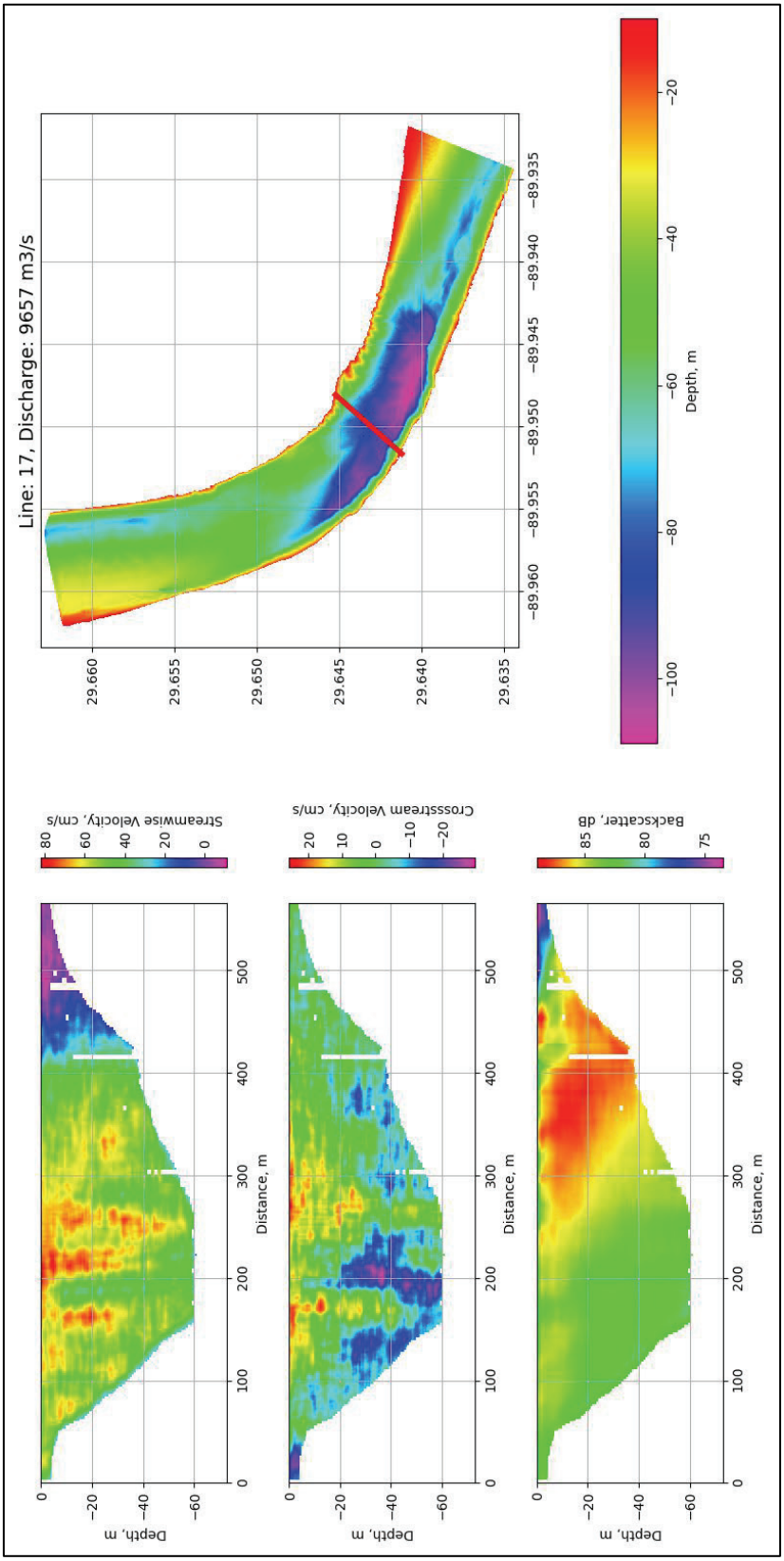
Line: 17, Discharge: 9657 m3/s
29.660
29.655
29.650
29.645
29.640
29.635
−89.960
−89.955
−89.950
−89.945
−89.940
−89.935
Depth, m
−20
−40
−60
−80
−100
Backscatter, dB
75
80
85
Crossstream Velocity, cm/s
20
10
0
−10
−20
Streamwise Velocity, cm/s
0
20
40
60
80
Depth, m
0
−20
−40
−60
Distance, m
0
100
200
300
400
500

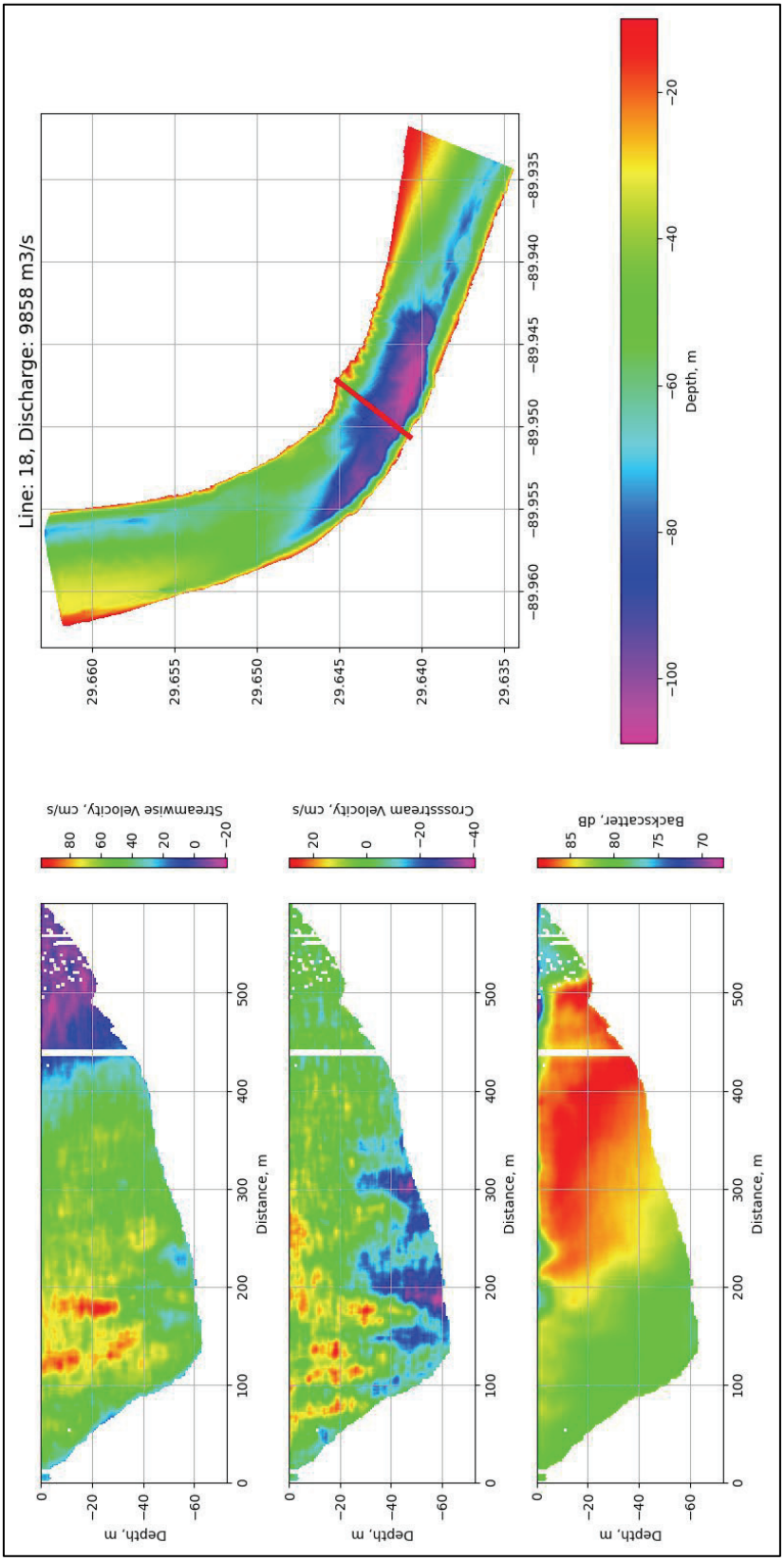
Line: 18, Discharge: 9858 m3/s
Depth, m
Backscatter, dB
Crossstream Velocity, cm/s
Streamwise Velocity, cm/s
Distance, m
Depth, m

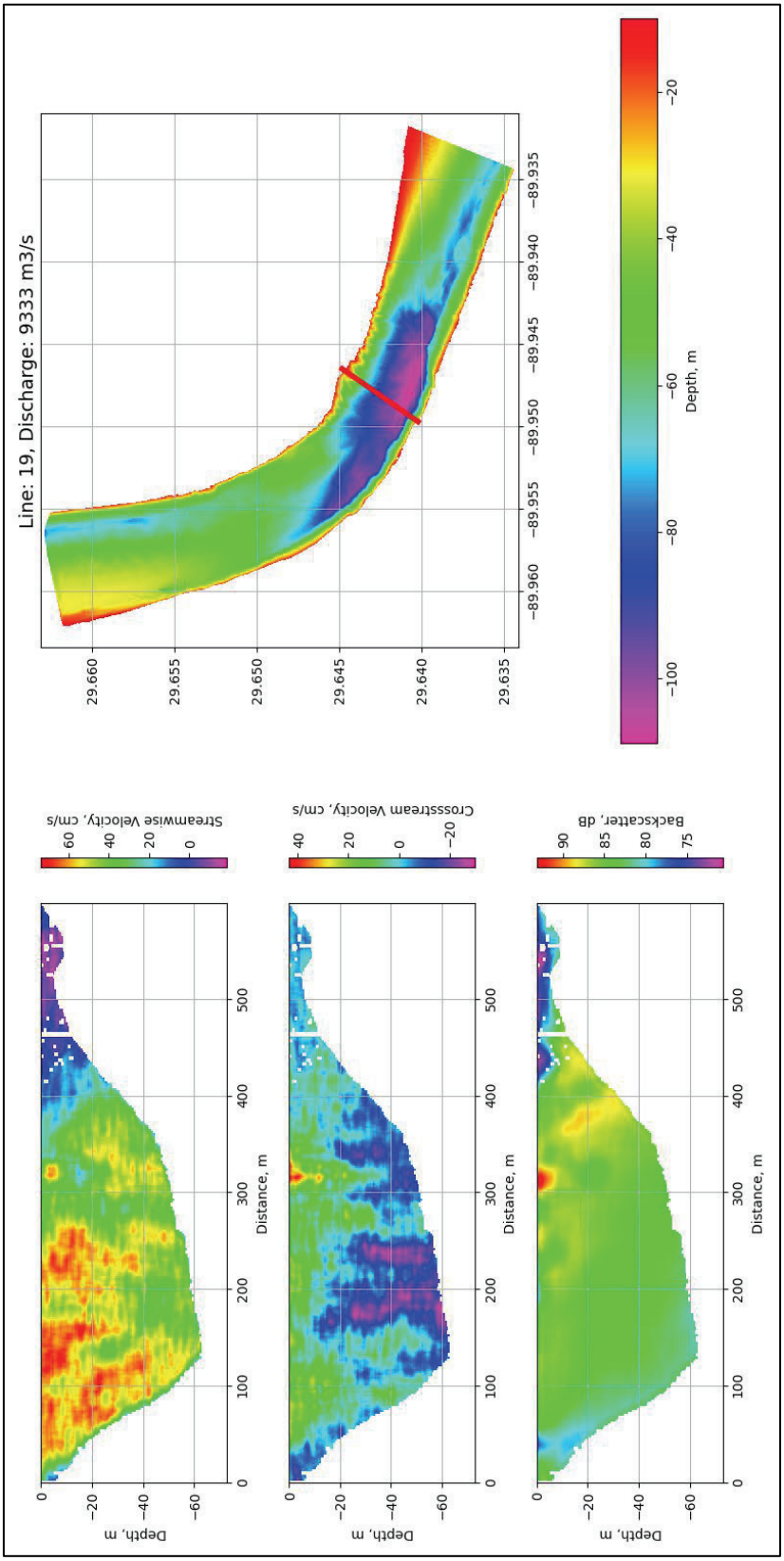
Line: 19, Discharge: 9333 m3/s
29.660
29.655
29.650
29.645
29.640
29.635
−89.960
−89.955
−89.950
−89.945
−89.940
−89.935
−20
−40
−60
−80
−100
Depth, m
Streamwise Velocity, cm/s
60
40
20
0
Crossstream Velocity, cm/s
40
20
0
−20
Backscatter, dB
90
85
80
75
Depth, m
0
−20
−40
−60
Distance, m
0
100
200
300
400
500

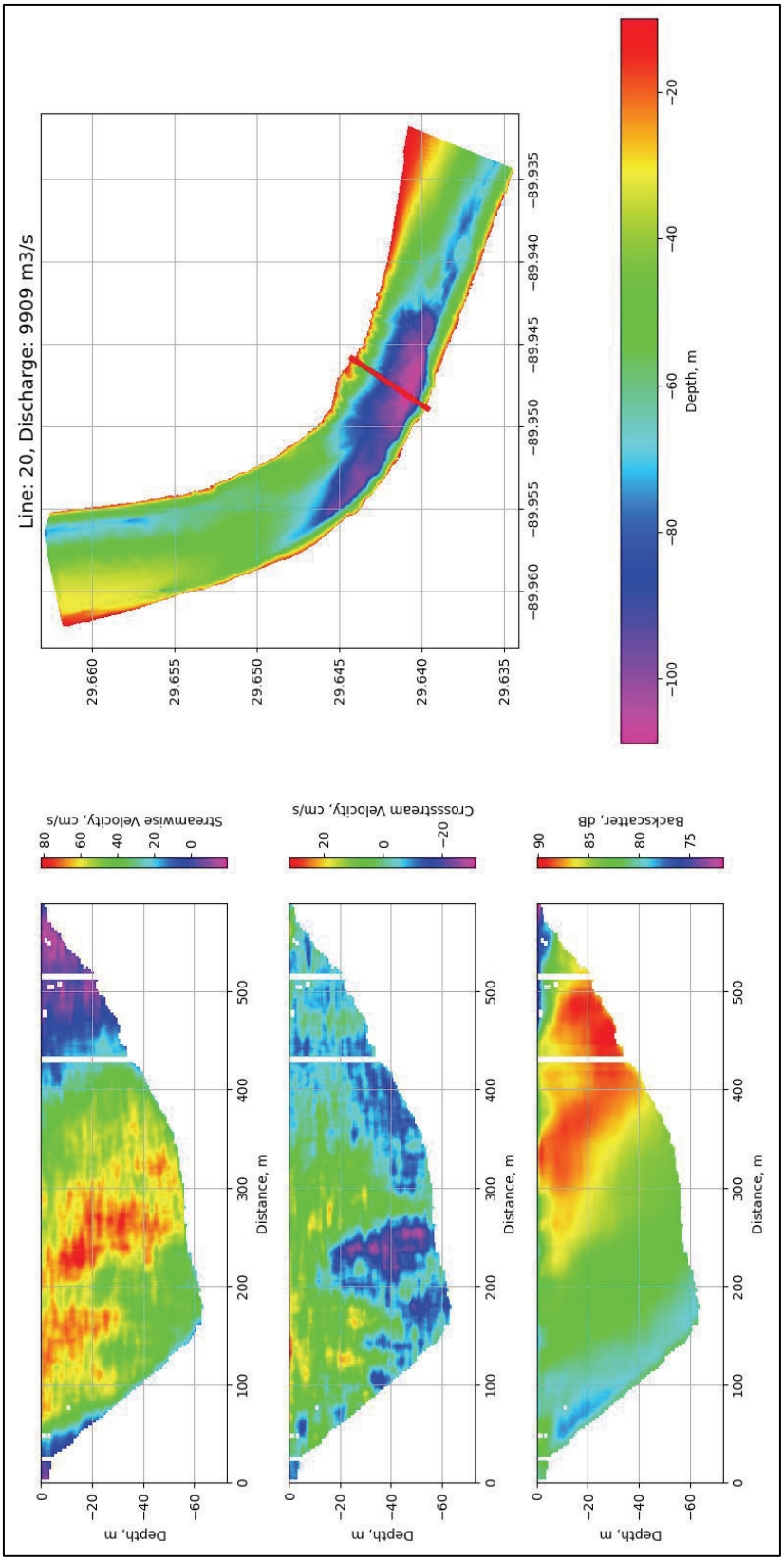
Line: 20, Discharge: 9909 m3/s
29.660
29.655
29.650
29.645
29.640
29.635
−89.960
−89.955
−89.950
−89.945
−89.940
−89.935
Depth, m
−20
−40
−60
−80
−100
Backscatter, dB
90
85
80
75
Crossstream Velocity, cm/s
20
0
−20
Streamwise Velocity, cm/s
80
60
40
20
0
Depth, m
Distance, m
0
100
200
300
400
500
−20
−40
−60

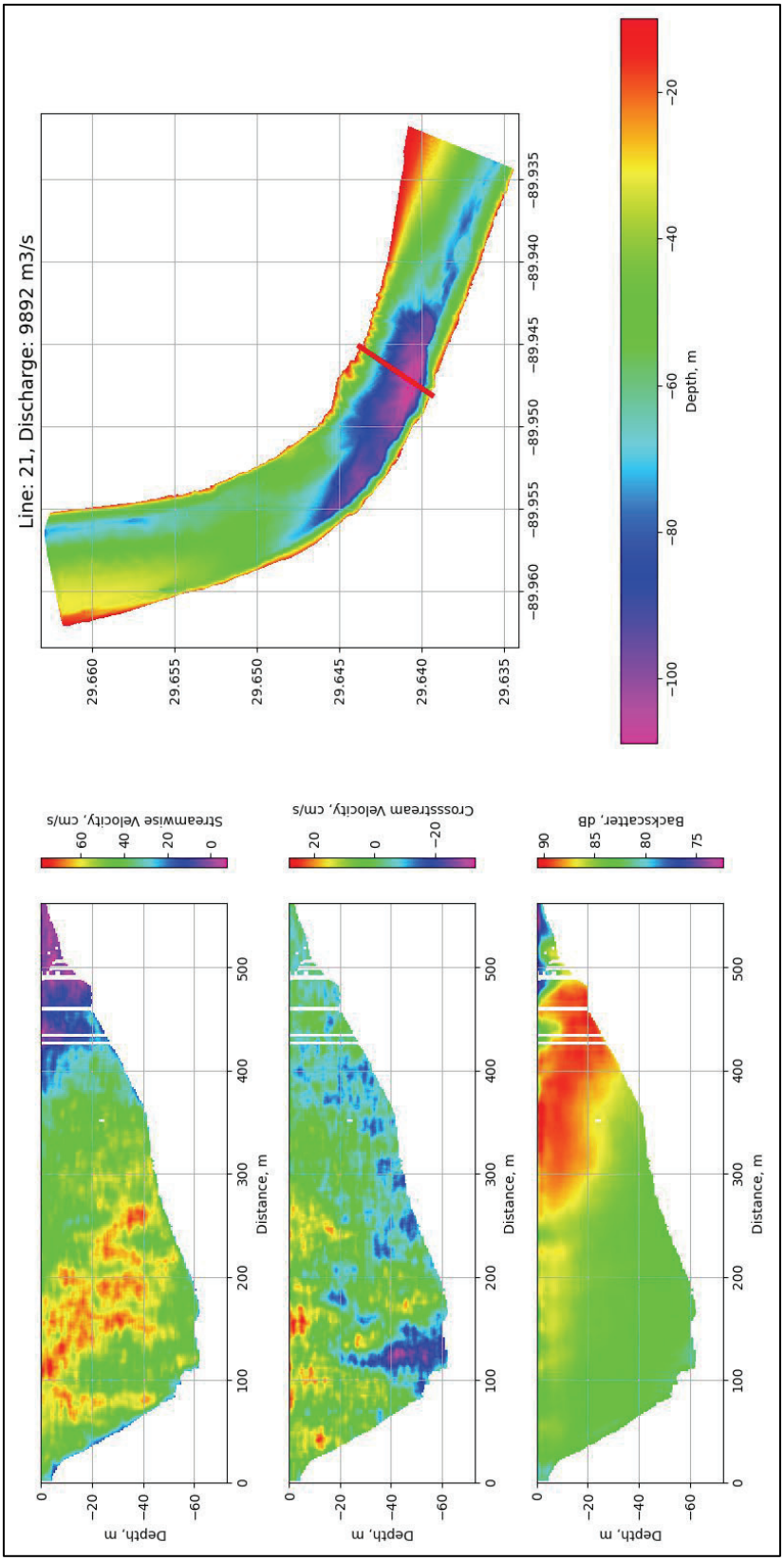
Line: 21, Discharge: 9892 m3/s
29.660
29.655
29.650
29.645
29.640
29.635
−89.960
−89.955
−89.950
−89.945
−89.940
−89.935
−20
−40
−60
−80
−100
Depth, m
Backscatter, dB
90
85
80
75
Crossstream Velocity, cm/s
20
0
−20
Streamwise Velocity, cm/s
60
40
20
0
Depth, m
Distance, m
0
100
200
300
400
500
−20
−40
−60

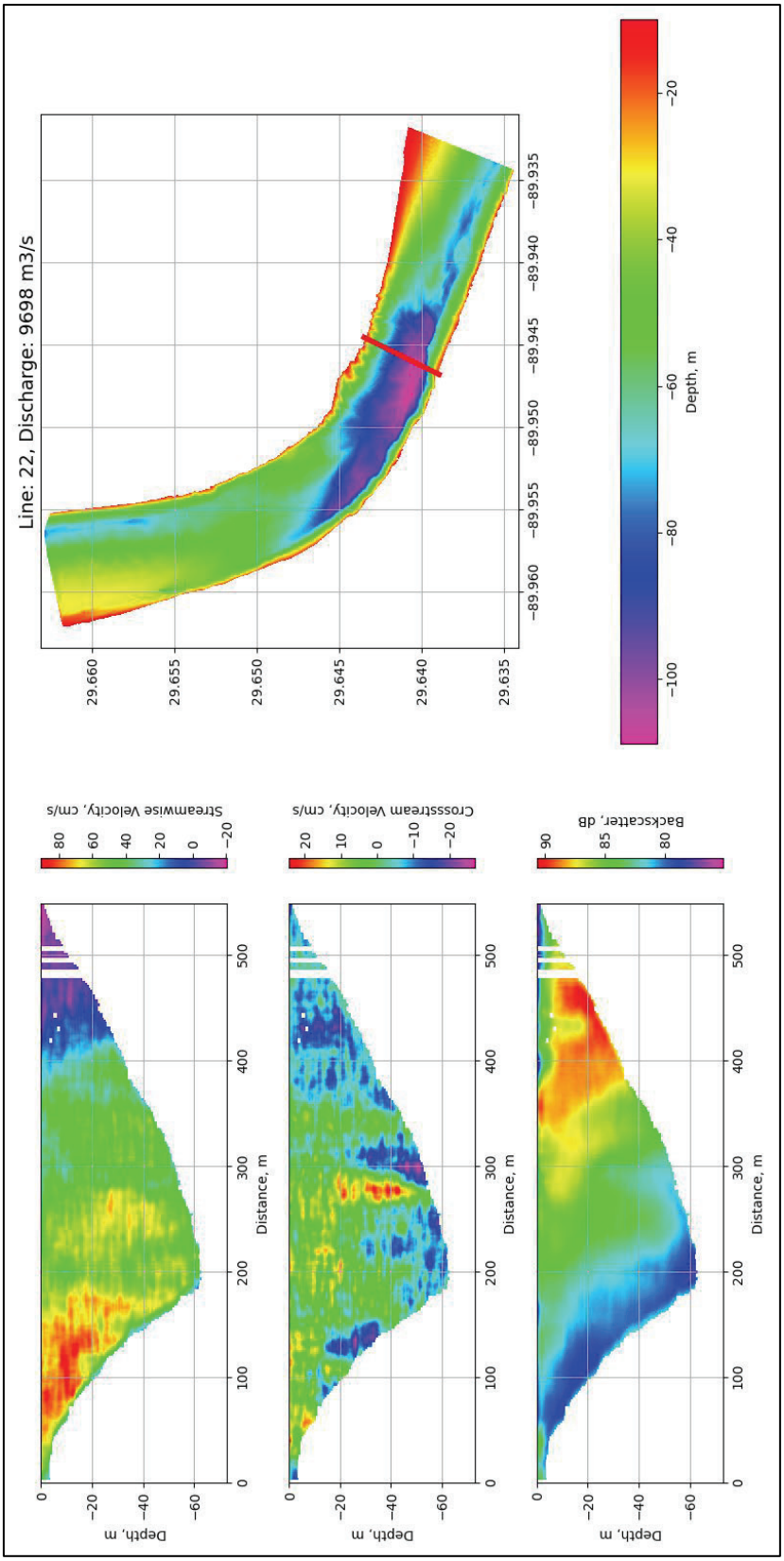
Line: 22, Discharge: 9698 m3/s
Depth, m
Streamwise Velocity, cm/s
Crossstream Velocity, cm/s
Backscatter, dB
Distance, m

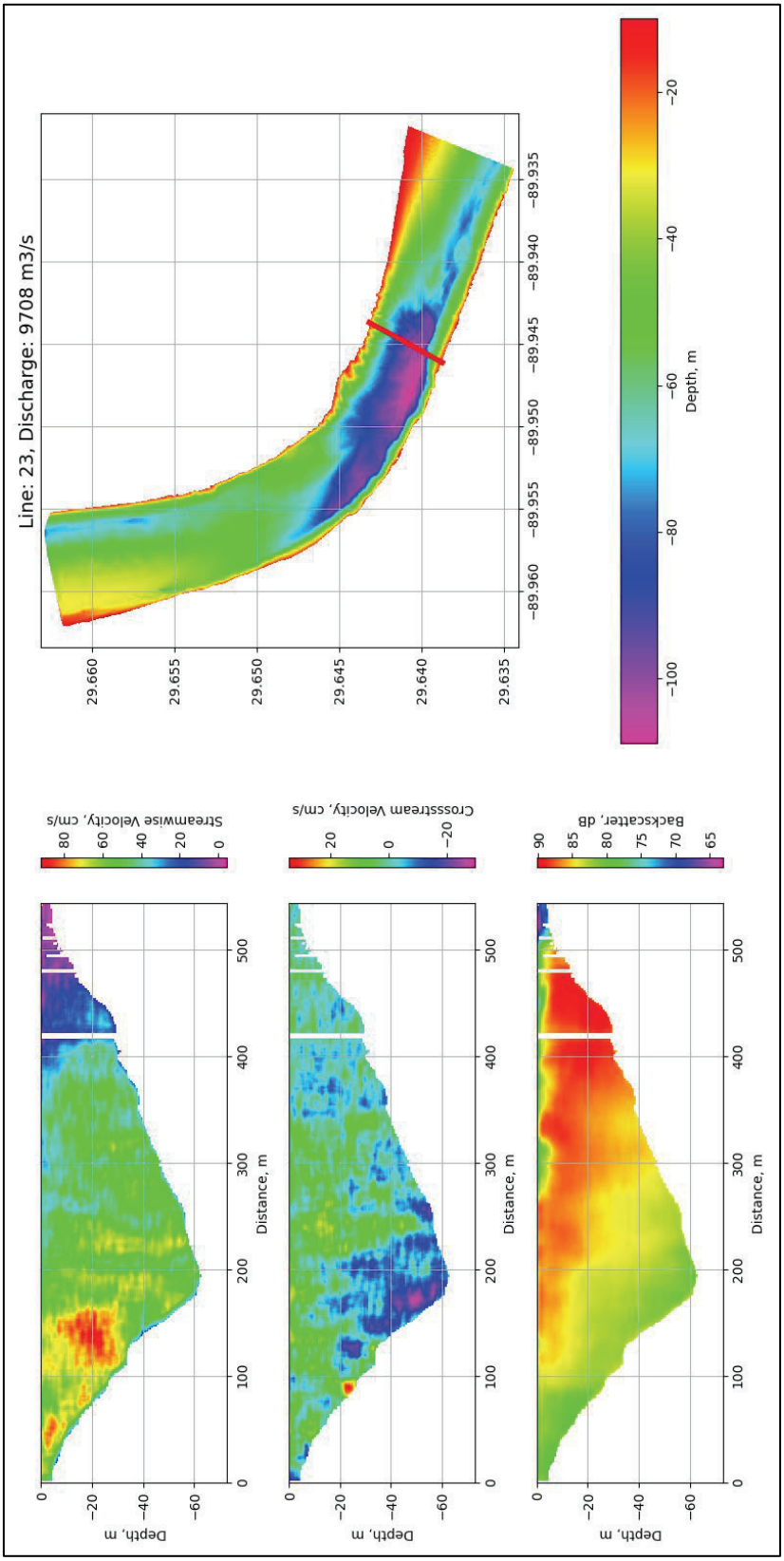
Line: 23, Discharge: 9708 m3/s
29.660
29.655
29.650
29.645
29.640
29.635
−89.960
−89.955
−89.950
−89.945
−89.940
−89.935
Depth, m
−20
−40
−60
−80
−100
Backscatter, dB
90
85
80
75
70
65
Crossstream Velocity, cm/s
20
0
−20
Streamwise Velocity, cm/s
80
60
40
20
0
Depth, m
Distance, m
0
100
200
300
400
500
−20
−40
−60

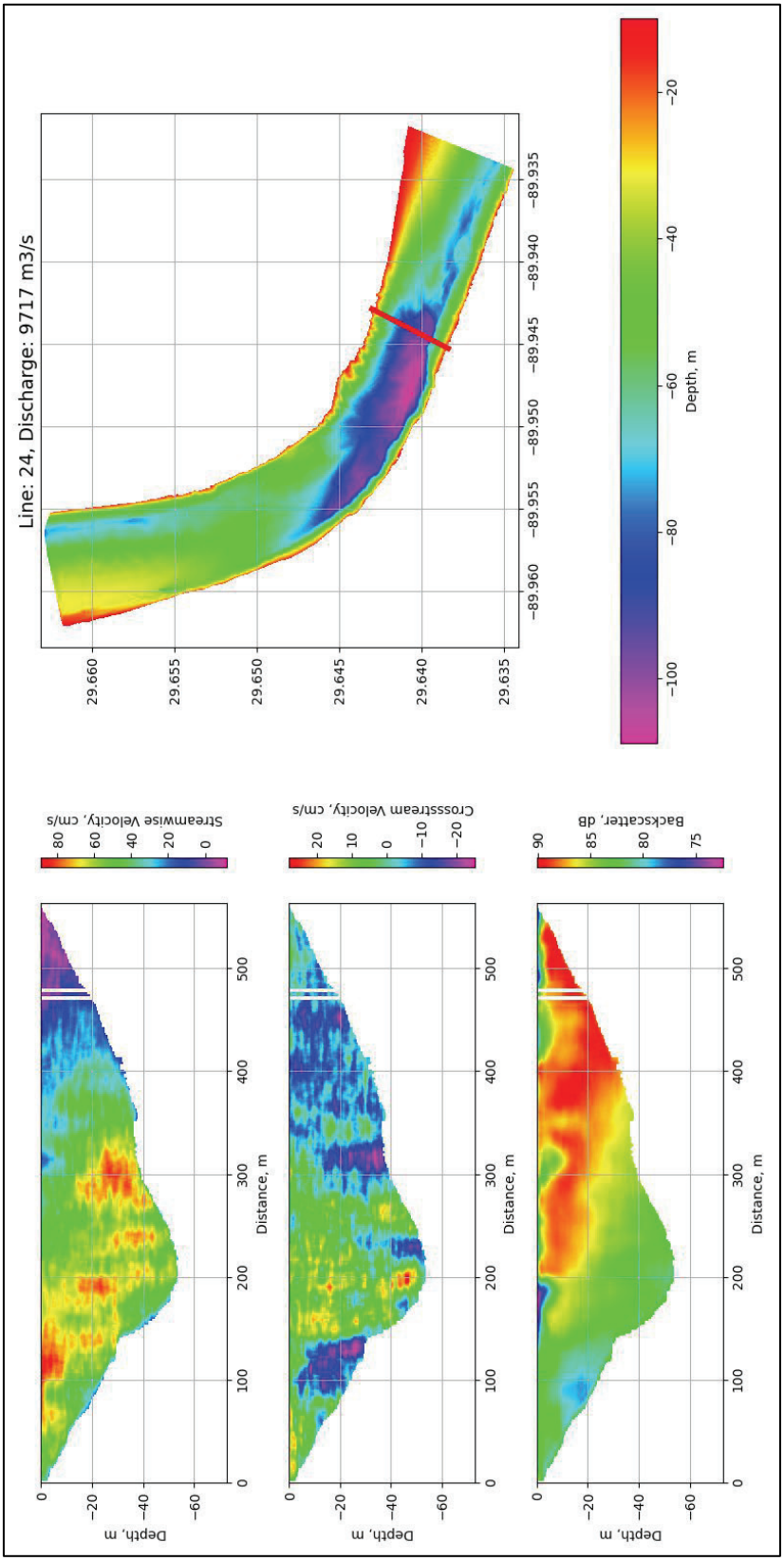
Line: 24, Discharge: 9717 m3/s
Depth, m
Distance, m
Backscatter, dB
Crossstream Velocity, cm/s
Streamwise Velocity, cm/s

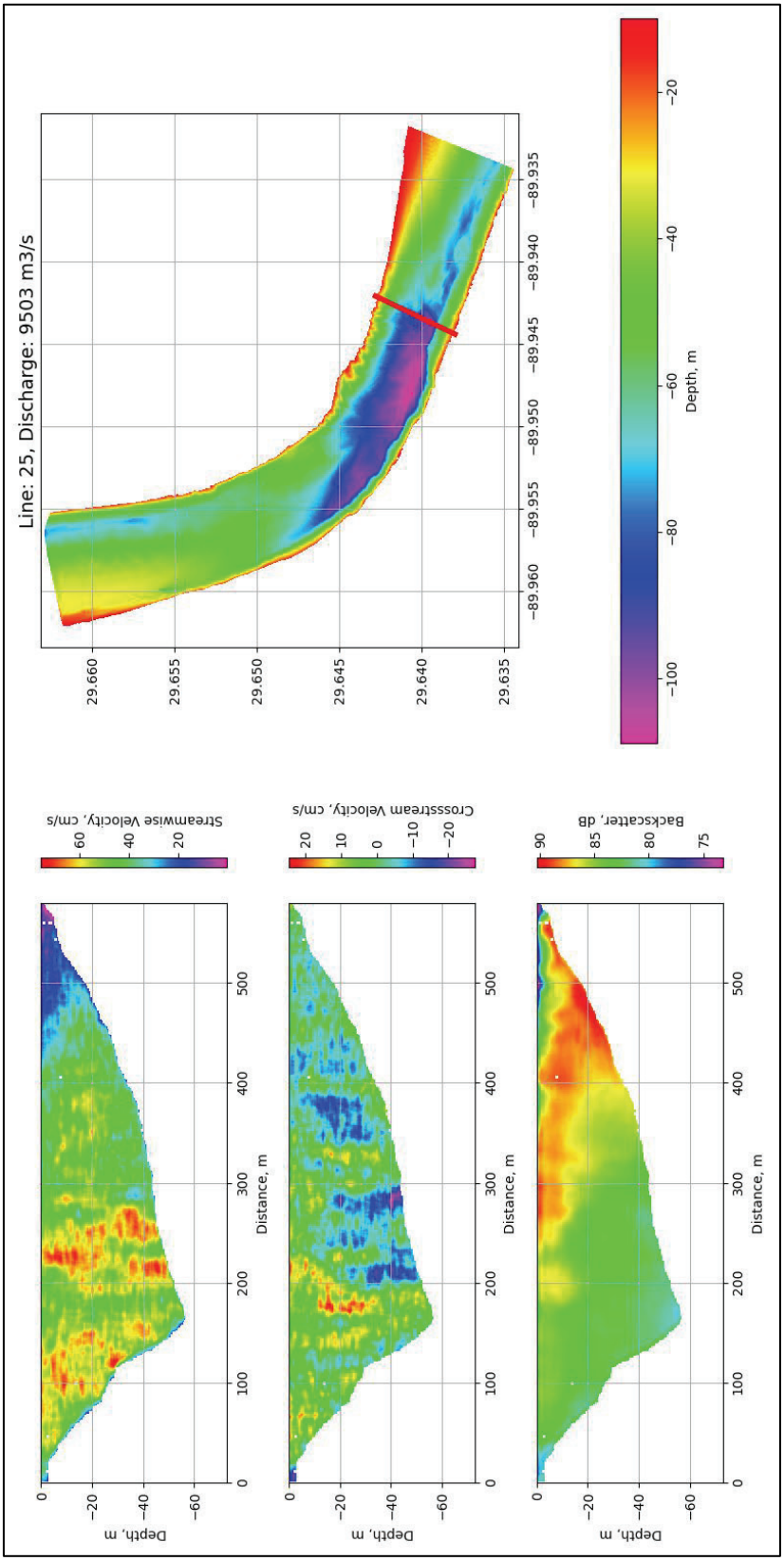
Line: 25, Discharge: 9503 m3/s
Depth, m
Backscatter, dB
Crossstream Velocity, cm/s
Streamwise Velocity, cm/s
Distance, m

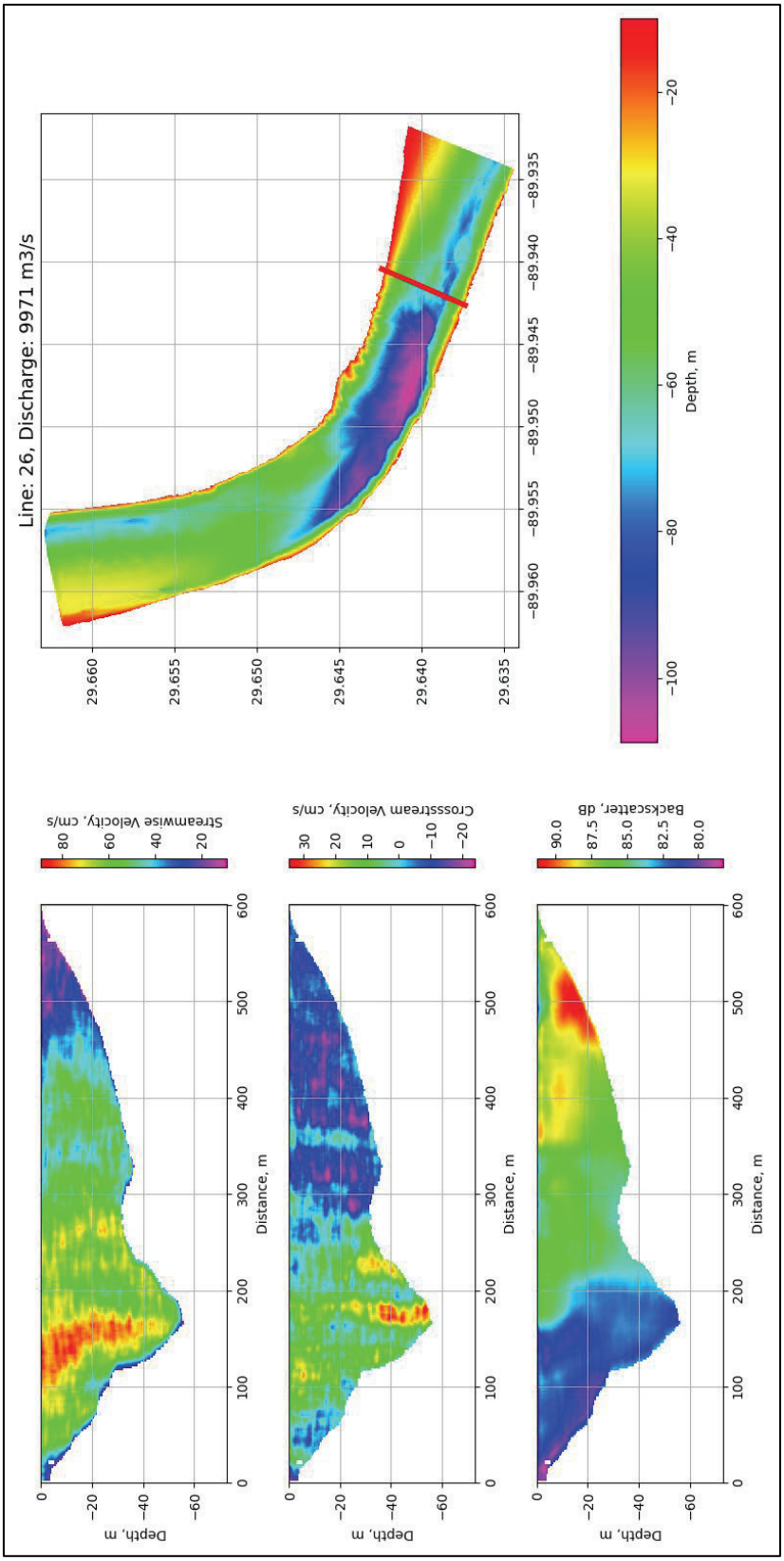
Line: 26, Discharge: 9971 m3/s
29.660
29.655
29.650
29.645
29.640
29.635
−89.960
−89.955
−89.950
−89.945
−89.940
−89.935
Depth, m
−20
−40
−60
−80
−100
Backscatter, dB
90.0
87.5
85.0
82.5
80.0
Crossstream Velocity, cm/s
30
20
10
0
−10
−20
Streamwise Velocity, cm/s
80
60
40
20
Depth, m
Distance, m
0
100
200
300
400
500
600
−20
−40
−60

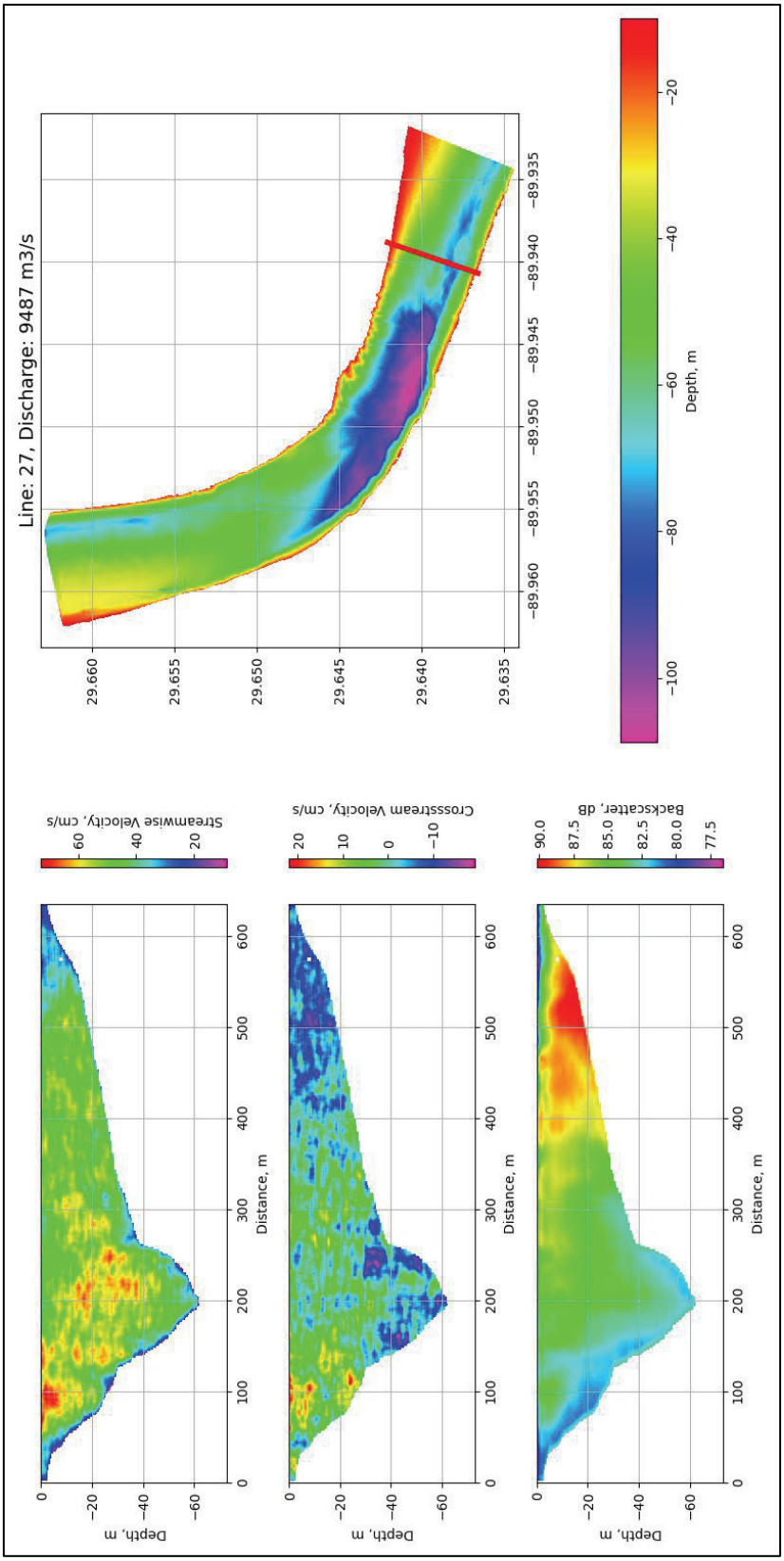
Line: 27, Discharge: 9487 m3/s
Depth, m
Distance, m
Streamwise Velocity, cm/s
Crossstream Velocity, cm/s
Backscatter, dB

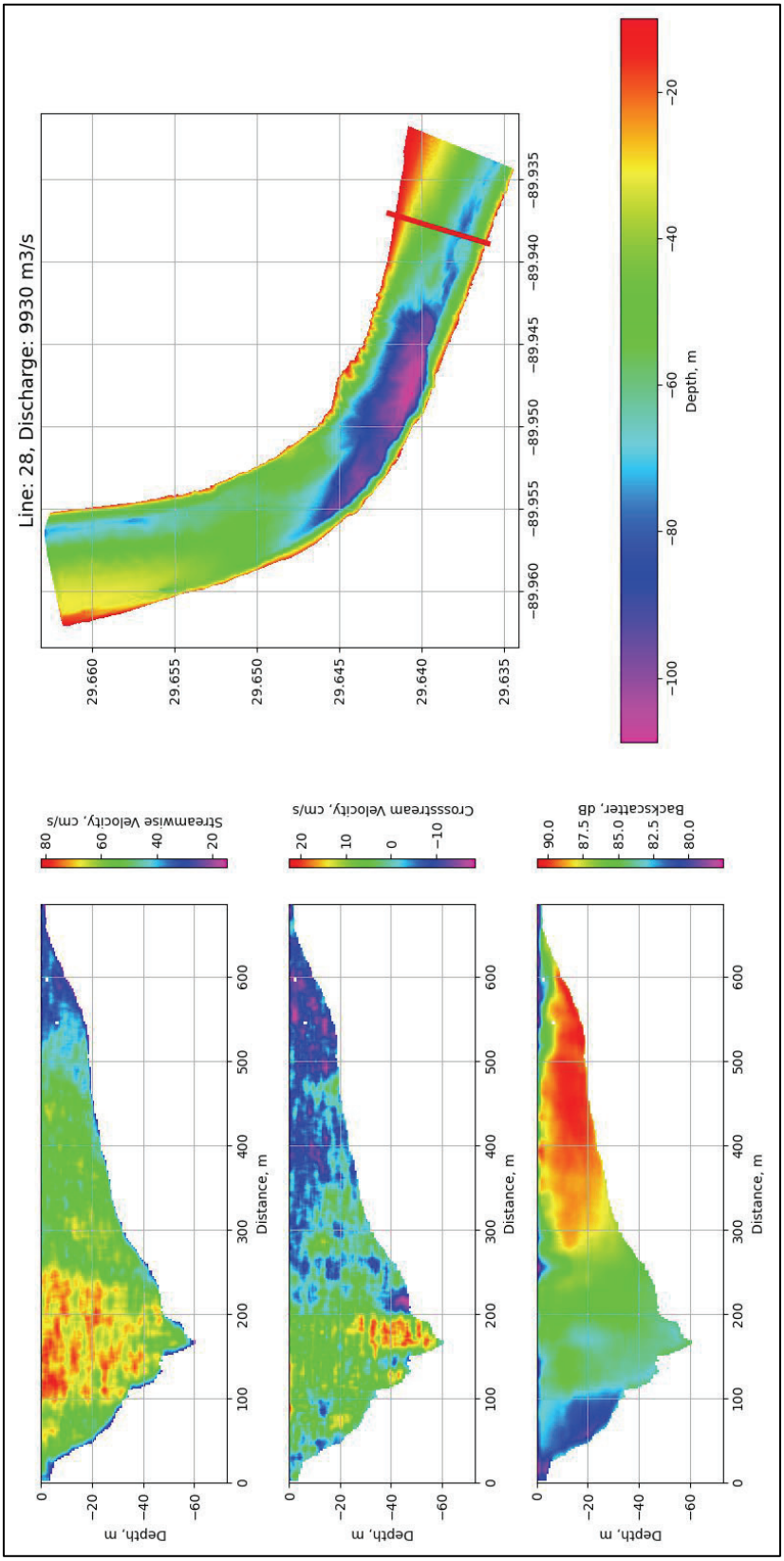
Line: 28, Discharge: 9930 m3/s
Depth, m
Streamwise Velocity, cm/s
Crossstream Velocity, cm/s
Backscatter, dB
Distance, m

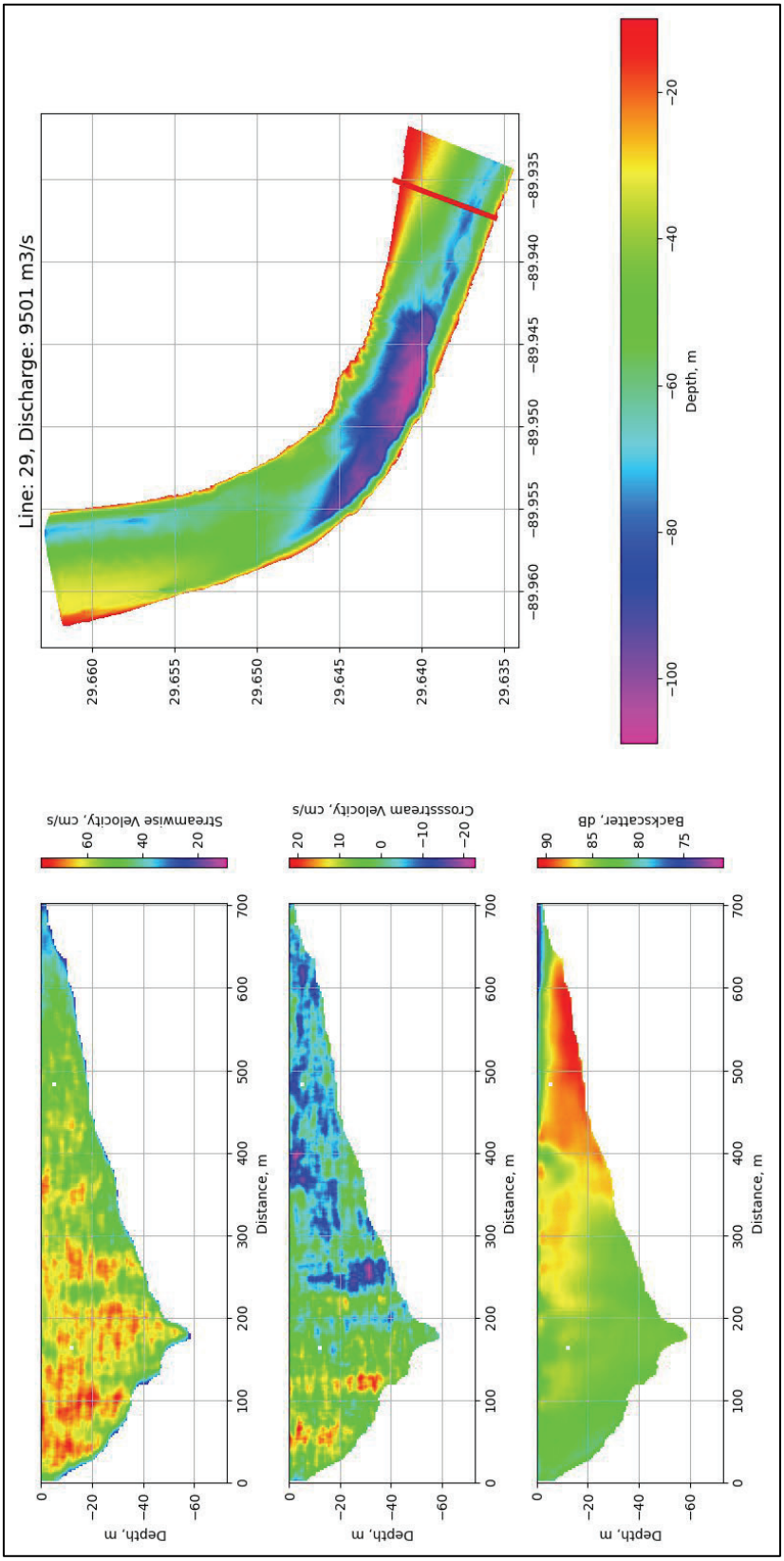
Line: 29, Discharge: 9501 m3/s
29.660
29.655
29.650
29.645
29.640
29.635
−89.960
−89.955
−89.950
−89.945
−89.940
−89.935
Depth, m
−20
−40
−60
−80
−100
Backscatter, dB
90
85
80
75
Crossstream Velocity, cm/s
20
10
0
−10
−20
Streamwise Velocity, cm/s
60
40
20
Depth, m
0
−20
−40
−60
Distance, m
0
100
200
300
400
500
600
700

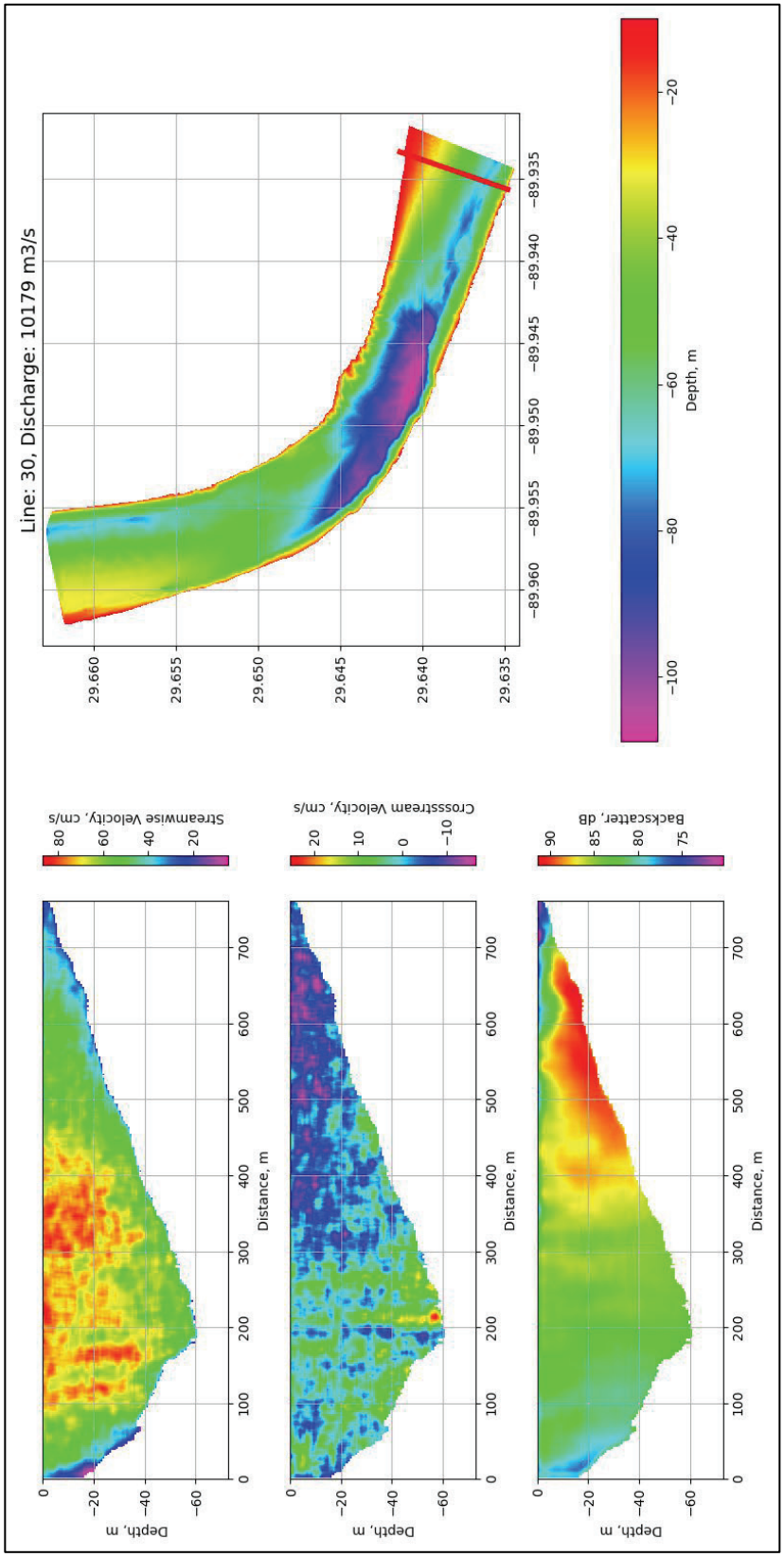
Line: 30, Discharge: 10179 m3/s
Depth, m
Distance, m
Backscatter, dB
Crossstream Velocity, cm/s
Streamwise Velocity, cm/s

Appendix B: ADCP Plots from 19 March 2021

The following 30 figures display the ADCP data collected on 19 March 2021. Each transect has its own figure. The *right side* of the figure indicates the location of the transect and bathymetric data for the reach. The panels on the *left side* show, from top to bottom, streamwise velocity, cross-stream velocity, and acoustic backscatter intensity.

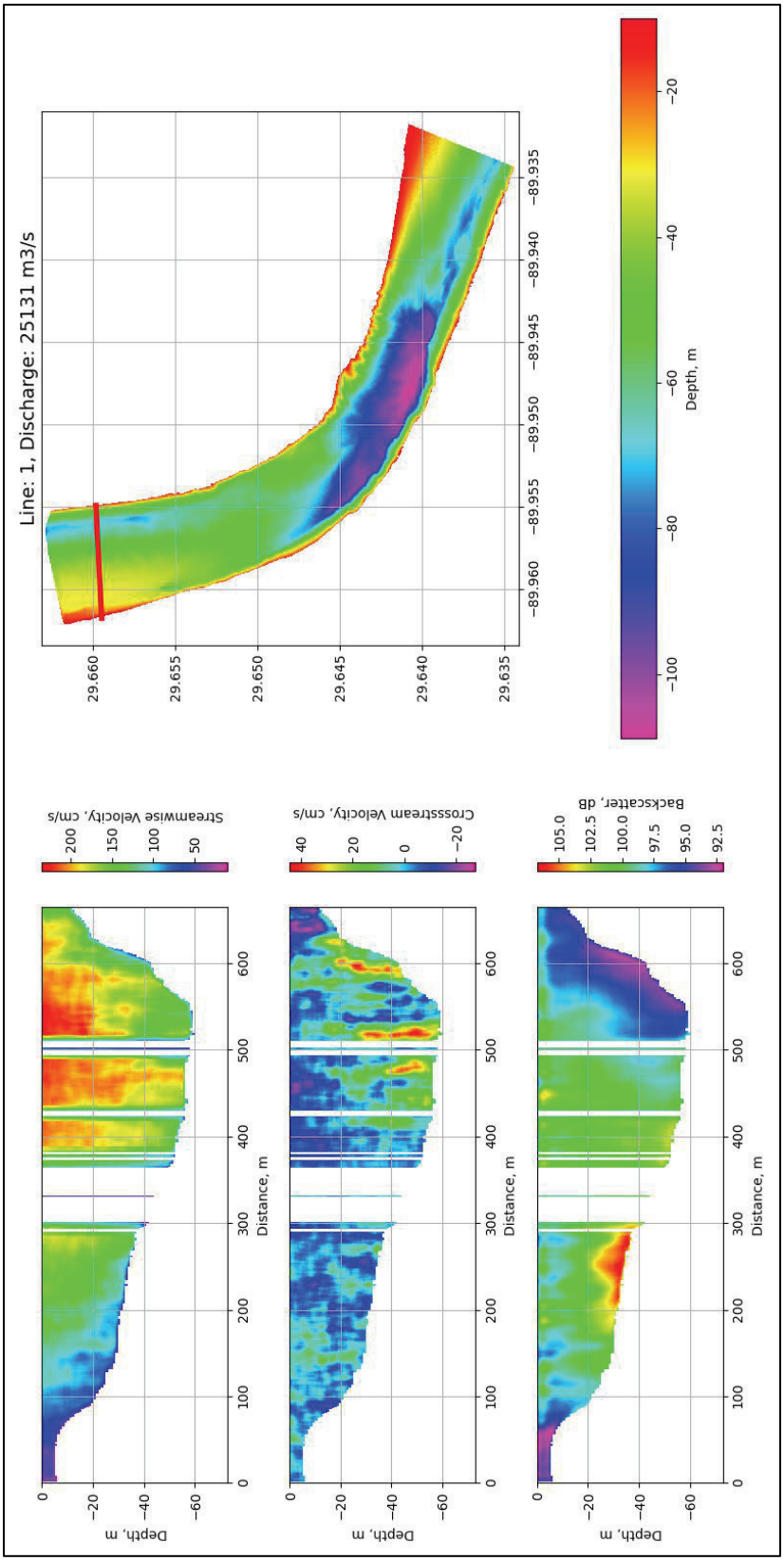
Line: 1, Discharge: 25131 m3/s
29.660
29.655
29.650
29.645
29.640
29.635
−89.960
−89.955
−89.950
−89.945
−89.940
−89.935
Depth, m
−20
−40
−60
−80
−100
Backscatter, dB
105.0
102.5
100.0
97.5
95.0
92.5
Crossstream Velocity, cm/s
40
20
0
−20
Streamwise Velocity, cm/s
200
150
100
50
Depth, m
Distance, m
0
100
200
300
400
500
600
−20
−40
−60

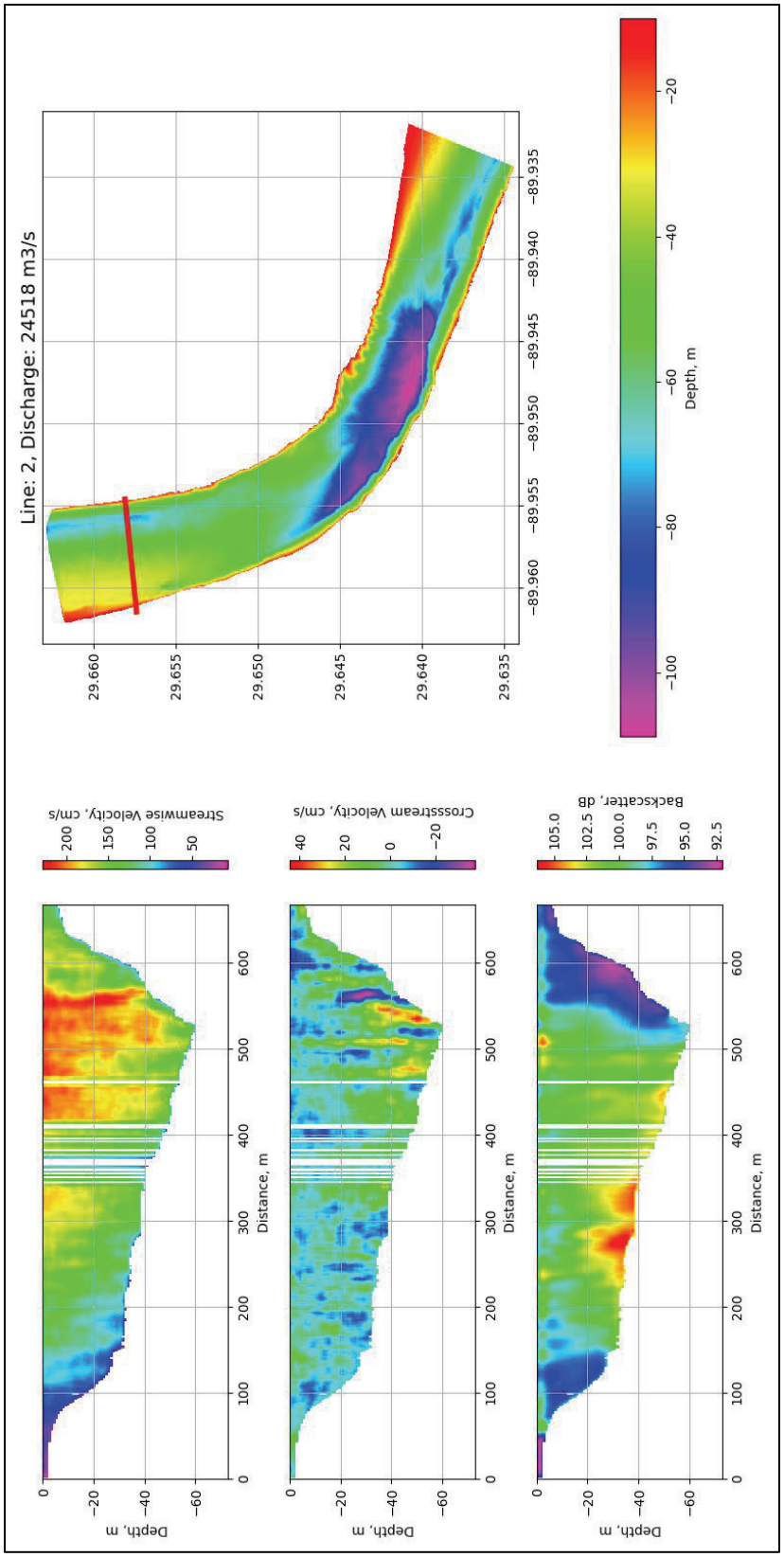
Line: 2, Discharge: 24518 m3/s
29.660
29.655
29.650
29.645
29.640
29.635
−89.960
−89.955
−89.950
−89.945
−89.940
−89.935
−20
−40
−60
−80
−100
Depth, m
Backscatter, dB
105.0
102.5
100.0
97.5
95.0
92.5
Crossstream Velocity, cm/s
40
20
0
−20
Streamwise Velocity, cm/s
200
150
100
50
Depth, m
Distance, m
0
100
200
300
400
500
600
−20
−40
−60

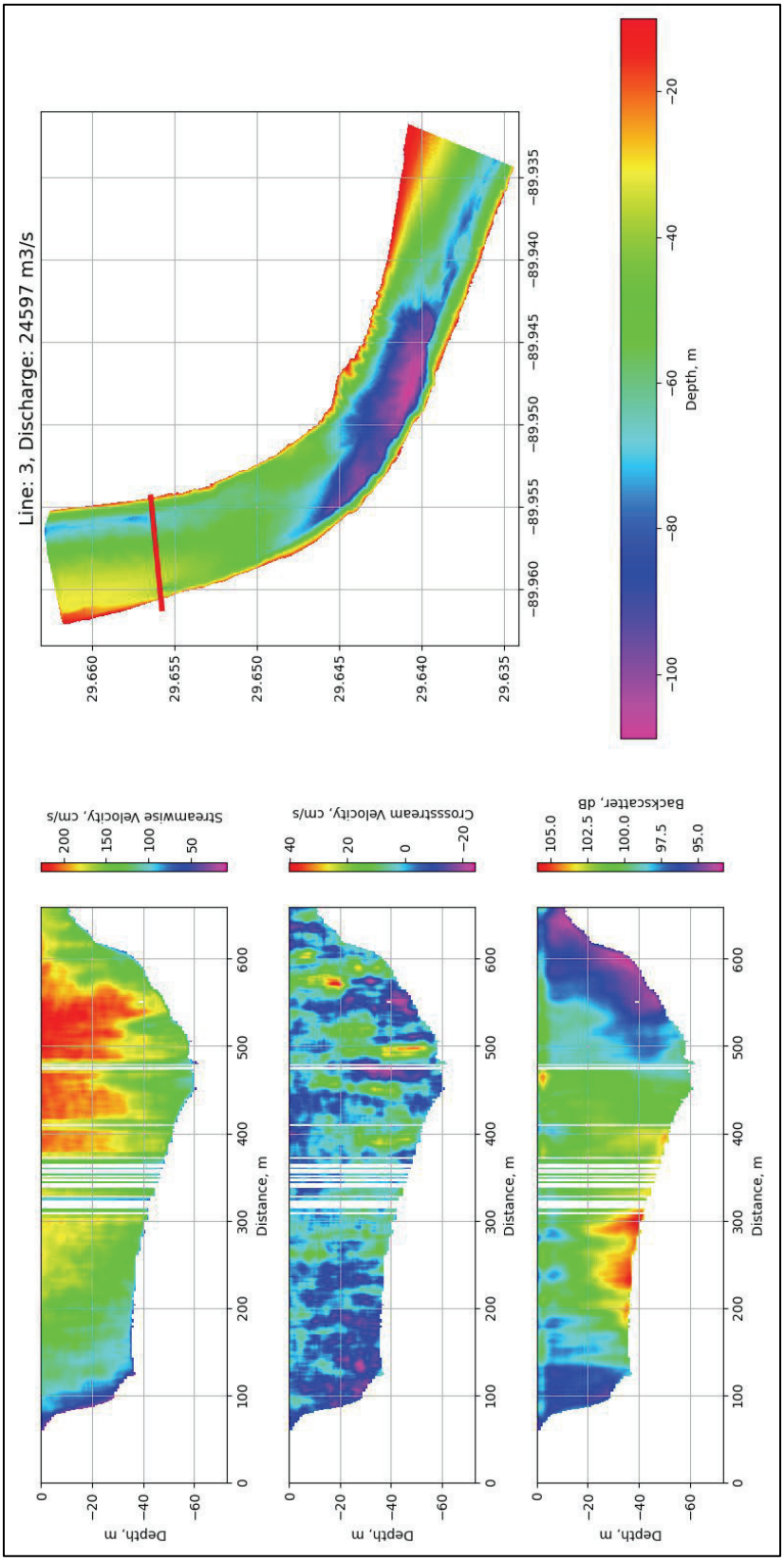
Line: 3, Discharge: 24597 m3/s
29.660
29.655
29.650
29.645
29.640
29.635
−89.960
−89.955
−89.950
−89.945
−89.940
−89.935
Depth, m
−20
−40
−60
−80
−100
Backscatter, dB
105.0
102.5
100.0
97.5
95.0
Crossstream Velocity, cm/s
40
20
0
−20
Streamwise Velocity, cm/s
200
150
100
50
Depth, m
Distance, m
0
100
200
300
400
500
600
−20
−40
−60

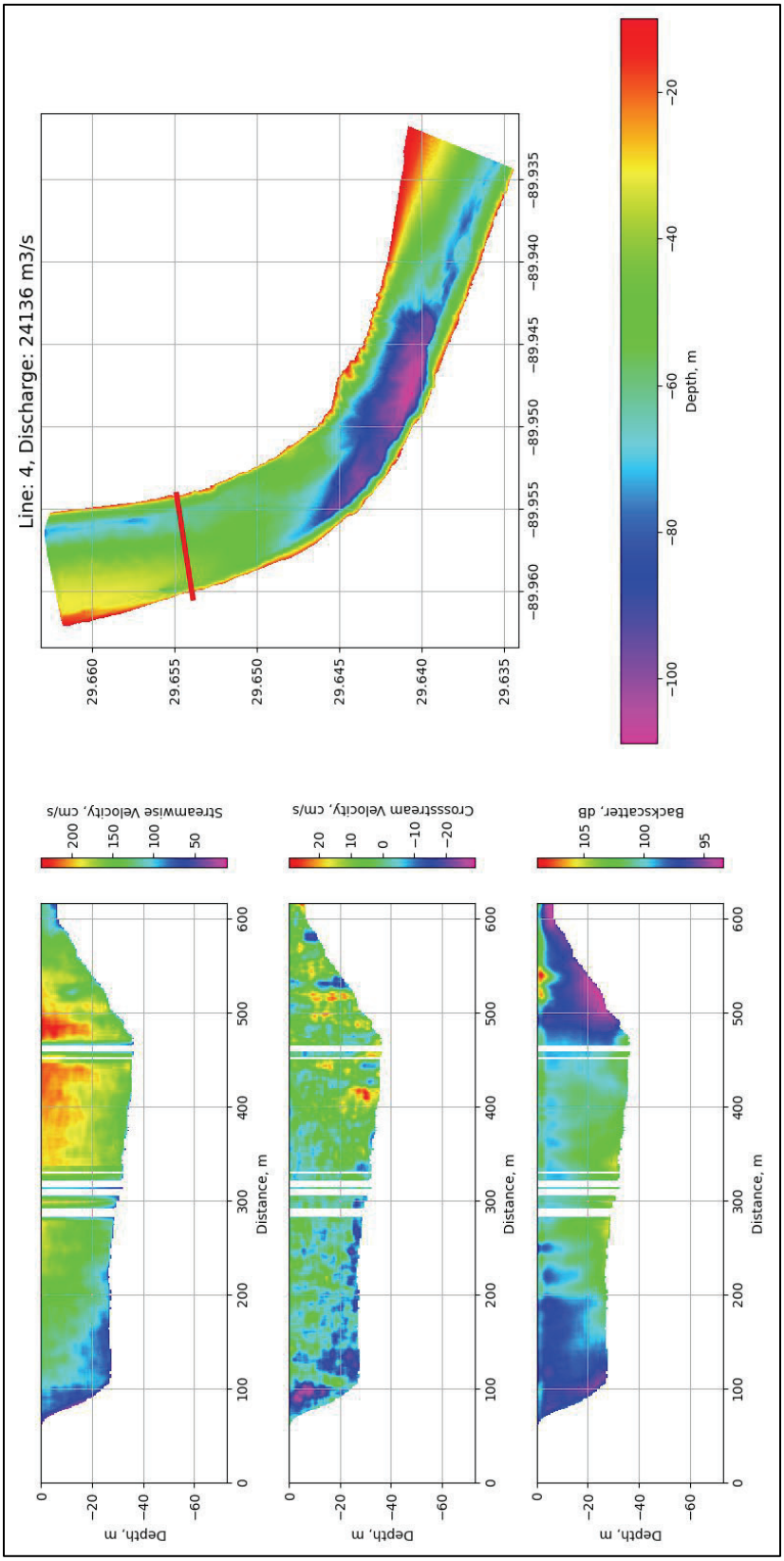
Line: 4, Discharge: 24136 m3/s
29.660
29.655
29.650
29.645
29.640
29.635
−89.960
−89.955
−89.950
−89.945
−89.940
−89.935
Depth, m
−20
−40
−60
−80
−100
Backscatter, dB
105
100
95
Crossstream Velocity, cm/s
20
10
0
−10
−20
Streamwise Velocity, cm/s
200
150
100
50
Depth, m
0
−20
−40
−60
Distance, m
0
100
200
300
400
500
600

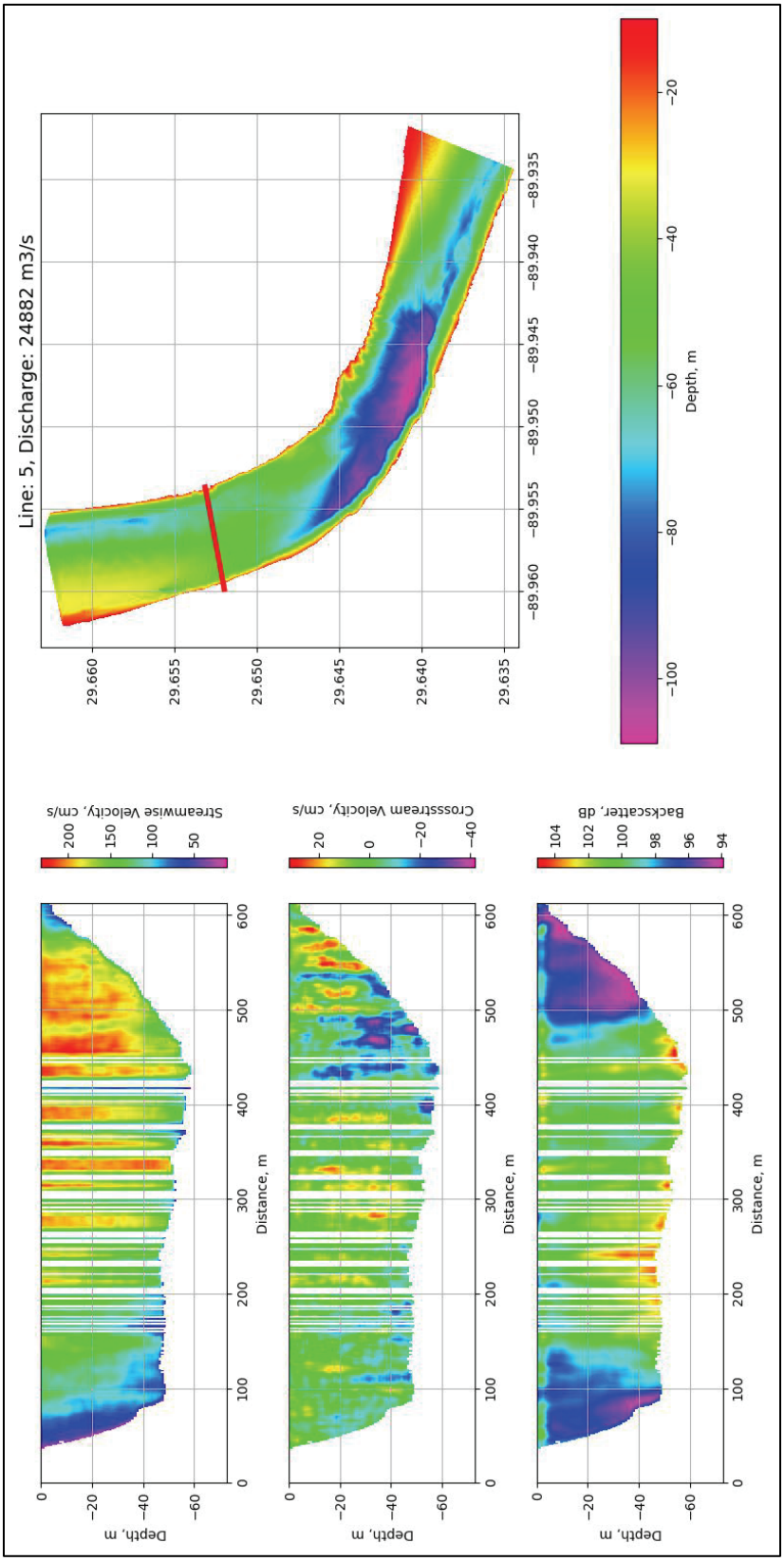
Line: 5, Discharge: 24882 m3/s
29.660
29.655
29.650
29.645
29.640
29.635
−89.960
−89.955
−89.950
−89.945
−89.940
−89.935
Depth, m
−20
−40
−60
−80
−100
Backscatter, dB
104
102
100
98
96
94
Crossstream Velocity, cm/s
20
0
−20
−40
Streamwise Velocity, cm/s
200
150
100
50
Depth, m
0
−20
−40
−60
Distance, m
0
100
200
300
400
500
600

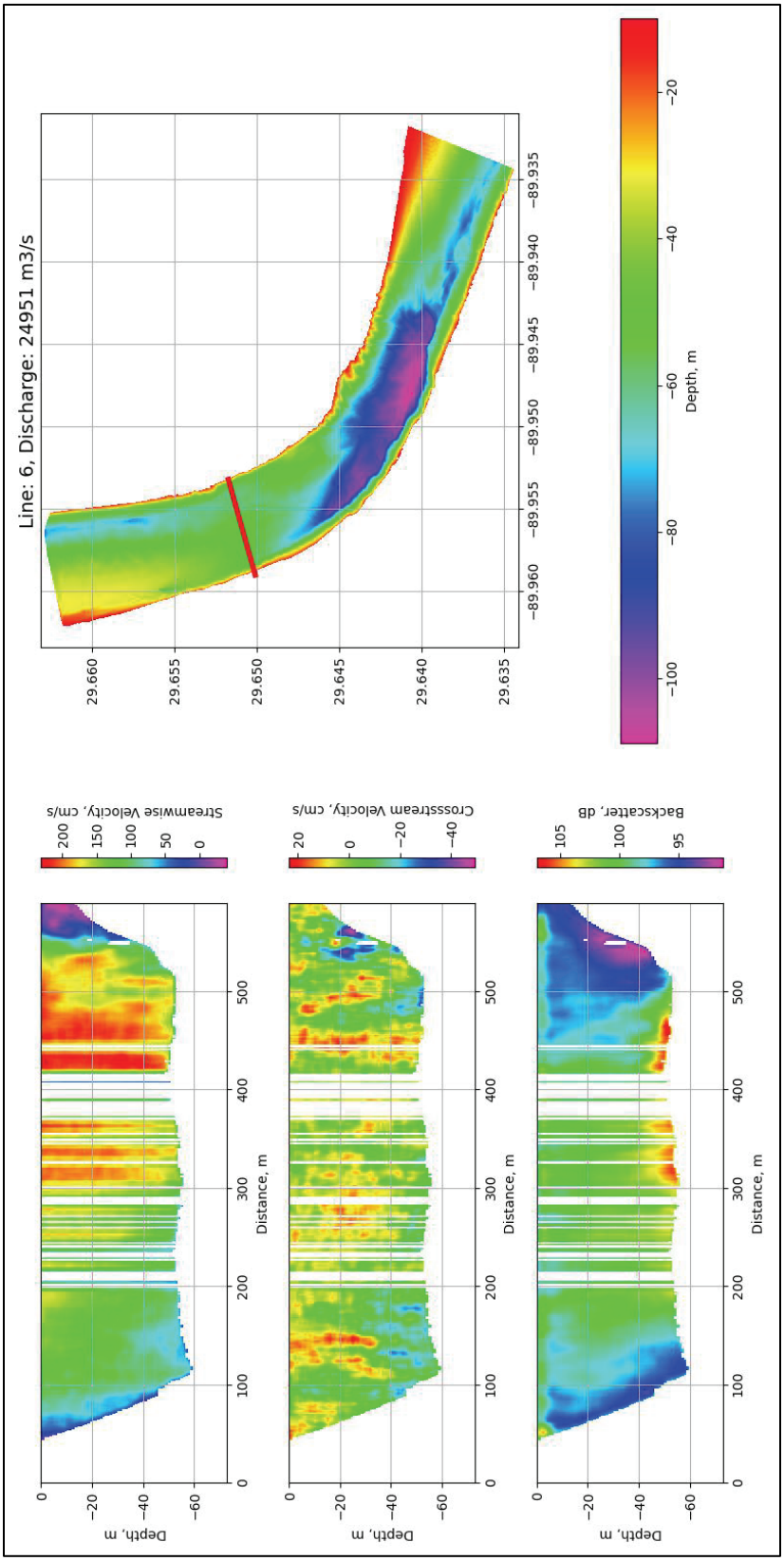
Line: 6, Discharge: 24951 m3/s
29.660
29.655
29.650
29.645
29.640
29.635
−89.960
−89.955
−89.950
−89.945
−89.940
−89.935
Depth, m
−20
−40
−60
−80
−100
Backscatter, dB
105
100
95
Crossstream Velocity, cm/s
20
0
−20
−40
Streamwise Velocity, cm/s
200
150
100
50
0
Depth, m
0
−20
−40
−60
Distance, m
0
100
200
300
400
500

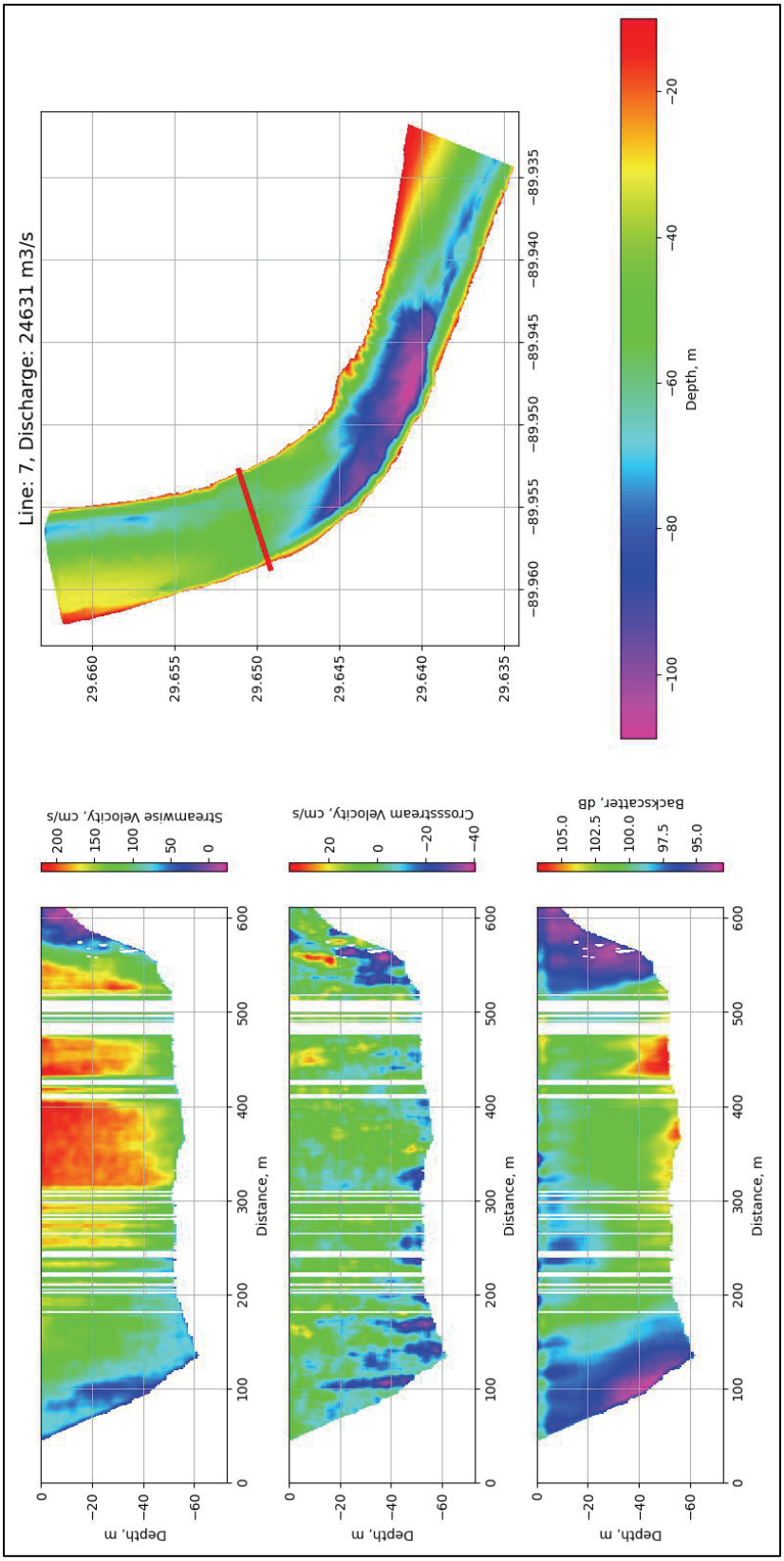
Line: 7, Discharge: 24631 m3/s
29.660
29.655
29.650
29.645
29.640
29.635
−89.960
−89.955
−89.950
−89.945
−89.940
−89.935
Depth, m
−20
−40
−60
−80
−100
Backscatter, dB
105.0
102.5
100.0
97.5
95.0
Crossstream Velocity, cm/s
20
0
−20
−40
Streamwise Velocity, cm/s
200
150
100
50
0
Depth, m
Distance, m
0
100
200
300
400
500
600
−20
−40
−60

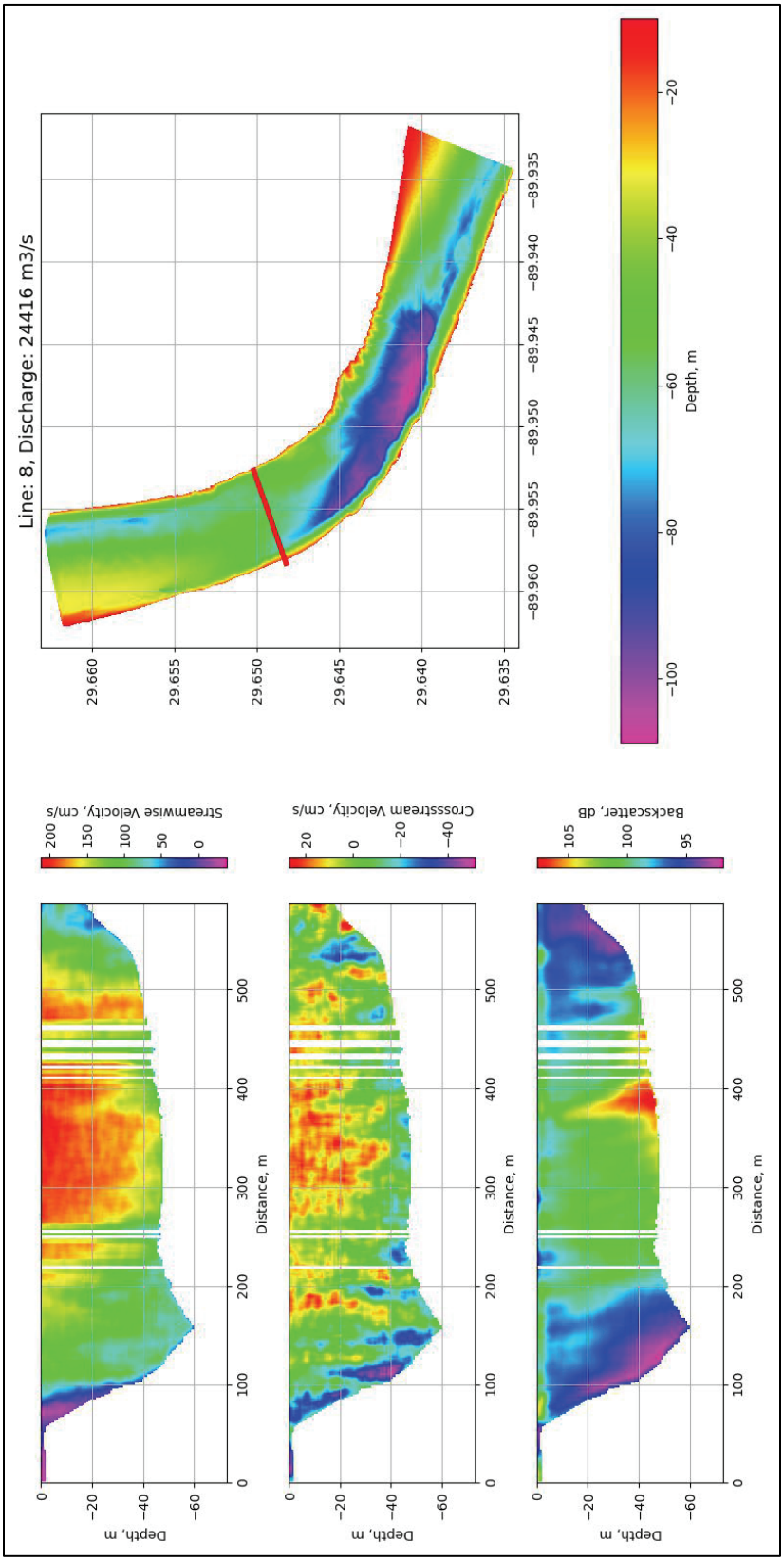
Line: 8, Discharge: 24416 m3/s
29.660
29.655
29.650
29.645
29.640
29.635
−89.960
−89.955
−89.950
−89.945
−89.940
−89.935
Depth, m
−20
−40
−60
−80
−100
Backscatter, dB
105
100
95
Crossstream Velocity, cm/s
20
0
−20
−40
Streamwise Velocity, cm/s
200
150
100
50
0
Depth, m
0
−20
−40
−60
Distance, m
0
100
200
300
400
500

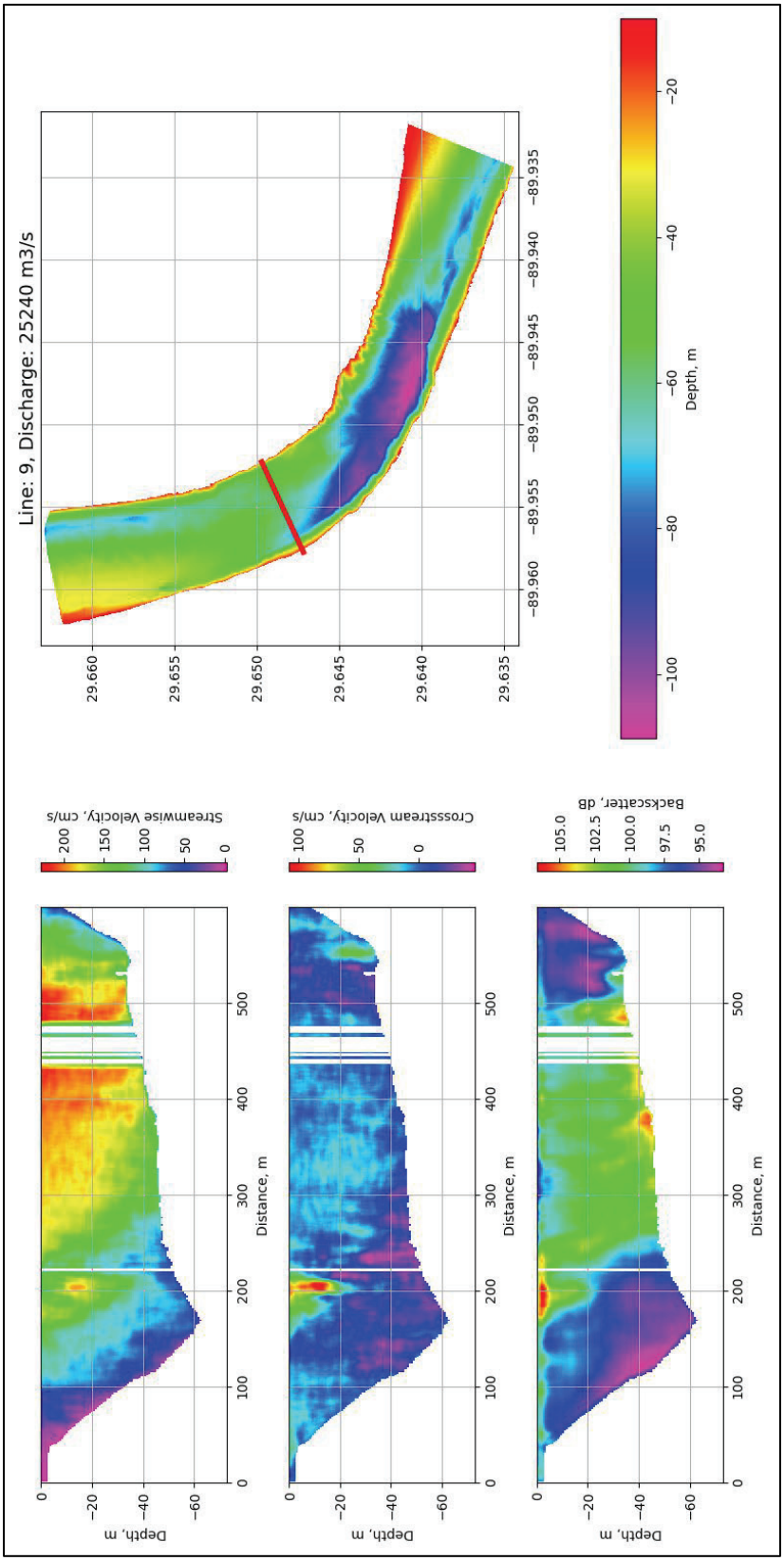
Line: 9, Discharge: 25240 m3/s
29.660
29.655
29.650
29.645
29.640
29.635
−89.960
−89.955
−89.950
−89.945
−89.940
−89.935
Depth, m
−20
−40
−60
−80
−100
Backscatter, dB
105.0
102.5
100.0
97.5
95.0
Crossstream Velocity, cm/s
100
50
0
Streamwise Velocity, cm/s
200
150
100
50
0
Depth, m
Distance, m
0
100
200
300
400
500
−20
−40
−60

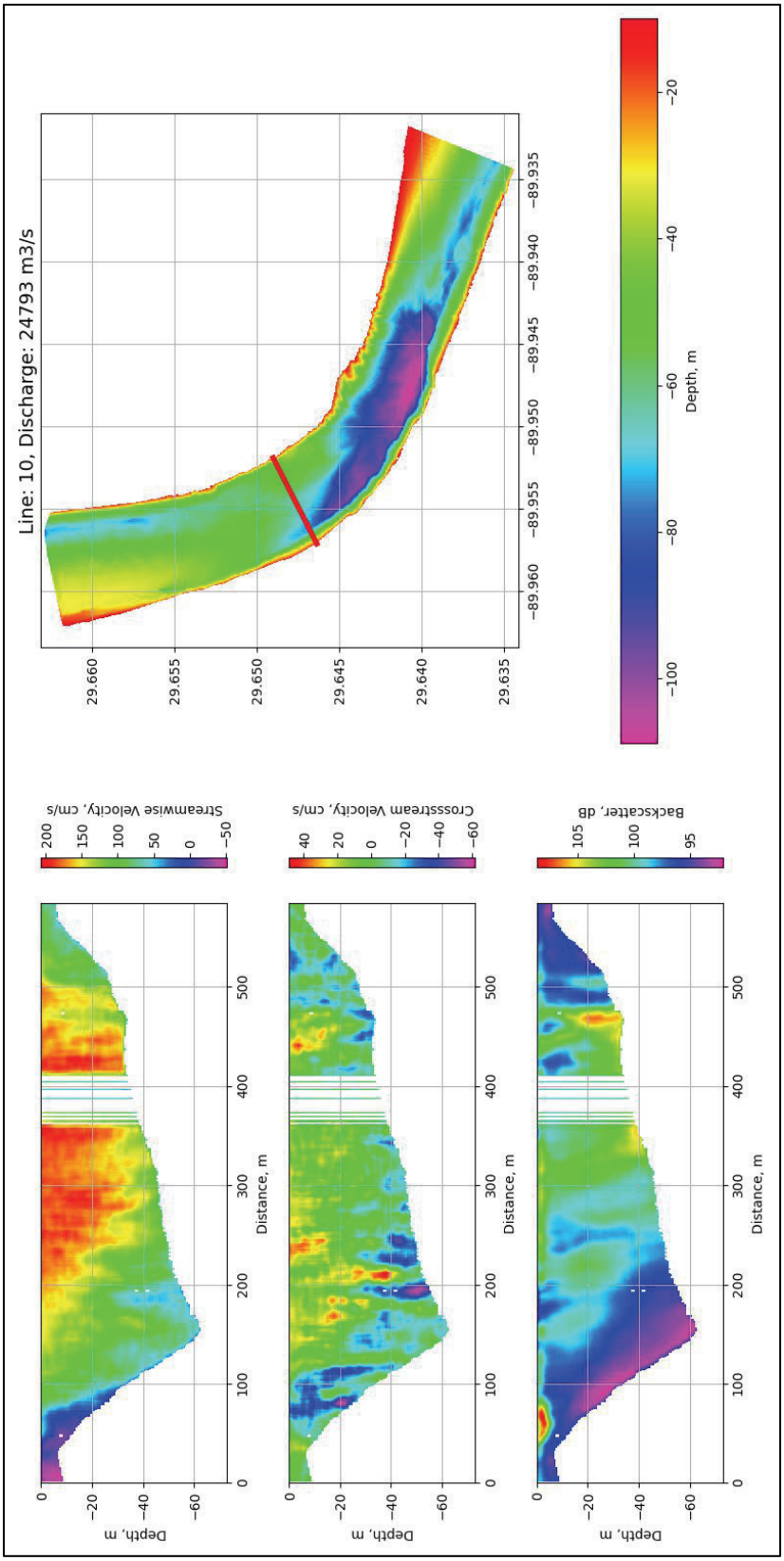
Line: 10, Discharge: 24793 m3/s
29.660
29.655
29.650
29.645
29.640
29.635
−89.960
−89.955
−89.950
−89.945
−89.940
−89.935
Depth, m
−20
−40
−60
−80
−100
Backscatter, dB
105
100
95
Crossstream Velocity, cm/s
40
20
0
−20
−40
−60
Streamwise Velocity, cm/s
200
150
100
50
0
−50
Depth, m
Distance, m
0
100
200
300
400
500
−20
−40
−60

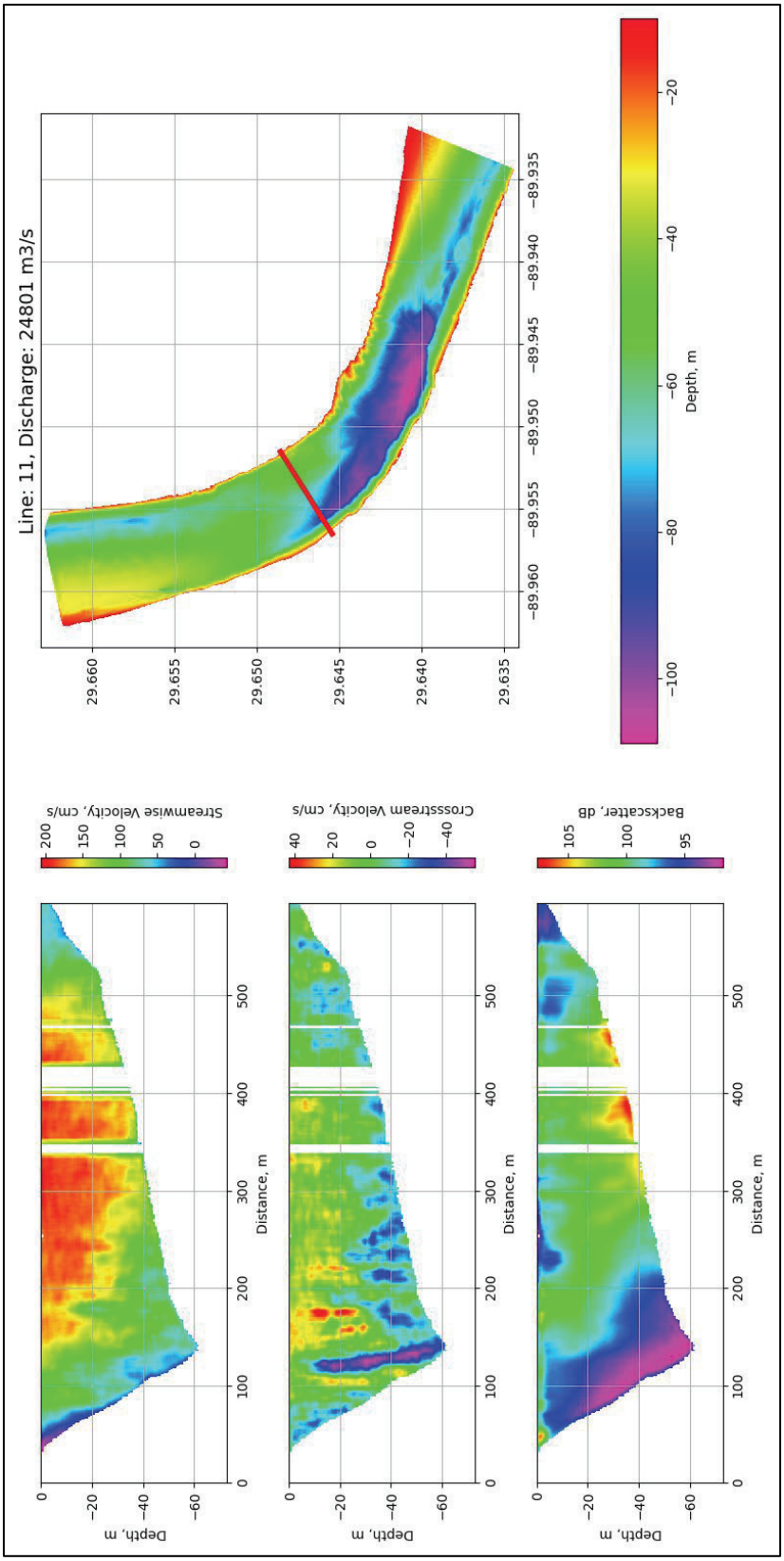
Line: 11, Discharge: 24801 m3/s
29.660
29.655
29.650
29.645
29.640
29.635
−89.960
−89.955
−89.950
−89.945
−89.940
−89.935
Depth, m
−20
−40
−60
−80
−100
Backscatter, dB
105
100
95
Crossstream Velocity, cm/s
40
20
0
−20
−40
Streamwise Velocity, cm/s
200
150
100
50
0
Depth, m
0
−20
−40
−60
Distance, m
0
100
200
300
400
500

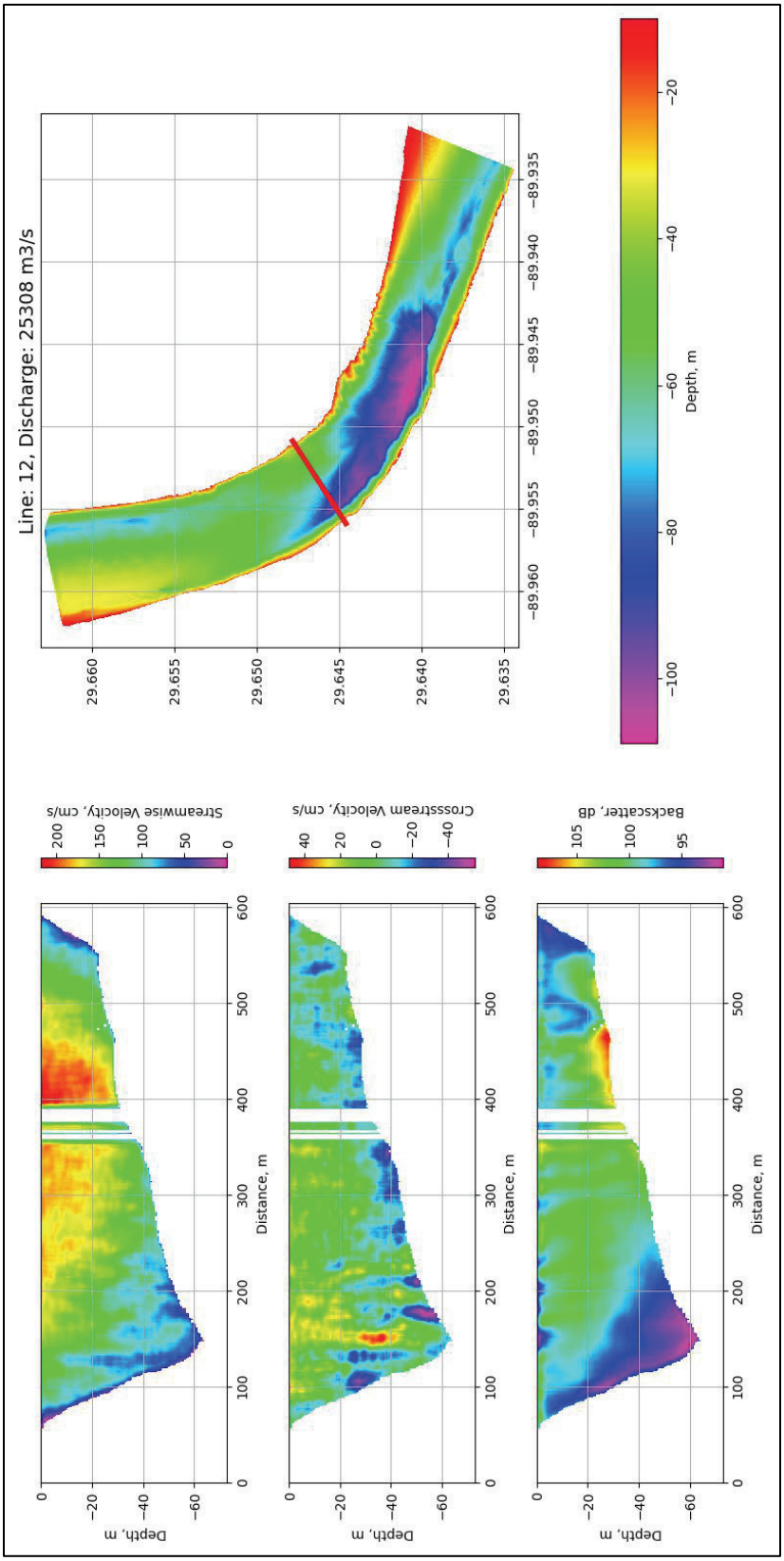
Line: 12, Discharge: 25308 m3/s
29.660
29.655
29.650
29.645
29.640
29.635
−89.960
−89.955
−89.950
−89.945
−89.940
−89.935
Depth, m
−20
−40
−60
−80
−100
Backscatter, dB
105
100
95
Crossstream Velocity, cm/s
40
20
0
−20
−40
Streamwise Velocity, cm/s
200
150
100
50
0
Depth, m
0
−20
−40
−60
Distance, m
0
100
200
300
400
500
600

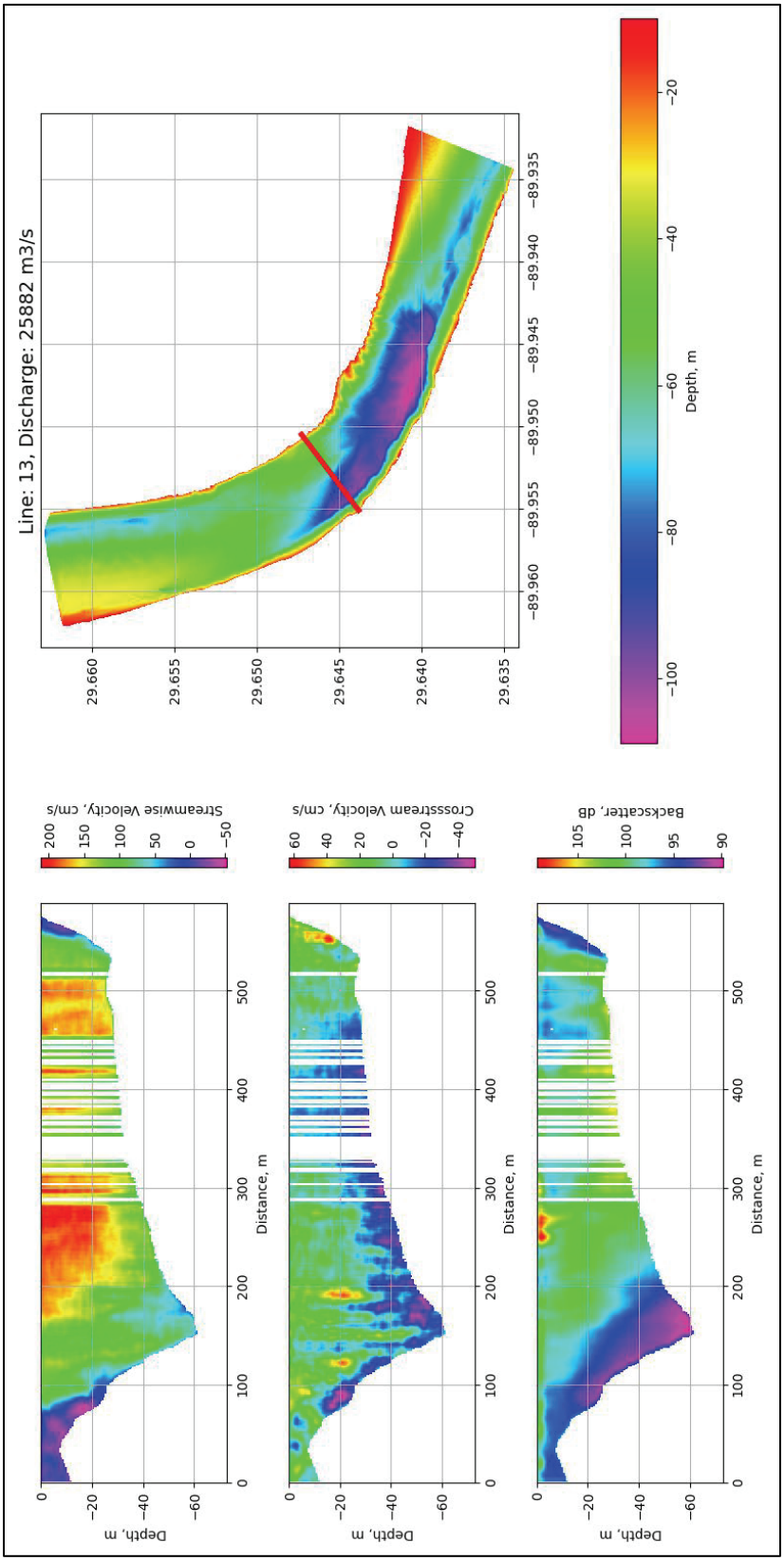
Line: 13, Discharge: 25882 m3/s
29.660
29.655
29.650
29.645
29.640
29.635
−89.960
−89.955
−89.950
−89.945
−89.940
−89.935
Depth, m
−20
−40
−60
−80
−100
Backscatter, dB
105
100
95
90
Crossstream Velocity, cm/s
60
40
20
0
−20
−40
Streamwise Velocity, cm/s
200
150
100
50
0
−50
Depth, m
0
−20
−40
−60
Distance, m
0
100
200
300
400
500

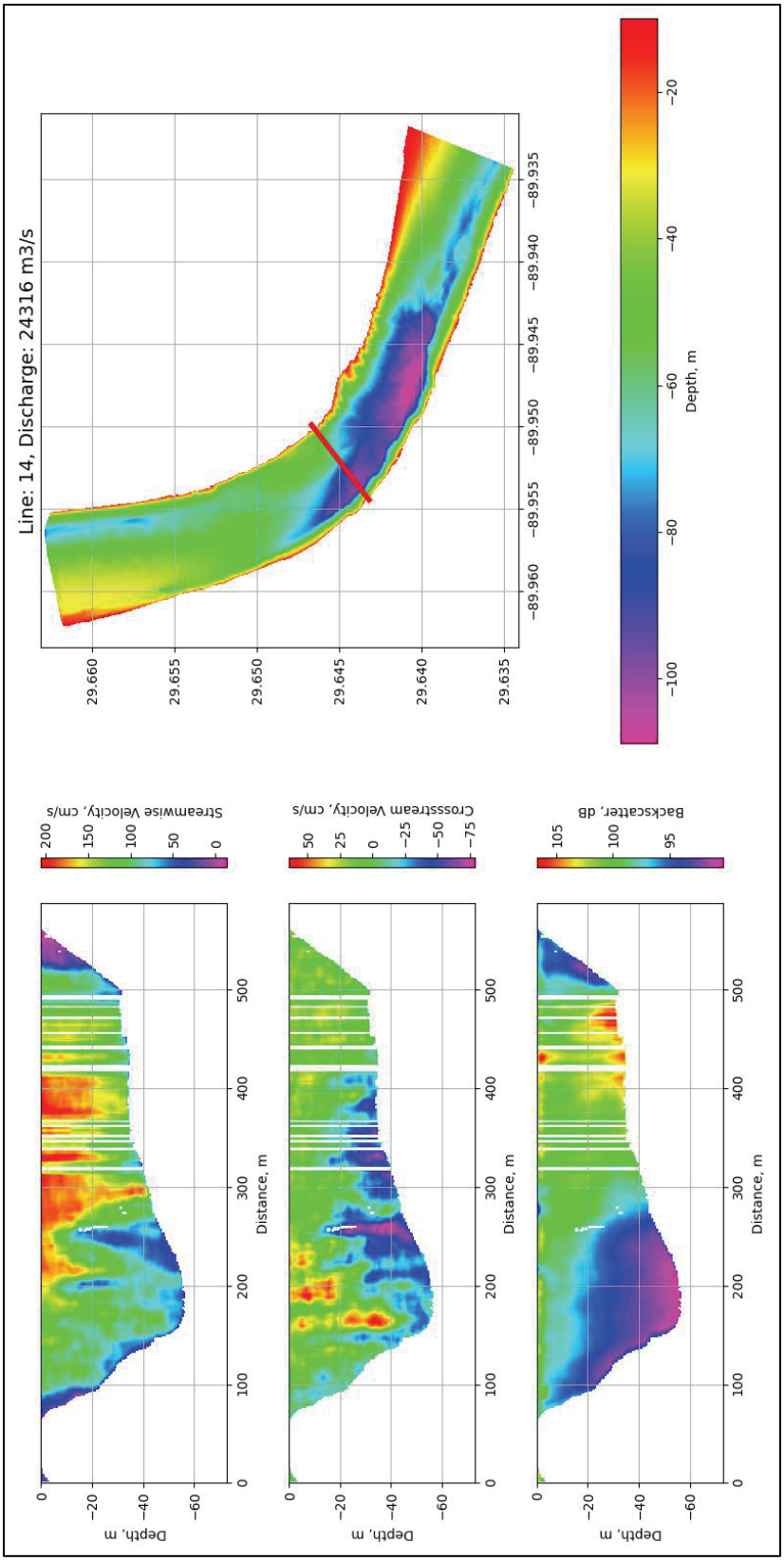
Line: 14, Discharge: 24316 m3/s
29.660
29.655
29.650
29.645
29.640
29.635
−89.960
−89.955
−89.950
−89.945
−89.940
−89.935
Depth, m
−20
−40
−60
−80
−100
Backscatter, dB
105
100
95
Crossstream Velocity, cm/s
50
25
0
−25
−50
−75
Streamwise Velocity, cm/s
200
150
100
50
0
Depth, m
0
−20
−40
−60
Distance, m
0
100
200
300
400
500

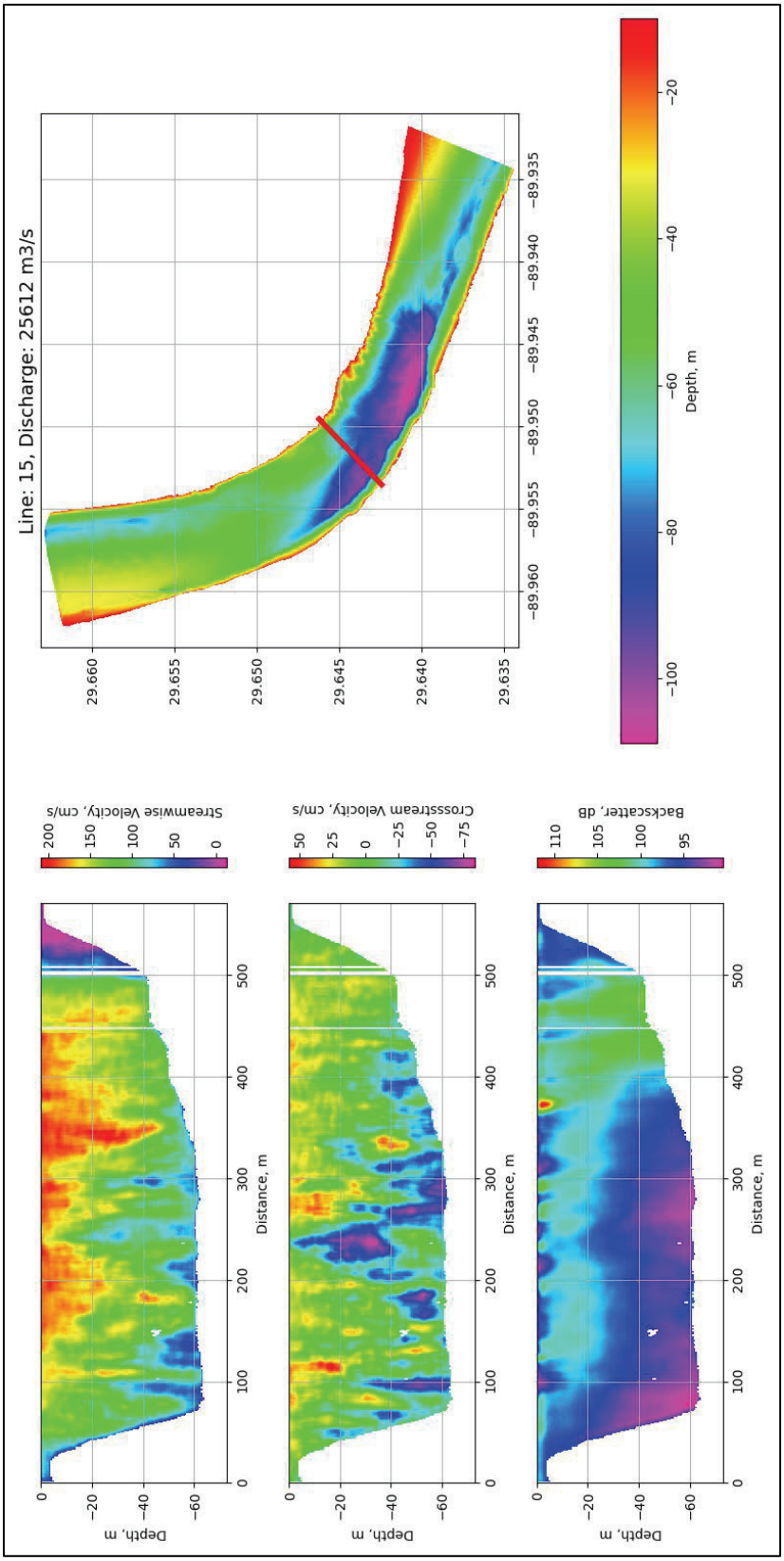
Line: 15, Discharge: 25612 m3/s
29.660
29.655
29.650
29.645
29.640
29.635
−89.960
−89.955
−89.950
−89.945
−89.940
−89.935
Depth, m
−20
−40
−60
−80
−100
Backscatter, dB
110
105
100
95
Crossstream Velocity, cm/s
50
25
0
−25
−50
−75
Streamwise Velocity, cm/s
200
150
100
50
0
Depth, m
Distance, m
0
100
200
300
400
500
−20
−40
−60

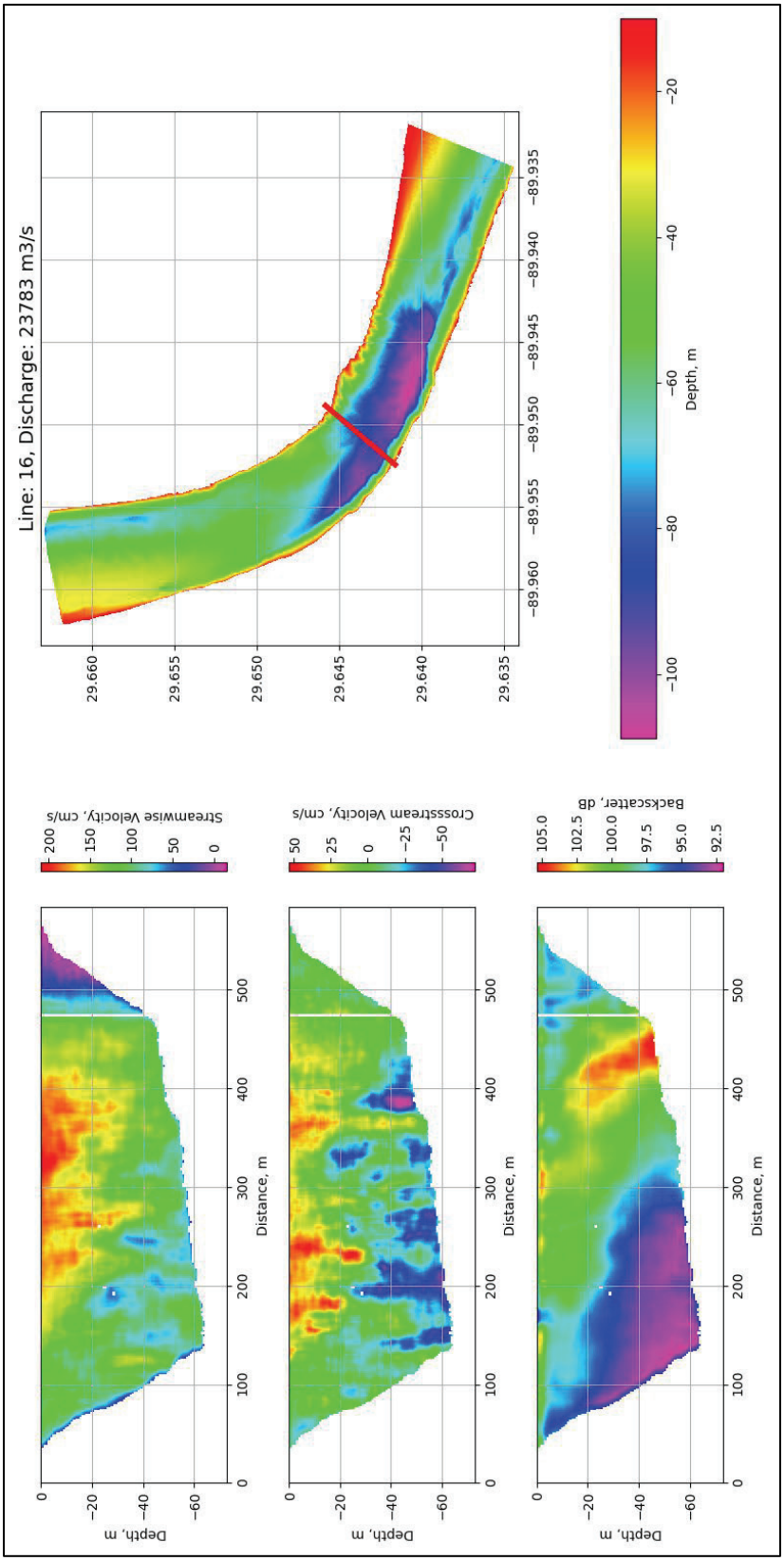
Line: 16, Discharge: 23783 m3/s
29.660
29.655
29.650
29.645
29.640
29.635
−89.960
−89.955
−89.950
−89.945
−89.940
−89.935
Depth, m
−20
−40
−60
−80
−100
Backscatter, dB
105.0
102.5
100.0
97.5
95.0
92.5
Crossstream Velocity, cm/s
50
25
0
−25
−50
Streamwise Velocity, cm/s
200
150
100
50
0
Depth, m
Distance, m
0
100
200
300
400
500
−20
−40
−60

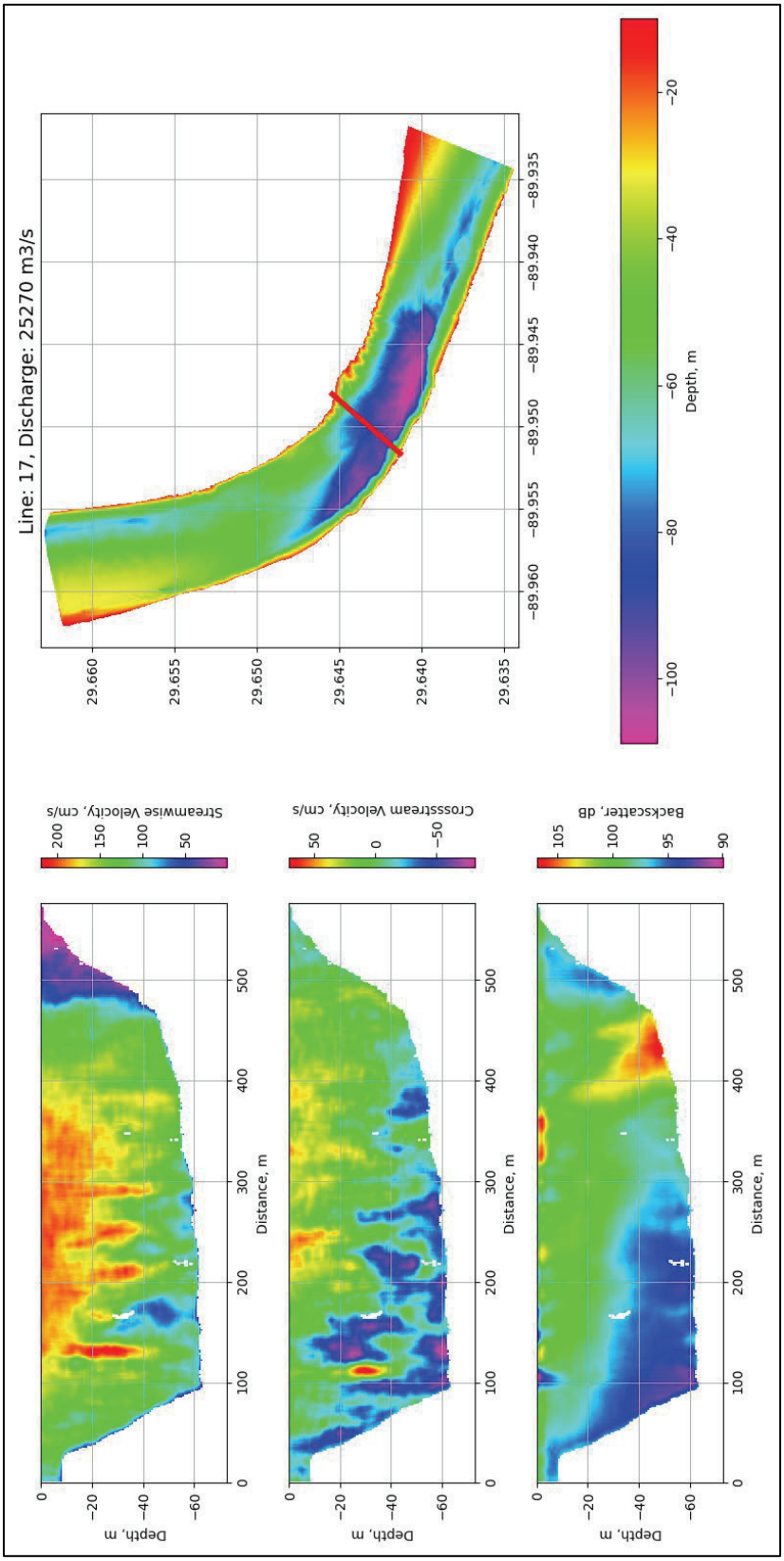
Line: 17, Discharge: 25270 m3/s
29.660
29.655
29.650
29.645
29.640
29.635
−89.960
−89.955
−89.950
−89.945
−89.940
−89.935
Depth, m
−20
−40
−60
−80
−100
Backscatter, dB
105
100
95
90
Crossstream Velocity, cm/s
50
0
−50
Streamwise Velocity, cm/s
200
150
100
50
Depth, m
Distance, m
0
100
200
300
400
500
−20
−40
−60

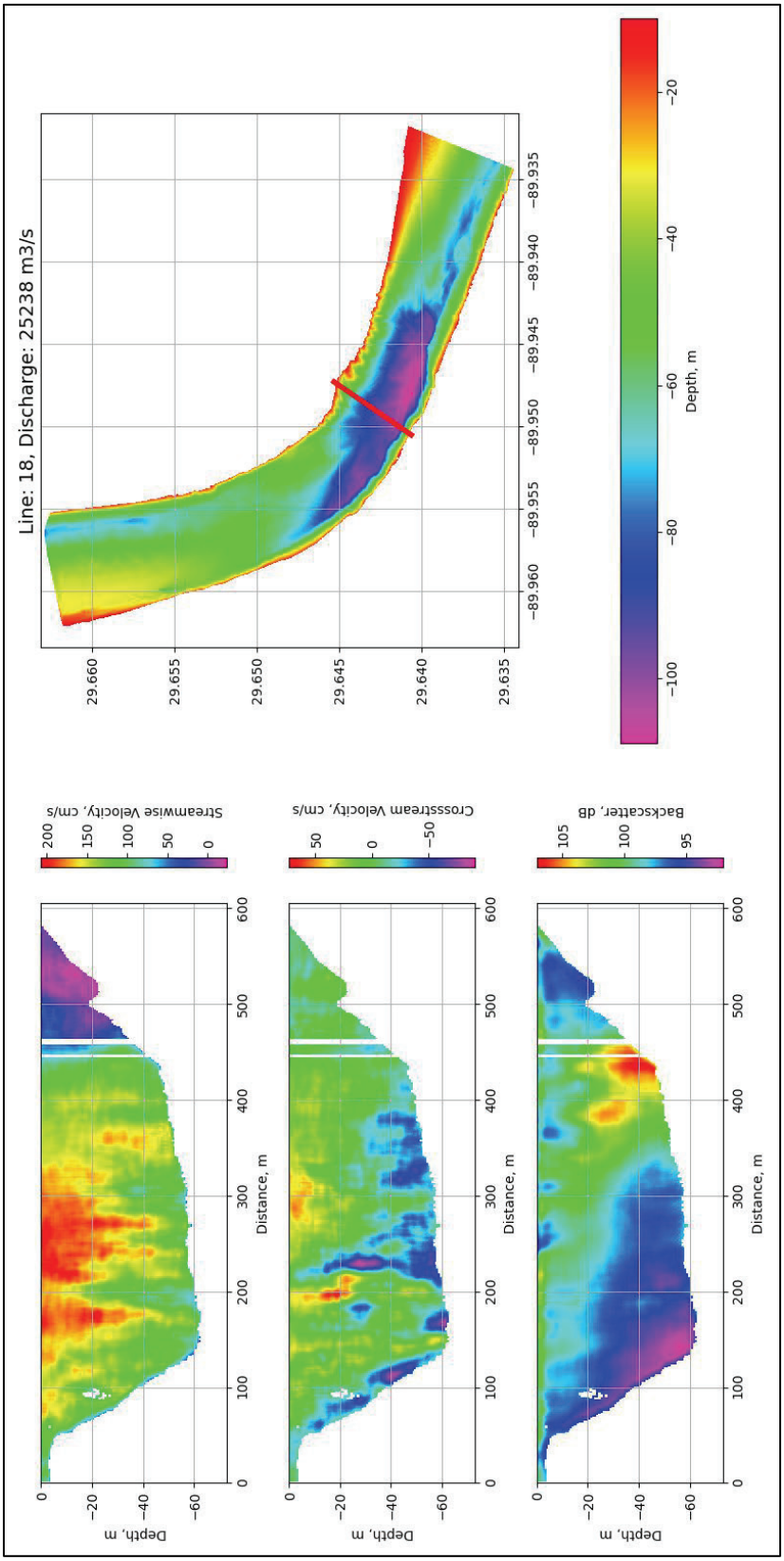
Line: 18, Discharge: 25238 m3/s
29.660
29.655
29.650
29.645
29.640
29.635
−89.960
−89.955
−89.950
−89.945
−89.940
−89.935
Depth, m
−20
−40
−60
−80
−100
Backscatter, dB
105
100
95
Crossstream Velocity, cm/s
50
0
−50
Streamwise Velocity, cm/s
200
150
100
50
0
Depth, m
Distance, m
0
100
200
300
400
500
600
−20
−40
−60

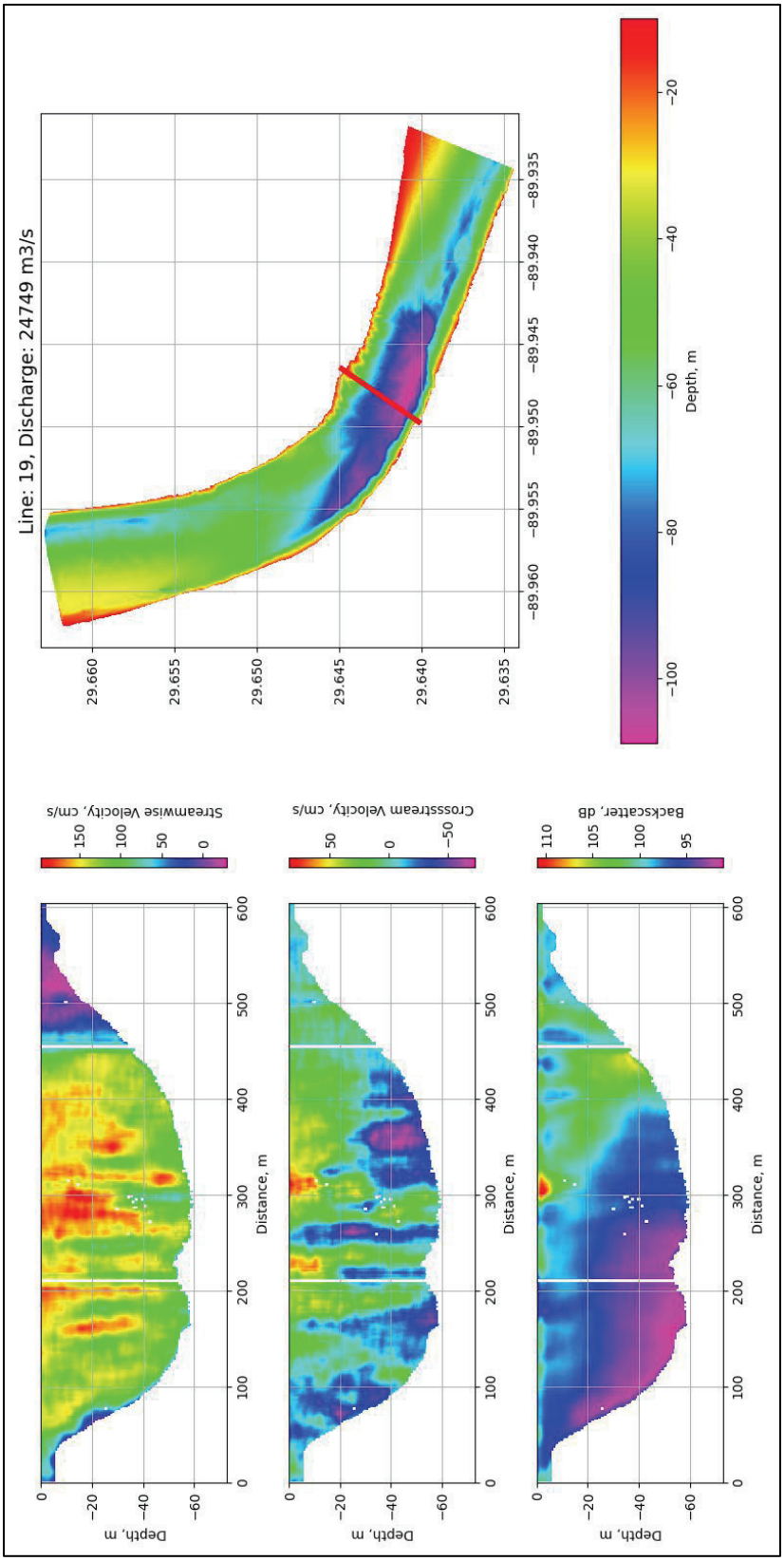
Line: 19, Discharge: 24749 m3/s
29.660
29.655
29.650
29.645
29.640
29.635
−89.960
−89.955
−89.950
−89.945
−89.940
−89.935
Depth, m
−20
−40
−60
−80
−100
Backscatter, dB
110
105
100
95
Crossstream Velocity, cm/s
50
0
−50
Streamwise Velocity, cm/s
150
100
50
0
Depth, m
Distance, m
0
100
200
300
400
500
600
−20
−40
−60

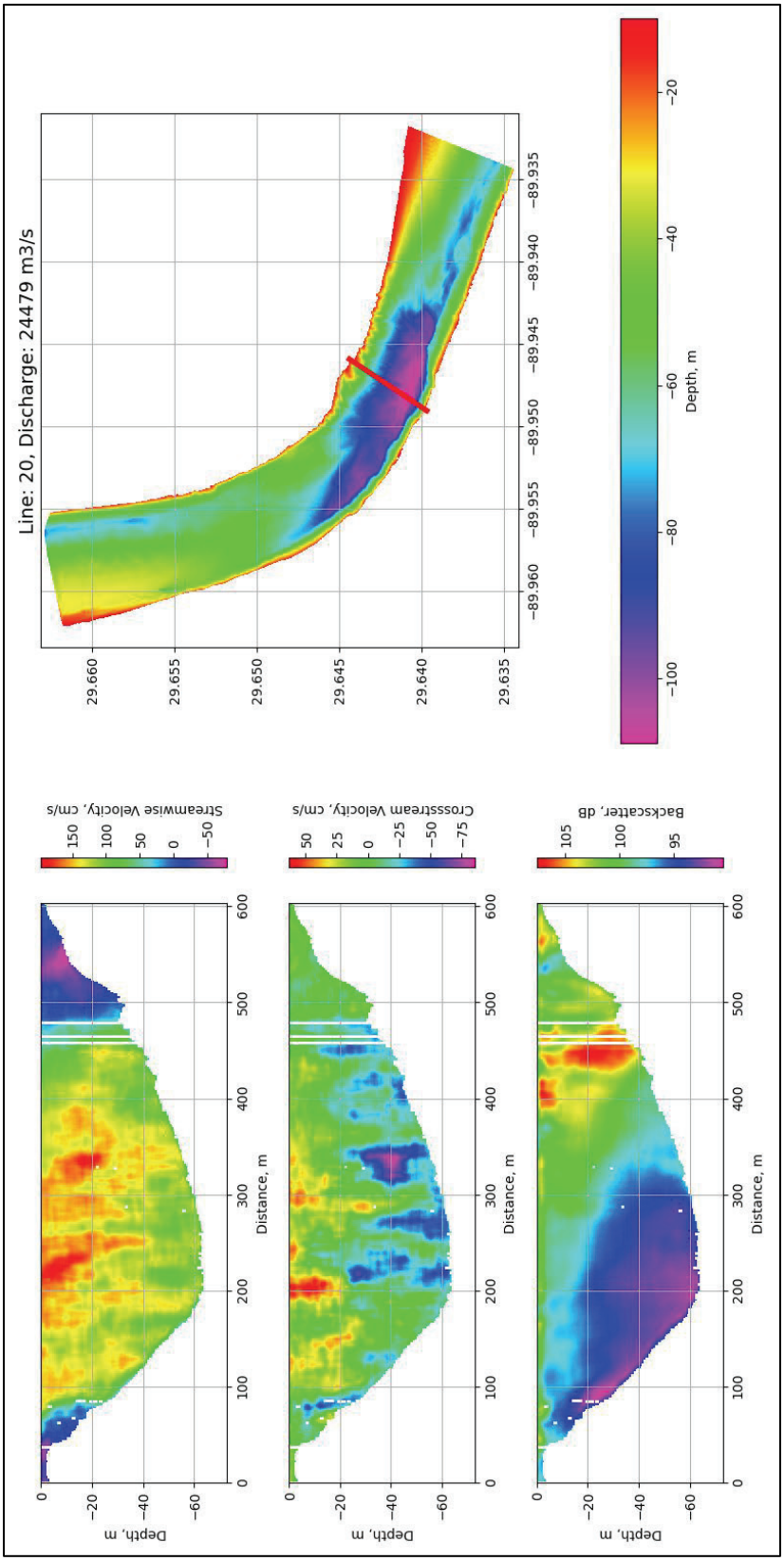
Line: 20, Discharge: 24479 m3/s
29.660
29.655
29.650
29.645
29.640
29.635
−89.960
−89.955
−89.950
−89.945
−89.940
−89.935
−20
−40
−60
−80
−100
Depth, m
Backscatter, dB
105
100
95
Crossstream Velocity, cm/s
50
25
0
−25
−50
−75
Streamwise Velocity, cm/s
150
100
50
0
−50
Depth, m
0
−20
−40
−60
Distance, m
0
100
200
300
400
500
600

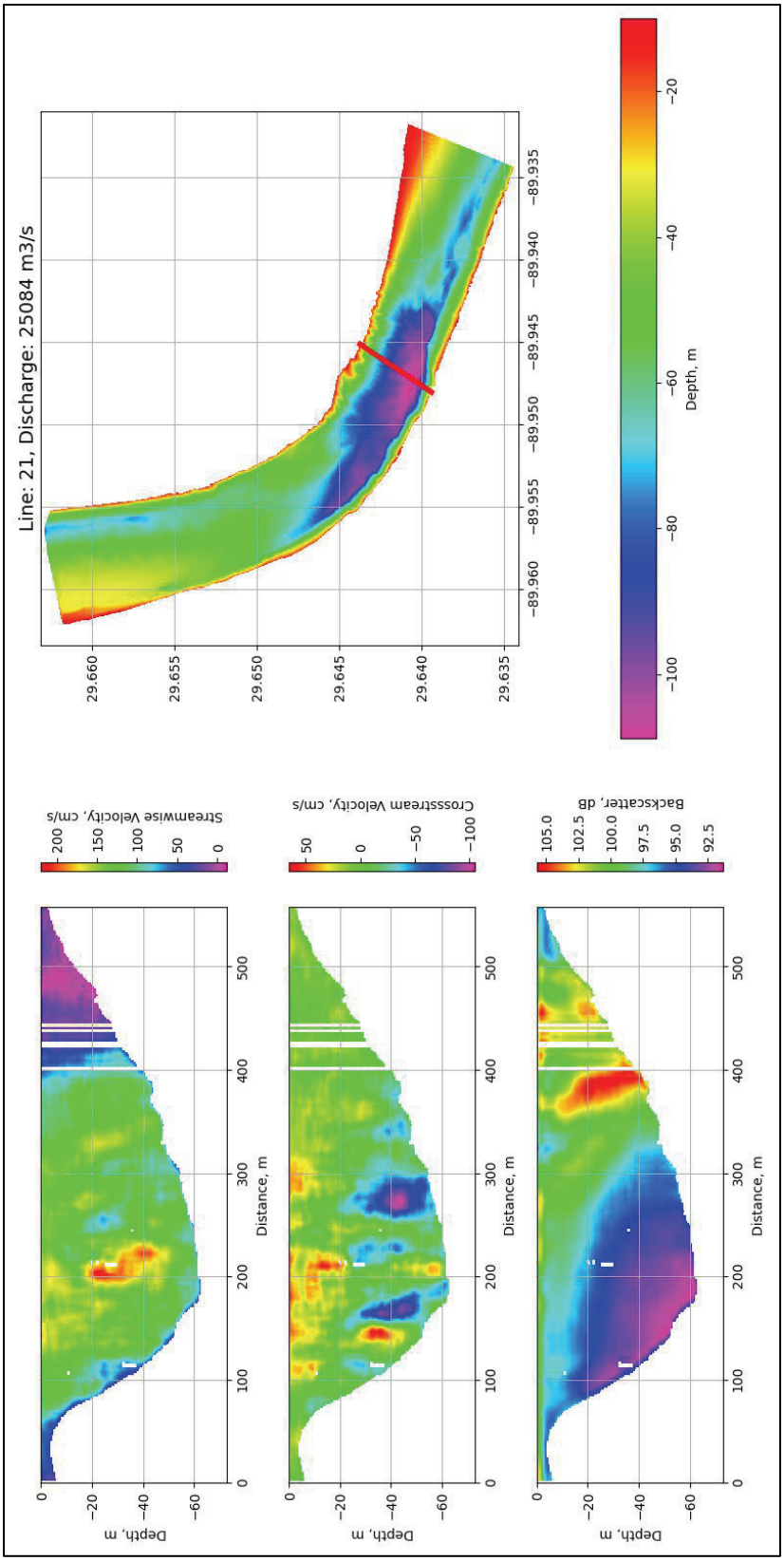
Line: 21, Discharge: 25084 m3/s
29.660
29.655
29.650
29.645
29.640
29.635
−89.960
−89.955
−89.950
−89.945
−89.940
−89.935
Depth, m
−20
−40
−60
−80
−100
Backscatter, dB
105.0
102.5
100.0
97.5
95.0
92.5
Crossstream Velocity, cm/s
50
0
−50
−100
Streamwise Velocity, cm/s
200
150
100
50
0
Depth, m
Distance, m
0
100
200
300
400
500
−20
−40
−60

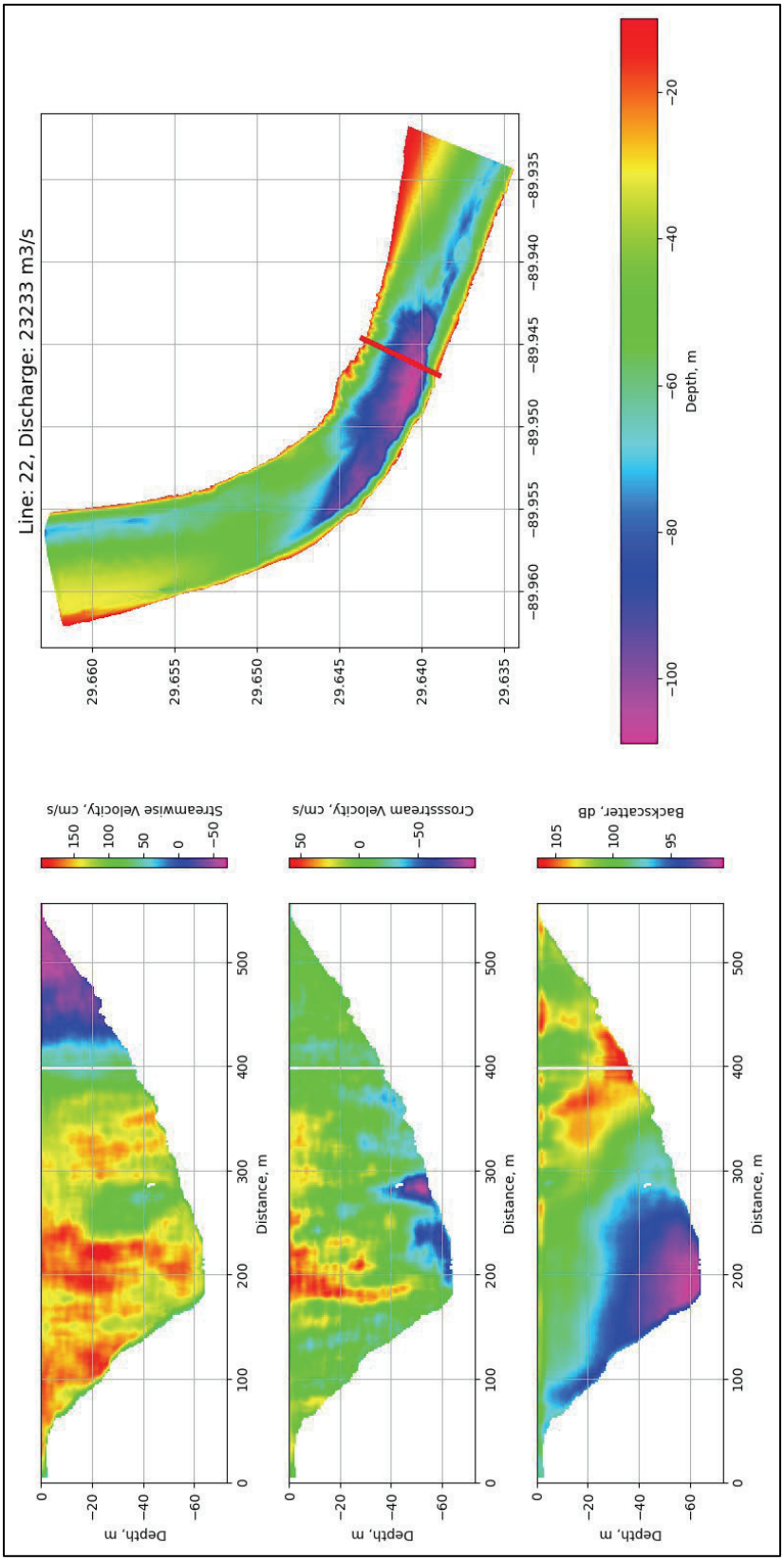
Line: 22, Discharge: 23233 m3/s
29.660
29.655
29.650
29.645
29.640
29.635
−89.960
−89.955
−89.950
−89.945
−89.940
−89.935
Depth, m
−20
−40
−60
−80
−100
Backscatter, dB
105
100
95
Crossstream Velocity, cm/s
50
0
−50
Streamwise Velocity, cm/s
150
100
50
0
−50
Depth, m
Distance, m
0
100
200
300
400
500
−20
−40
−60

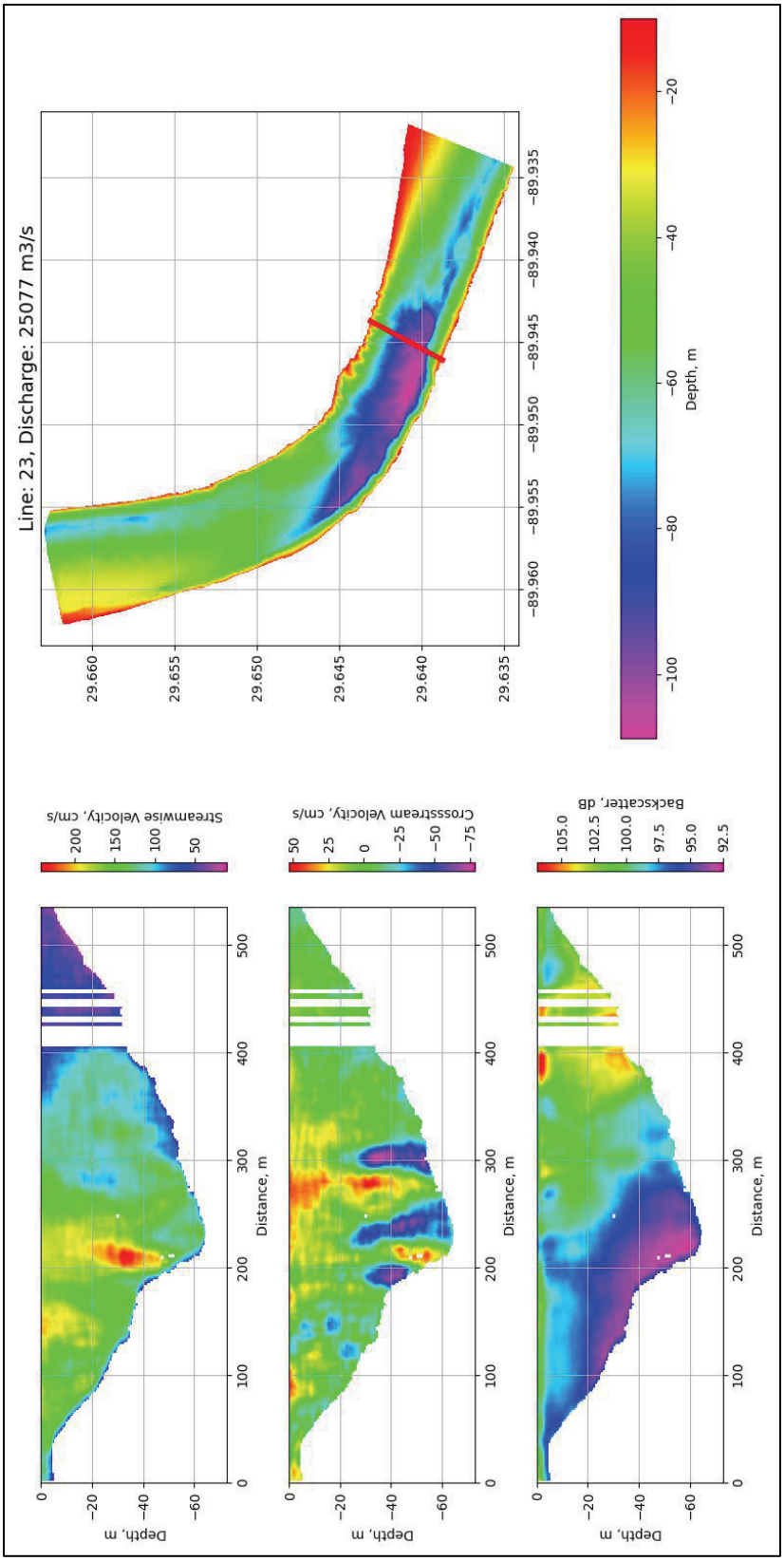
Line: 23, Discharge: 25077 m3/s
29.660
29.655
29.650
29.645
29.640
29.635
−89.960
−89.955
−89.950
−89.945
−89.940
−89.935
Depth, m
−20
−40
−60
−80
−100
Backscatter, dB
105.0
102.5
100.0
97.5
95.0
92.5
Crossstream Velocity, cm/s
50
25
0
−25
−50
−75
Streamwise Velocity, cm/s
200
150
100
50
Depth, m
Distance, m
0
100
200
300
400
500
−20
−40
−60

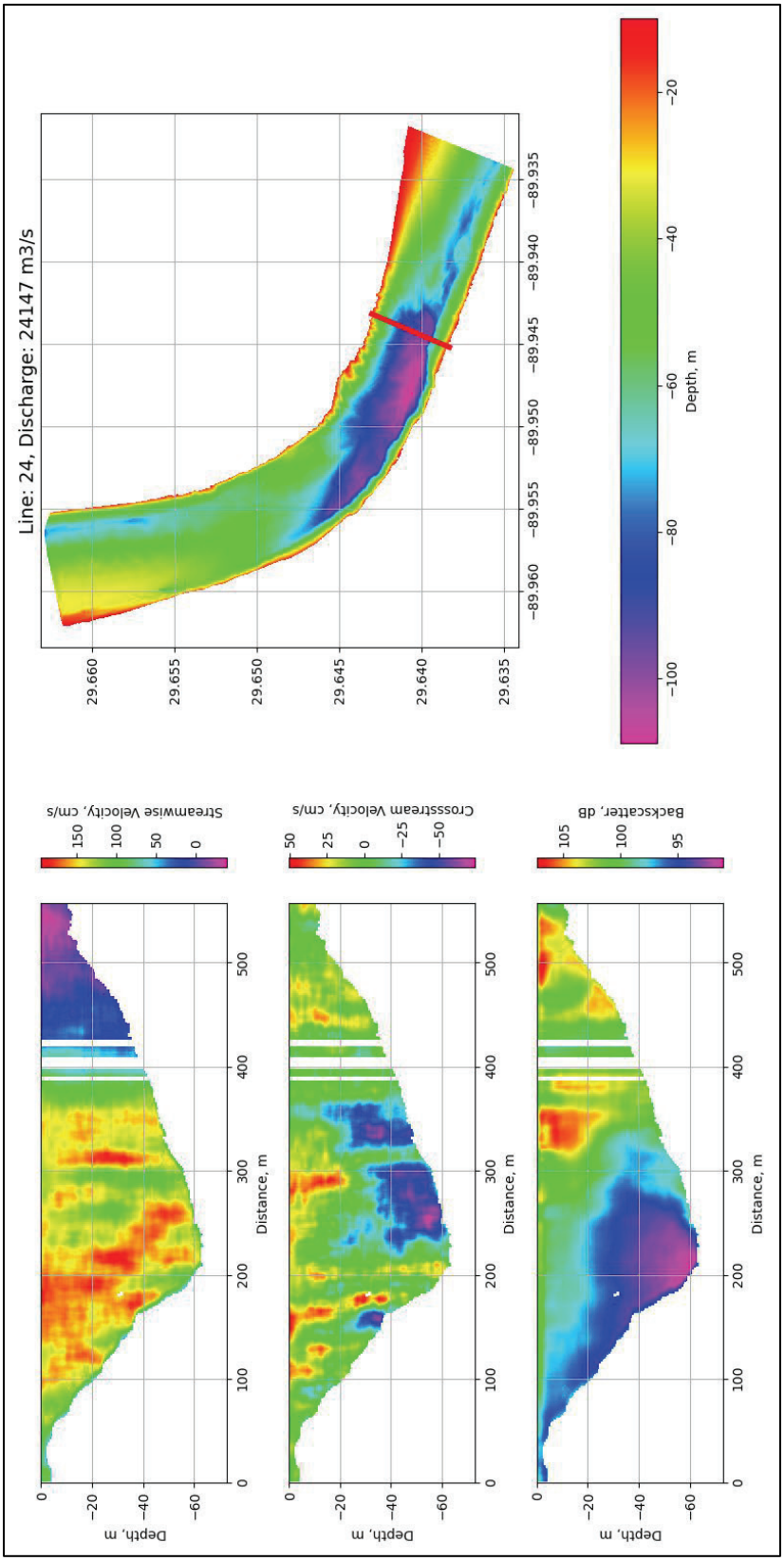
Line: 24, Discharge: 24147 m3/s
29.660
29.655
29.650
29.645
29.640
29.635
−89.960
−89.955
−89.950
−89.945
−89.940
−89.935
Depth, m
−20
−40
−60
−80
−100
Backscatter, dB
105
100
95
Crossstream Velocity, cm/s
50
25
0
−25
−50
Streamwise Velocity, cm/s
150
100
50
0
Depth, m
0
−20
−40
−60
Distance, m
0
100
200
300
400
500

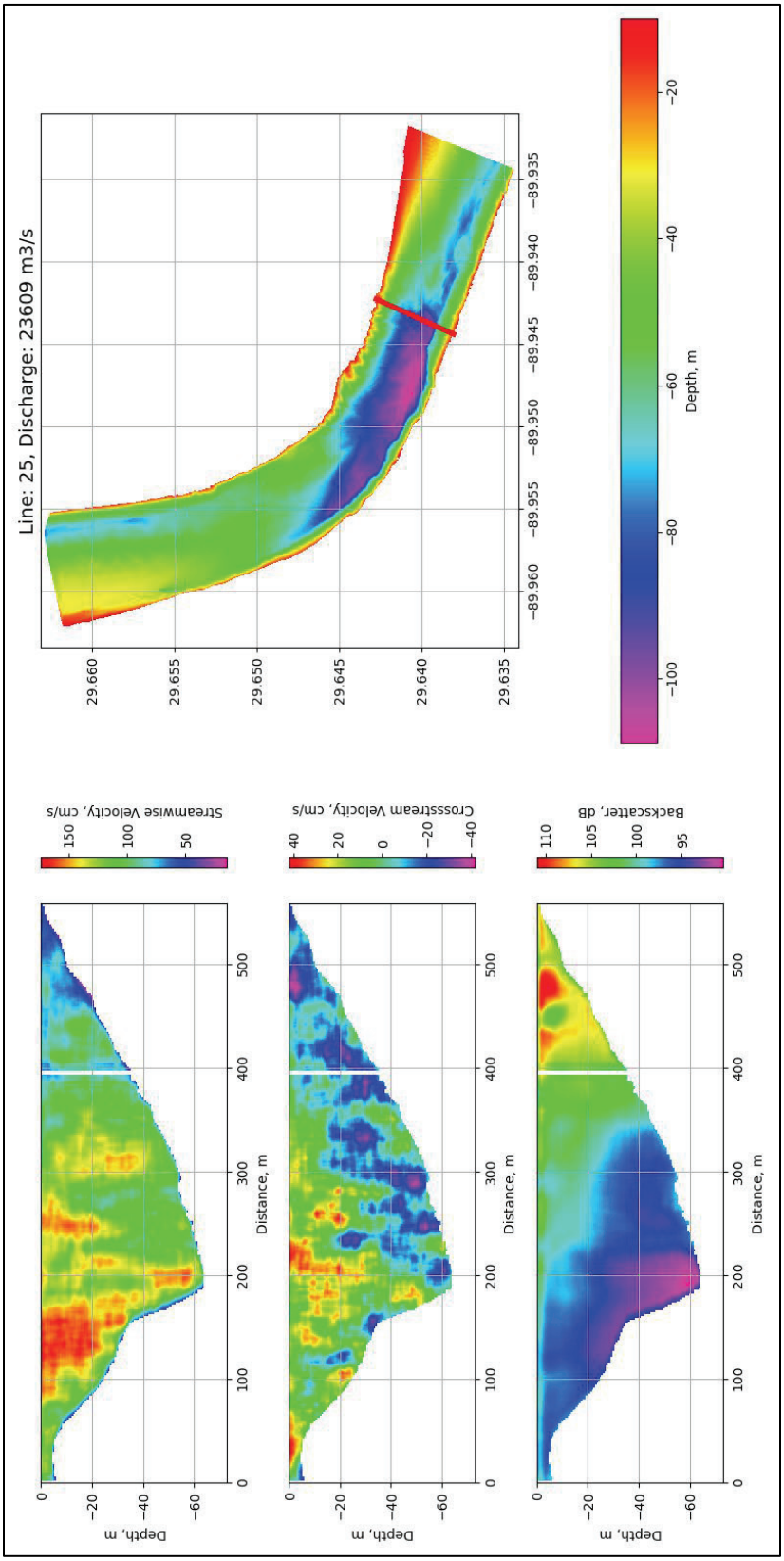
Line: 25, Discharge: 23609 m3/s
29.660
29.655
29.650
29.645
29.640
29.635
−89.960
−89.955
−89.950
−89.945
−89.940
−89.935
Depth, m
−20
−40
−60
−80
−100
Backscatter, dB
110
105
100
95
Crossstream Velocity, cm/s
40
20
0
−20
−40
Streamwise Velocity, cm/s
150
100
50
Depth, m
0
−20
−40
−60
Distance, m
0
100
200
300
400
500

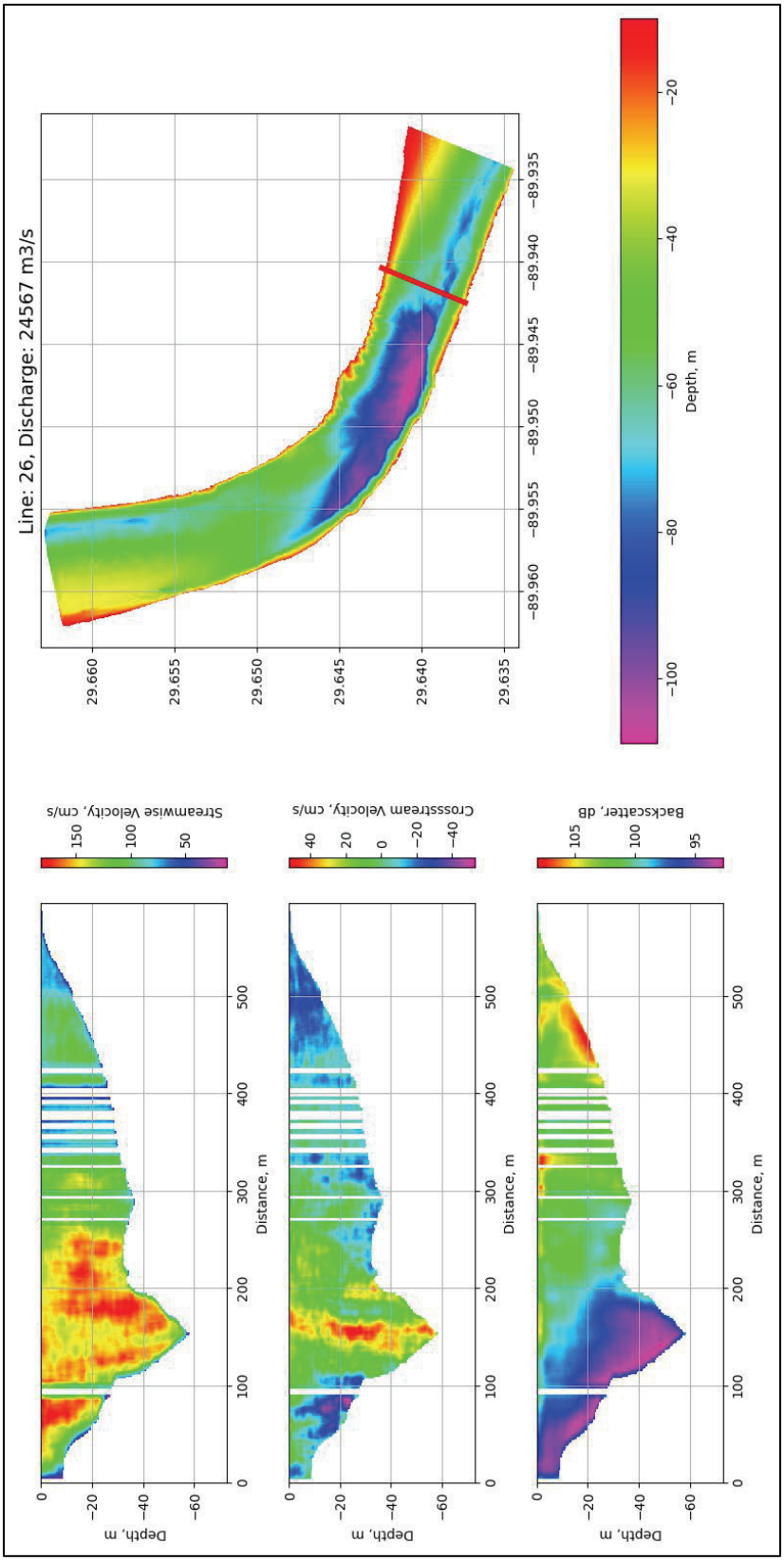
Line: 26, Discharge: 24567 m3/s
29.660
29.655
29.650
29.645
29.640
29.635
−89.960
−89.955
−89.950
−89.945
−89.940
−89.935
Depth, m
−20
−40
−60
−80
−100
Backscatter, dB
105
100
95
Crossstream Velocity, cm/s
40
20
0
−20
−40
Streamwise Velocity, cm/s
150
100
50
Depth, m
0
−20
−40
−60
Distance, m
0
100
200
300
400
500

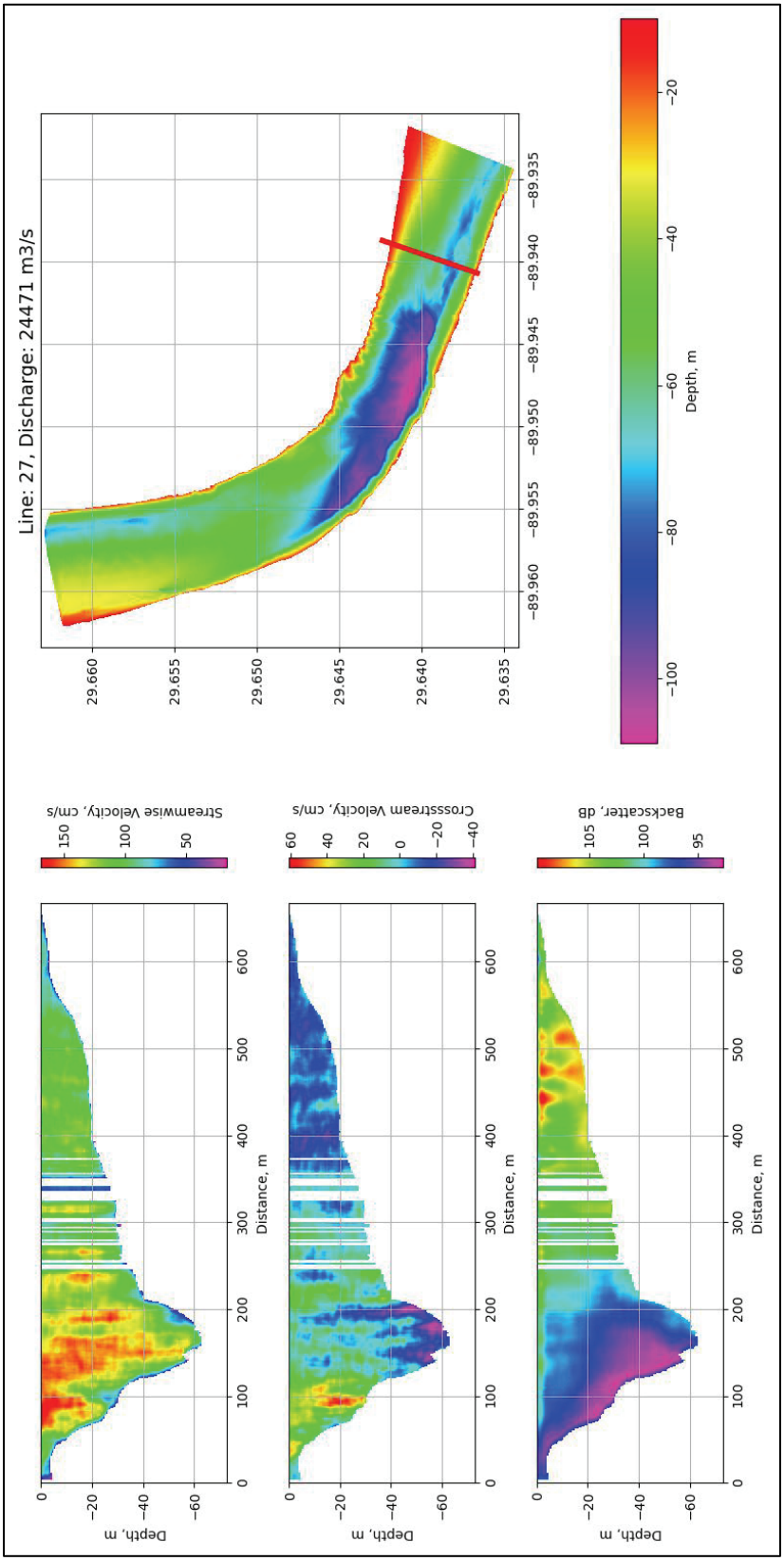
Line: 27, Discharge: 24471 m3/s
29.660
29.655
29.650
29.645
29.640
29.635
−89.960
−89.955
−89.950
−89.945
−89.940
−89.935
Depth, m
−20
−40
−60
−80
−100
Backscatter, dB
105
100
95
Crossstream Velocity, cm/s
60
40
20
0
−20
−40
Streamwise Velocity, cm/s
150
100
50
Depth, m
Distance, m
0
100
200
300
400
500
600
−20
−40
−60

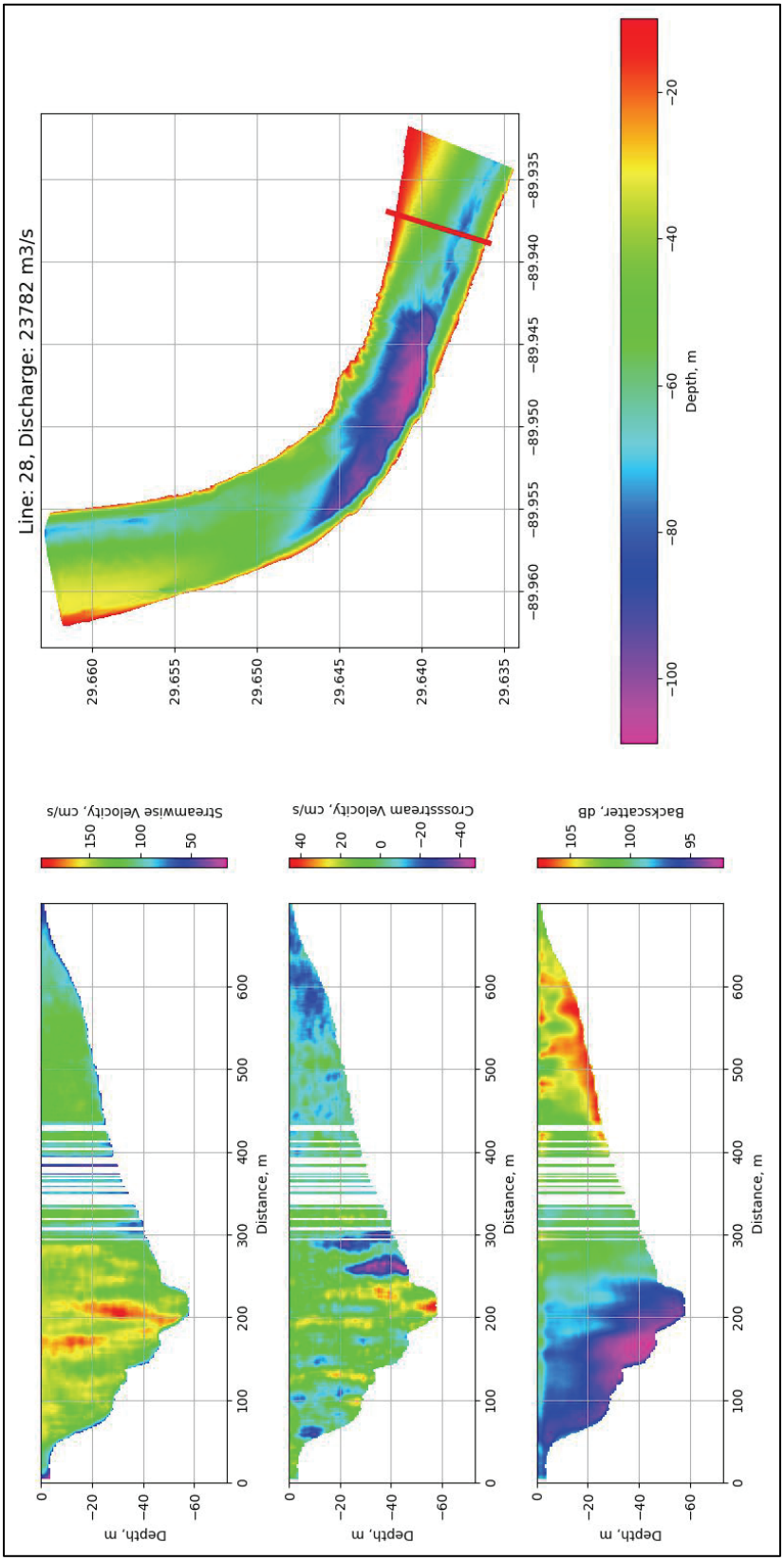
Line: 28, Discharge: 23782 m3/s
29.660
29.655
29.650
29.645
29.640
29.635
−89.960
−89.955
−89.950
−89.945
−89.940
−89.935
Depth, m
−20
−40
−60
−80
−100
Backscatter, dB
105
100
95
Crossstream Velocity, cm/s
40
20
0
−20
−40
Streamwise Velocity, cm/s
150
100
50
Depth, m
0
−20
−40
−60
Distance, m
0
100
200
300
400
500
600

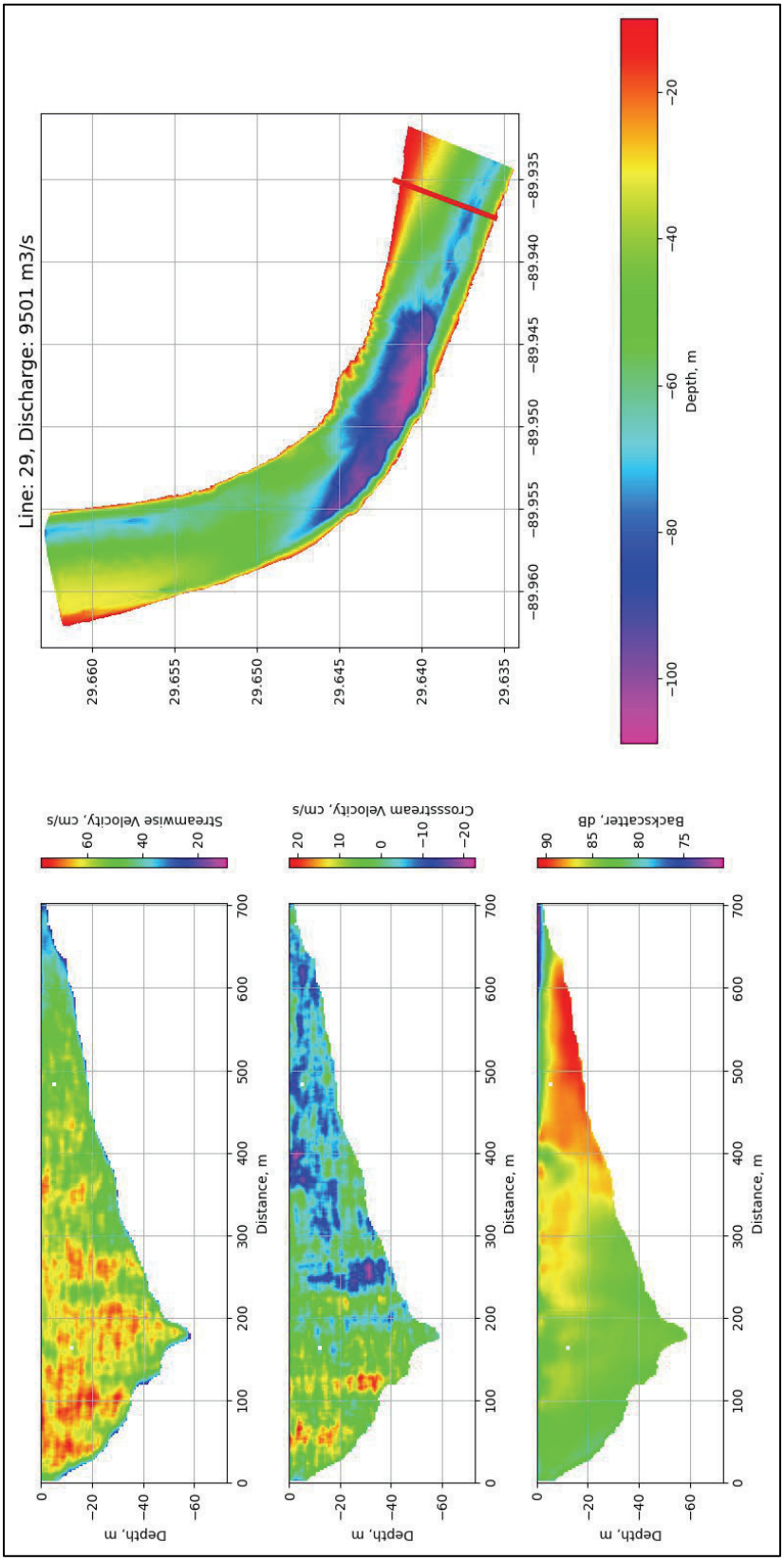
Line: 29, Discharge: 9501 m3/s
29.660
29.655
29.650
29.645
29.640
29.635
−89.960
−89.955
−89.950
−89.945
−89.940
−89.935
Depth, m
−20
−40
−60
−80
−100
Backscatter, dB
90
85
80
75
Crossstream Velocity, cm/s
20
10
0
−10
−20
Streamwise Velocity, cm/s
60
40
20
Depth, m
0
−20
−40
−60
Distance, m
0
100
200
300
400
500
600
700

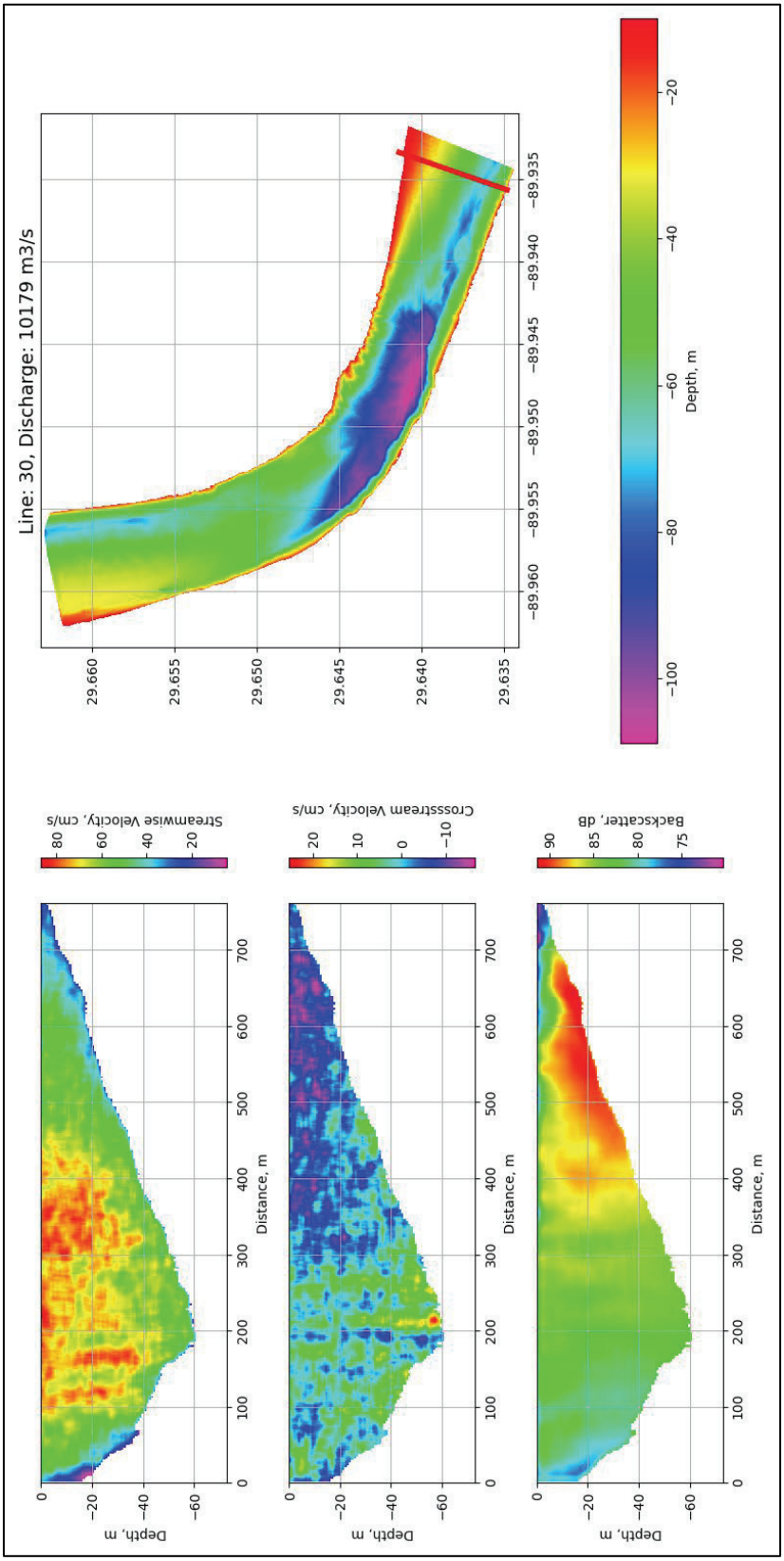
Line: 30, Discharge: 10179 m3/s
29.660
29.655
29.650
29.645
29.640
29.635
−89.960
−89.955
−89.950
−89.945
−89.940
−89.935
Depth, m
−20
−40
−60
−80
−100
Backscatter, dB
90
85
80
75
Crossstream Velocity, cm/s
20
10
0
−10
Streamwise Velocity, cm/s
80
60
40
20
Depth, m
0
−20
−40
−60
Distance, m
0
100
200
300
400
500
600
700

REPORT DOCUMENTATION PAGE

1. REPORT DATE	2. REPORT TYPE	3. DATES COVERED	
		START DATE	END DATE
August 2023	Final report	FY20	FY21

4. TITLE AND SUBTITLE

Acoustic Doppler Current Profiler Study of Water and Sediment Movement through a Deep Scour Hole in the Lower Mississippi River

5a. CONTRACT NUMBER	5b. GRANT NUMBER	5c. PROGRAM ELEMENT
5d. PROJECT NUMBER	**5e. TASK NUMBER**	**5f. WORK UNIT NUMBER**

6. AUTHOR(S)

Michael T. Ramirez, Travis A. Dahl, and Gary L. Brown

7. PERFORMING ORGANIZATION NAME(S) AND ADDRESS(ES)

US Army Engineer Research and Development Center
Coastal and Hydraulics Laboratory
3909 Halls Ferry Road
Vicksburg, MS 39180-6199

8. PERFORMING ORGANIZATION REPORT NUMBER

MRG&P Report No. 45

9. SPONSORING/MONITORING AGENCY NAME(S) AND ADDRESS(ES)

Mississippi River Geomorphology and Potamology Program
US Army Corps of Engineers, Mississippi Valley Division
Vicksburg, MS 39180-0080

10. SPONSOR/MONITOR'S ACRONYM(S)

MRG&P MVD

11. SPONSOR/MONITOR'S REPORT NUMBER(S)

12. DISTRIBUTION/AVAILABILITY STATEMENT

Distribution Statement A: Approved for public release; distribution is unlimited.

13. SUPPLEMENTARY NOTES

Funding provided by the Mississippi Valley Division through the Mississippi River Geomorphology and Potamology Program.

14. ABSTRACT

A series of acoustic Doppler current profiler (ADCP) transects were collected through a deep scour hole at the bend near River Mile 60 on the Lower Mississippi River. The measurements were collected during both a low and a high flow. The ADCP results show a 3D flow field through the deep bend. The backscatter intensity of the ADCP measurements indicates the majority of the sediment remains close to the inside of the bed and high in the water column, with minimal concentrations at the bottom of the bend. These findings have implications for numerical sediment transport models, which tend to deposit material at the bottom of deep scour holes like the one in this study.

15. SUBJECT TERMS

Acoustic Doppler velocimeter; Mississippi River; Scour (Hydraulic engineering); Sediment transport; Velocimetry

16. SECURITY CLASSIFICATION OF:			17. LIMITATION OF ABSTRACT	18. NUMBER OF PAGES
a. REPORT	b. ABSTRACT	C. THIS PAGE		
Unclassified	Unclassified	Unclassified	SAR	97

19a. NAME OF RESPONSIBLE PERSON	19b. TELEPHONE NUMBER (include area code)
Travis A. Dahl	601-634-2371